

Polygonal faults in the northern North Sea

Amalie Sande Rødde

Master thesis in geodynamics and basin studies



Faculty of Mathematics and Natural Science

Department of Earth Science

University of Bergen

June 2020

Abstract

Polygonal faults have been studied in sedimentary basins at the Norwegian continental shelf and globally as non-tectonic normal faults. The polygonal faults have been recognized for a long time, but no one has described them collectively to understand the trigger mechanisms better. This study applied a 3D seismic data set of the North Viking Graben focusing on the Cenozoic sequences in the sedimentary basin. The polygonal faults in these stratigraphic sequences display a random distribution of strikes and develop in very fine-grained sediments of clays. A comprehensive seismic interpretation was conducted of the entire northern North Sea, focusing on seven sequence boundaries and six stratigraphic sequences in the period of Paleocene to Miocene. Detailed characteristics of the stratigraphic sequences were investigated by analyzing attribute maps, seismic data, and topological characteristics in minor subareas (each 56 km²). These data were applied to examine polygonal faults distribution, seismic signatures, and geometries in the area.

The most important observations in this study are: 1) the seismic expression of polygonal faults vary more between sequences than within different positions of the basin, 2) polygonal faults in the Cenozoic successions in the northern North Sea are restricted to the eastern half of the sedimentary basin. The distribution is thought to be due to reduced grain size and increased smectite content with increasing distance to the main provenance area at the East Shetland Platform, 3) the Eocene-Oligocene sequences cover the highest frequency and density of polygonal faults in the area and display evident remobilized structures of gravitational sliding from N-S trending mounds and strike sets of faults. The most evident trigger mechanism of polygonal faults in this study is an interaction between internal (dissolution, crushing, diagenesis, syneresis) and external (gravitational sliding, gravitational loading) mechanisms contributing to the formation of polygonal faults. Phases of uplift and sediments deposited from gravitational processes from the Early Paleocene to Pliocene and Pleistocene periods have impacted polygonal fault development in the basin. Late Paleocene-Early Eocene and Miocene periods are characterized by limited polygonal faults associated with uplifts, lithologies, and sand inputs.

Acknowledgements

This study is a part of my MSc degree in Structural Geology at the Department of Earth Science, University of Bergen. The thesis was completed with great assistance and feedback, and I wish to thank several people for valuable contributions to this project.

First, I would like to express my gratitude to my main supervisor Christian Hermanrud. He has been eager and interested in my studies, and I would like to thank you for valuable discussions, constructive feedback, and always being available during this period. In addition, I would like to thank him for giving me an exciting thesis with many interesting discoveries, more than we had time to go through. I want to thank my co-supervisors, Haakon Fossen, for much-appreciated discussions and valuable input, and Casey Nixon for introducing me to Network GT and Topology. Thank you for educational meetings and a great introduction to the tool. A big thanks to everyone in the PESTOH group for sharing your knowledge during the past two years.

I am grateful for all help by Leo Zijerveld and for always responding quickly and helping with any computer or Petrel problems. A big thanks to Philipp Müller for always being available for meetings, answering questions, contributions, and good guidance to my seismic work. Thank you to CGG for providing me with a 3D seismic data set of the northern North Sea.

Thanks to everyone at Hjørnerommet and all my friends at the university for two fun, challenging and educational years. A big thanks go to Philipp Müller, Serianna Kvarøy, Magomed Khadisov, Aleksey Fjodorov, and Halcyon Schepel for proofreading my thesis.

A special thanks go to my family and friends for always believing in me and motivating me during hard times.

Bergen, June 2021

Amalie Sande Rødde

Content

- 1. Introduction.....1**
- 2. Geological background.....4**
 - 2.1 Pre-Cenozoic4
 - 2.2 The Cenozoic6
 - 2.2.1 Summary of the lithology of Cenozoic sediments11
- 3. Theoretical background13**
 - 3.1 Polygonal faults13
 - 3.1.1 Occurrence14
 - 3.1.2 Lithologies.....15
 - 3.1.3 Trigger mechanisms15
 - 3.1.3 Diagenesis in the Cenozoic successions21
 - 3.1.4 Geometries and seismic identification22
 - 3.2 Soft sediment remobilization24
 - 3.3 Network topology24
 - 3.5 Seismic attributes26
- 4. Data and methodology.....27**
 - 4.1 Seismic and well data.....27
 - 4.2 Seismic interpretation31
 - 4.2.1 Interpreted sequence boundaries33
 - 4.2.2 Seismic expression of sequences37
 - 4.2.3 Uncertainties39
 - 4.3 Topology and Geometry Analysis39
 - 4.3.1 Spatial visualization of fracture networks.....41
 - 4.3.3 Uncertainties42
 - 4.4 Workflow42
 - 4.4.1 Fault distribution maps43
 - 4.4.2 Subareas44
- 5. Seismic observations and topological characteristics of polygonal faults48**
 - 5.1 CSS-0 (Upper Mesozoic sequence)48
 - 5.2 CSS-1 (Paleocene-Early Eocene sequence)53
 - 5.3 CSS-2 (Largely Eocene sequence).....62

5.4 CSS-3 (Lower Oligocene sequence)	68
5.5 CSS-4 (Upper Oligocene sequence)	74
5.6 CSS-5/6 (Lower Miocene sequence)	85
5.7 CSS-7 (Upper Miocene sequence)	88
5.8 Summary of seismic and topological observations	91
6. Summary and interpretation of observations	93
6.1 Seismic expression of polygonal faults.....	93
6.2 Kinematics for polygonal fault systems	95
6.2.1 Basin distribution	95
6.2.2 Fault plane geometries	97
6.2.3 Fault displacement	99
6.2.4 Fault orientation	101
6.3 Proposed classification of polygonal faults	104
6.4 Suggested trigger mechanisms.....	107
7. Future work.....	117
8. Conclusion	118
References.....	120

1. Introduction

Polygonal faults are small-scale extensional faults situated in fine-grained sedimentary successions and are introduced as non-tectonic normal faults, exhibiting a wide range of fault strikes (Cartwright, 1994; Dewhurst et al., 1999; Cartwright et al., 2003; Stuevold et al., 2003; Wrona et al., 2017). Polygonal faults were first recognized as a deformational feature in soft sediments in the late 1980s and were first appreciated through seismic images from plan view (Henriet et al., 1988; Cartwright, 1994; Cartwright et al., 2003). The fault systems are confined to fine-grained rocks, in most cases with high content of smectite or biogenic silica represented as clays, that hold a set of chemical and physical properties influencing the behavior of sedimentary successions (Kloprogge et al., 1999; Cartwright et al., 2003; Stuevold et al., 2003; Sun et al., 2009). Sedimentary successions accommodating high clay ratios compact easily from additional overburden by decreasing voids within the clays, which can initiate lithification processes, such as cementation and diagenesis (Skempton, 1969).

Polygonal fault systems have been observed in sedimentary basins on passive margins and cratonic basins, but not in active margins (Dewhurst et al., 1999; Watterson et al., 2000; Stuevold et al., 2003; Cartwright, 2011). Global studies on polygonal faults have been conducted by Lonergan et al. (1998), Dewhurst et al. (1999), Clausen et al. (1999), Watterson et al. (2000), Stuevold et al. (2003), Cartwright et al. (2003), Sun et al. (2009), Laurent et al. (2012), and Wrona et al. (2017), where the studies found that polygonal faults are distributed on the basin floor, along the slope, and at the basin flank in a sedimentary basin. In addition, has extensive polygonal fault systems on the Norwegian continental shelf been studied by a set of authors in areas of the northern North Sea (Cartwright & Dewhurst, 1998; Clausen et al., 1999; Wrona et al., 2017), Central North Sea basin (Dewhurst et al., 1999), Møre Basin (Stuevold et al., 2003), and Vøring Basin (Laurent et al., 2012), where vertical variations of polygonal fault systems are commonly discussed. Stuevold et al. (2003) argued that the observed vertical variation of polygonal faults is related to lithological variations within restricted sequences. The polygonal faults in the northern North Sea are observed in the sediments of the Cenozoic period and has been considered to initiate in the successions of Eocene-Early Oligocene and reactive in Late Oligocene-Mid-Miocene (Cartwright & Dewhurst, 1998; Clausen et al., 1999; Wrona et al., 2017).

While a lot of work has been done to map the occurrences of polygonal faults concerning lithology, basinal setting, and characteristics, significant knowledge gaps exist concerning what processes led to these observations. The formation of polygonal fault systems is crucial to fully understand the interaction of deformational structures and basin evolution. Polygonal faults display a wide range of geometries, fault patterns, lithologies, and distribution, where numerous potential trigger mechanisms have been proposed: (1) density inversion by differential compaction of a denser viscous fluid overlying a less dense viscous fluid (Henriet et al., 1988), (2) gravitational sliding driven by gravity processes (Higgs & McClay, 1993), (3) syneresis generating a spontaneous contraction of marine clay driven by electrochemical forces (Dewhurst et al., 1999), (4) gravitational loading by a low coefficient of friction when sediment failure occurs under vertical loading (Goult, 2001, 2002), and (5) particle dissolution, driven by temperature, pressure, and mineralogy, leading to a contraction-driven shear failure (Cartwright, 2011).

Clausen et al. (1999) investigated Oligocene polygonal faults at the Horda Platform and found a close link between polygonal faults and sediment loading. The mechanisms driving sediment loading are density inversion, where there is a compactional state of underlying fine-grained sediments, where a similar relationship was suggested by Cartwright et al. (2003) that reviewed suggested trigger mechanisms. Arguments by Dewhurst et al. (1999) proposed syneresis as a mechanism for the formation of polygonal faults based on three-dimensional extraction from smectite-rich gels through attractive forces between clay particles in seawater. They further argued that syneresis was valid for compaction and faulting as gravity processes and tectonic events. Cartwright (2011) argued that particle dissolution can explain changes in nucleation and growth of shear fractures and that the process of diagenesis can trigger shear failure. Wrona et al. (2017) investigated polygonal faults in the North Horda Platform and argued that fault growth likely was triggered by a low coefficient of friction and gravitational loading. They rejected a gravity-driven mechanism based on the uniform strike distribution of the polygonal faults. Previous studies have mainly investigated individual locations and stratigraphic levels. A comparison between sets of stratigraphic levels and locations within a basin seems to be less investigated in the North Sea and globally. Hopefully, a better understanding of the spatial variation of polygonal fault systems can provide new supporting information about the trigger mechanisms of polygonal faults.

This study examines the seismic signatures of polygonal faults in the Cenozoic succession of the northern North Sea by analyzing seismic data to improve the understanding of the Cenozoic sediments. Interpretation of significant sequence boundaries was conducted to get an increased understanding of the depositional history of the sedimentary basin. The seismic signatures display a range of patterns and behaviors of the fault systems. Mapping of the polygonal faults' various distribution within the basin at stratigraphic levels has been conducted to improve the understanding of differences between diverse stratigraphic levels and basin locations. An investigation of the geometry and physical properties of polygonal faults has been done to comprehend fault plane geometries and sites of maximum displacements fully. The lithology of clays has been the main factor forming polygonal faults in the sedimentary basin. The anisotropic strike displayed by the polygonal fault systems display has been investigated to examine correlations of visible orientation trends, which is interesting as it gives an insight into whether the trends are related to geological processes or random distribution. The seismic interpretation and topological analysis done in this study have improved the understanding of the polygonal fault systems, which have further been used to give a suggested polygonal fault classification and proposed trigger mechanisms for the classes.

2. Geological background

This thesis's main objective is the polygonal faults situated in the Cenozoic successions in the sedimentary basin of the northern North Sea. Since the polygonal fault systems are most prominent in the Cenozoic sequences, the Pre-Cenozoic geology of the area will be discussed briefly. A further detailed description of the Cenozoic will follow as this the main time interval considered in this study.

2.1 Pre-Cenozoic

The North Sea sedimentary basin has been affected by a complex geological evolution since the Cambrian time, including phases of extension, which established a low relief through subsidence and thermal cooling (Ziegler, 1975; Færseth, 1996). The architecture and signature of the basin expose dominant extensional structures of normal faults and grabens (figure 2-1A).

The most comprehensive event occurring in the Pre-Cenozoic was the formation of the Caledonian orogeny, which was formed due to the collision of Laurentia and Baltica in the Late Silurian–Early Devonian (Ziegler, 1975; Glennie, 2009). The collision led to the merging of the North American–Greenland plate (Laurentia) and the Northwest European plate (Baltica) along the Caledonian fold belt, which led to the formation of a crystalline basement in the North Sea, containing intrusive and metamorphic rocks of Caledonian age (Fossen et al., 2017). The closure of the Iapetus ocean led to the collapse of the Caledonian orogeny due to a change in the tectonic regime, where the previous compressional regime was substituted by an extensional regime (Ziegler, 1975). The extensional regime influenced a long-term continental lithospheric extension that involved polyphase stretching and thermal cooling, that led to complex extension events in the Late Permian–Triassic, Late Jurassic–Early Cretaceous, and Middle Cretaceous (Nottvedt et al., 1995; Nøttvedt, 2000). The numerous rifting events resulted in the North Sea rift system, a paleorift system that includes Viking and Sogn graben. Viking graben formed as a central graben structure from the rifting event in the Late Permian–Early Triassic and are situated extended upper crust, bounded by the Norwegian mainland to the east and Shetland Platform to the west (Nottvedt et al., 1995; Fazlikhani et al., 2017).

The characteristic graben structures formed in the North Sea became important depocenters for the accumulation of sediments, which later developed into significant petroleum sources and reservoirs (figure 2-1A). Dypvik (1983) described the sediments deposited in the graben

structures during the Mesozoic. The Triassic deposits are comprised mainly of beds consisting of continental sandstones of interbedded with shale intervals, representing the Hegre Group (Hesthammer & Fossen, 1999). After the Late Permian-Triassic rifting episode, the thermal subsidence of the whole area continued, which resulted in a gradual transgression. Thus, the depositional environment changed the strictly continental (Hegre Group) to shallow marine environment, and the Statfjord Group marks this change. Statfjord Group is mainly comprised of the fluvial sandstones interbedded with shales that progressively become more marine (Goldsmith et al., 2003). As the area became progressively submerged, the Dunlin Group shales were deposited. However, the Middle Jurassic, doming of the North Sea has resulted in the deposition of the thick progradational sequences (Husmo et al., 2003). The sandstones of the Middle Jurassic age coincide with the Brent Group, which exhibits the highest hydrocarbon-bearing level in the northern North Sea (Helland-Hansen et al., 1992). The initiation of the Late Jurassic rifting has diminished the importance of the North Sea dome, which had two effects on the petroleum play in the northern North Sea. First, rotation of the fault blocks has given the area its final structural architecture. Secondly, this has caused a transgression in the area (Fraser et al., 2003). The sediments deposited in the Late Jurassic are made of the clays deposited in an anaerobic marine environment which is the primary source rock of petroleum in the North Sea. Cretaceous sediments hold deposits of clastic sources from marine environments in the northern areas and chalk sediments as hemipelagic composition in the southern regions. Rifting gradually ceased during the early Cretaceous, starting a period of thermal subsidence (Copestake et al., 2003; Surlyk et al., 2003).

The previously described sediments have become important hydrocarbon sources, reservoir rocks, and seal rocks within the graben structures, where the primary hydrocarbon source are the Upper Jurassic shales and coals (Ziegler, 1975; Dypvik, 1983; Isaksen, 2004). The Triassic-Middle Jurassic reservoirs are represented by the shoreface, gravity flow, and fluvial sandstone deposits. The main top of the Mesozoic reservoir contains shales and marls from the Upper Jurassic-Cretaceous. In summary, the Caledonian orogeny and the extensional post-Caledonian events have led to prominent modifications and variations in structural architecture, sediment supply, and accommodation space in the sedimentary basin of the North Sea (Nottvedt et al., 1995; Ravnås et al., 2000).

2.2 The Cenozoic

The Cenozoic era was a relatively tectonic passive period, compared to earlier post-Caledonian times, as the rift phase moved further west (Isaksen & Tonstad, 1989). The period was affected by passive subsidence from the Cretaceous period resulting in rifting and opening the Atlantic Ocean. Evidence of several stages of flank uplift and subsidence is a passive impact resulting from the Atlantic Ocean opening, in addition to the development of a wide area with low relief, suitable for the deposition of sediments (Faleide et al., 2002).

The low relief contains thick, massive Cenozoic sediment packages holding the Rogaland, Hordaland, and Nordland Group (figure 2-1) (Isaksen & Tonstad, 1989; Jordt et al., 1995). In the early Cenozoic, the beginning of the Paleogene, the regions of the Shetland Platform and mainland Norway became uplifted from volcanic activity, which shaped an important depocenter and source area for clastic sources for the remaining time of the Cenozoic (figure 2-1) (Ziegler, 1975; Jordt et al., 2000; Løseth et al., 2003).

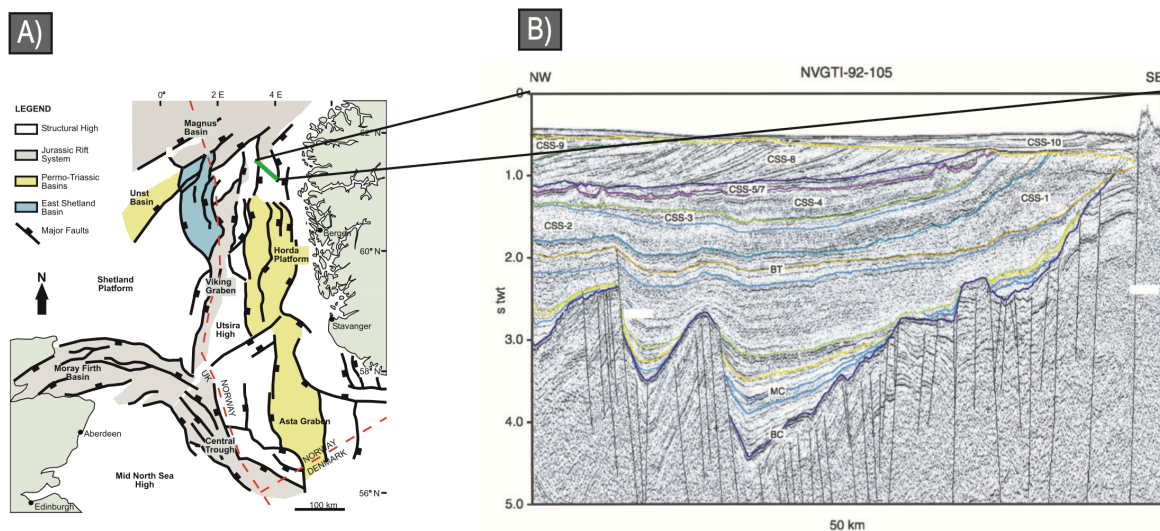


Figure 2-1: A) Structural overview map modified of Dominguez (2017) and Færseth (1996), displaying the dominant structural features and highs of normal faults in the North, B) NVGTI-92-105 Regional seismic line retrieved from Faleide et al. (2002) displaying sedimentary sequences deposited above Base Cretaceous. BT marks Base Tertiary, MS marks Mid-Cretaceous, and BC marks Base Cretaceous. Cenozoic sequences overlying BT are marked as CSS, a sequence stratigraphic framework introduced in chapter 4.

Paleocene

An acceleration in tectonic subsidence initiated an uplift of surrounding areas in the Paleocene resulting from a magmatic plume arriving from Iceland, which led to an increase in sediment supply due to erosion (Faleide et al., 2002). Two main depocenters of Viking Graben and outside Sognefjord were identified from the period's sediment distribution (Jordt et al., 1995). Increased sediment supply fed into the sedimentary basin resulted from flank uplift and an increased relief influencing sandy clinoforms to prograde from the East Shetland Platform and southern Norway (Faleide et al., 2002). Thickness variations of sediments display more prominent sediments along the continental margin than in the basin center, and biostratigraphic data show deepest areas of the period indicating a roughly 800 m deep sea-level, suggesting shallow marine conditions along the margin in the east and west (Jordt et al., 1995). In the Late Paleocene, a transgression resulted in a relatively deep sea-level that marks the Late Paleocene-Early Eocene transition, resulting in an aggradational stacking pattern and even sediment thickness (Faleide et al., 2002). However, ash-fall deposits interrupt the sedimentation in the period, which laid a foundation for the Balder formation, resulting from volcanic activity in combination with active rifting (Isaksen & Tonstad, 1989; Løseth et al., 2003). The volcanic deposits lay the foundation of smectite-rich sediments of the Hordaland Group.

Eocene

The Late Paleocene-Early Eocene transition is characterized by a hiatus, most pronounced along the basin flanks (Faleide et al., 2002). The Eocene period is characterized by relatively deep-water levels, associated with slope to basin-floor setting displaying traces of sand alternations and thin clay intervals (Martinsen et al., 1999). The sand alternations are recognized as the Frigg sand, consisting of thick, immature sand with thin intervals of clay and siltstone, resulting from submarine fan deposited in deep marine conditions in the Early Eocene (Jordt et al., 1995; Faleide et al., 2002). The mudrocks deposited in Eocene are characterized by a high smectite content caused by alternations of volcanic ash, which originated from volcanism due to the opening of the Atlantic ocean in the Mid-Eocene (Jordt et al., 1995; Marcussen et al., 2009). Balder formation results from deposits from volcanic activity and consists of interbedded layers of shale and tuff (Faleide et al., 2002). Sediment deposits from the Eocene display depocenters along Viking and Central Graben and are observed to thin eastward, which is proposed to be deposited from the uplifted East Shetland Platform. The sediments signature suggests deposition through gravity processes, resulting in turbidity

currents in deep water (Faleide et al., 2002). The areas along the Horda Platform display traces of regional thinning related to the topography of Scandinavia, acting as a limit for sufficient sediment supply of clastic material and could be a barrier for the progradation of sediments to the east (Jordt et al., 1995). A relative sea-level fall or uplift event during Late Eocene influenced a delta system to prograde into the basin from the west, characterized as the Grid sand (Isaksen & Tonstad, 1989; Faleide et al., 2002).

Oligocene

The Oligocene successions are dominated by mudrocks and shale, with a high smectite content, equivalent to underlying sequences of the Eocene age (Isaksen & Tonstad, 1989). A significant sand deposit emerged in the Early Oligocene, likely from a sandy gravity flow deposited in the Statfjord-Tampen, constrained to the easternmost basin margin (Martinsen et al., 1999). The sand influx resulted from a significant uplift and erosion of the Shetland Platform, which caused erosion of softer, underlying sediments (figure 2-2) (Rundberg & Eidvin, 2005). The sediments of the Early Oligocene age are disturbed through sediment remobilization that causes thickness and local variations within successions, thus is the lowermost boundary of the Oligocene nearly unaffected (Jordt et al., 1995). Intra Oligocene marks a boundary representing a eustatic sea-level fall, named the Mid-Oligocene sea-level fall (Jordt et al., 1995). A sea-level rise followed where sediments deposited show a well-defined outbuilding pattern from the East Shetland Platform, exhibiting a wedge-shaped geometry, thinning out towards the west with a progradational to aggradational stacking pattern (figure 2-2) (Jordt et al., 1995; Faleide et al., 2002; Marcussen et al., 2009). Skade formation was deposited in the Late Oligocene linked to sandy inputs from a low sea-level and are limited to the upper Oligocene sediments, onlapping onto an underlying Oligocene wedge unit Isaksen and Tonstad (1989); (Martinsen et al., 1999). An evident change in basin configuration occurred in the Oligocene period. The thickest Oligocene deposits are situated north of the Viking Graben and display a clear north–south trend, displaying thinning at the basin flanks at east and west (Faleide et al., 2002).

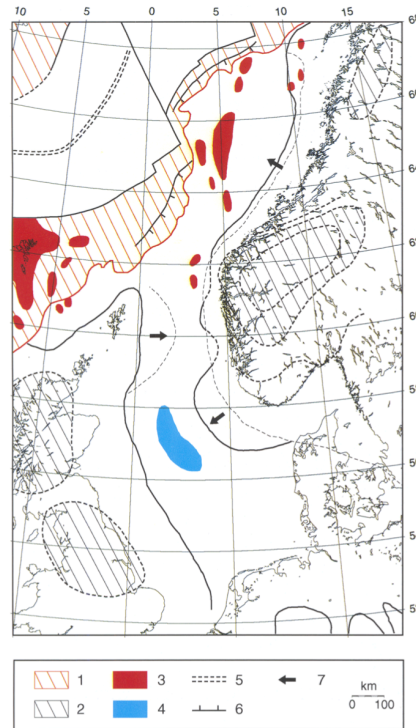


Figure 2-2: Overview map retrieved from Faleide et al. (2002) displaying the regional setting in the Early Oligocene. 2) Mark areas of uplift, 3) mark intrabasinal highs, 4) mark main depocenter, and 7) mark outbuilding directions.

Miocene

The Early Miocene is characterized by a hiatus that led to erosion of underlying Oligocene successions (Faleide et al., 2002). The Miocene sediments were deposited under a relatively shallow sea-level, resulting in a shallow marine basin, where depocenters were located south of 60 ° N, thinning and absent further north (Faleide et al., 2002). The high smectite content of mudrocks is a common denominator for the Early Miocene sediments and the previous sediments of the Hordaland Group. The high smectite content can cause variations in pore pressure, velocities, and densities (Marcussen et al., 2009). Mid-Miocene is characterized by the Mid-Miocene unconformity resulting from a sea-level fall due to glacio-eustatic changes that influenced a regional uplift (Jordt et al., 2000; Faleide et al., 2002; Løseth et al., 2003). The Mid-Miocene unconformity is prominent in the eastern margin of the northern North Sea and represents a break in sediment supply. Sediments deposited above the unconformity display coarse-grained lithologies of the Utsira sand, deposited under shallow marine conditions (Martinsen et al., 1999; Faleide et al., 2002). The Utsira formation act as a fill above the undulating topography of the Oligocene sediments and is located above the unconformity. Below the unconformity is underlain the mudrocks of the Hordaland Group, which exhibits

high-smectite content, sediment remobilization, and polygonal faults (Martinsen et al., 1999; Løseth et al., 2003; Zweigel et al., 2004).

Pliocene and Pleistocene

The Pliocene and Pleistocene age sediments contain mostly glacial sediments originating from the mainland of Norway, resulting from post-glacial uplift (Isaksen & Tonstad, 1989; Faleide et al., 2002; Løseth et al., 2003). The sediments from the period exhibit westward prograding clinoforms downlapping onto underlying Utsira formation, displaying a stacking pattern that expresses dominant sediment transport from the margin of Norway (figure 2-3) (Martinsen et al., 1999; Faleide et al., 2002). The outbuilding pattern indicates uplift and changes in the relative sea-level, influencing the accommodation space in the basin. The Pliocene and Pleistocene sediments are proposed as marine mudstones coarsening upwards into a more immature, glacially influenced sand (Jordt et al., 1995; Marcussen et al., 2009). The sediments of this period are related to high erosion rates associated with a colder climate, where boulder clay, moraines, and out-washed sands are the primary sediment source in the given period (Isaksen & Tonstad, 1989; Jordt et al., 2000; Thyberg et al., 2000; Faleide et al., 2002).

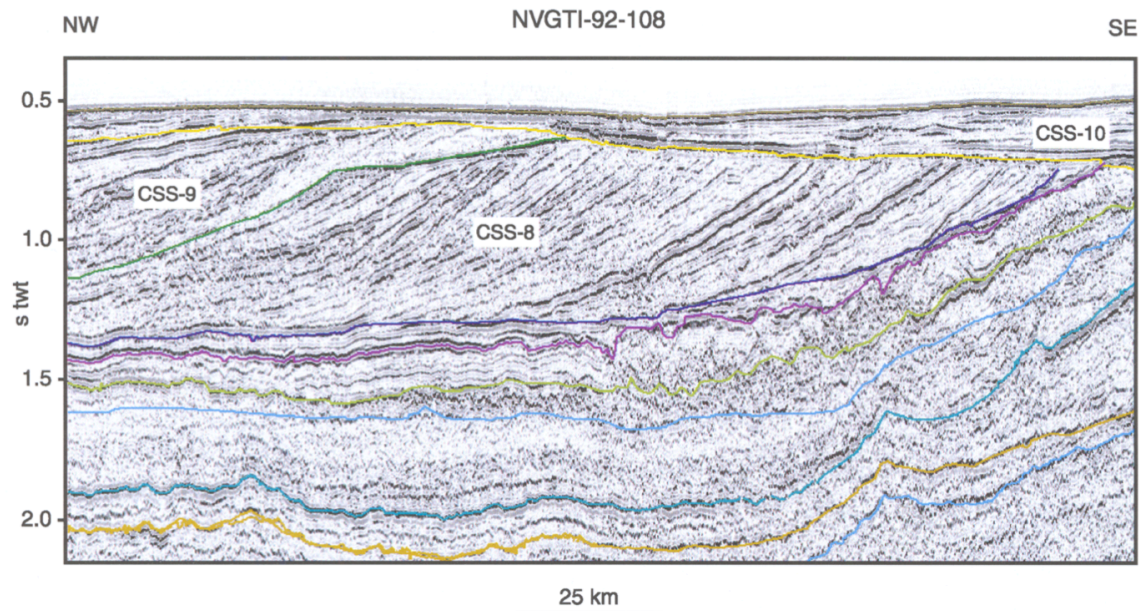


Figure 2-3: NVGTI-92-108 Regional seismic line retrieved from Faleide et al. (2002). The seismic line display outbuilding of prograding sequences above the Mid-Miocene unconformity and deposition from mainland Norway. Sequences are marked as CSS, which is a sequence stratigraphic framework introduced in chapter 4.

2.2.1 Summary of the lithology of Cenozoic sediments

The previously described outline of the Cenozoic illustrates significant variations in lithologies and tectonic activity. The successions covering the Hordaland Group hold lithologies of mudrock with high smectite content where several sandy influxes are identified (figure 2-4). The sandy units are generally fed into the basin from the flanks during uplift from submarine channels. In Paleocene, an uplift, caused by a magmatic plume, led to an increase in sediment supply and sand influxes combined with deposits of Balder, Sele, Lista, and Våle formations (Isaksen & Tonstad, 1989). Due to the rise of a magmatic plume, the mudstones of Paleocene to Lower Eocene age contain a high content of smectite-rich clay (Thyberg et al., 2000). Increasing velocities from well data can reflect a diagenetic change from smectite to illite and quartz (Marcussen et al., 2009). In Eocene, East Shetland Platform's uplift led to development of submarine fans and deposition of the Frigg and Grid sands through gravity flow (Isaksen & Tonstad, 1989). The Eocene sediments especially high smectite content, are caused by volcanic ash alternations and can vary laterally within the sediments due to pore pressure variations (Thyberg et al., 2000; Marcussen et al., 2009). The deposits of the Eocene age are several hundred meters thick and contain the erosion of soft, underlying sediments. Authors agree on less dense mudrocks and the highest smectite content of Eocene and Oligocene sediments of any mudrocks in the Cenozoic (Thyberg et al., 2000; Marcussen et al., 2009; Hermanrud & Undertun, 2019). The Utsira formation is the last significant sand input into the basin in the Cenozoic period, due to uplift from glacio-eustatic changes in Late Miocene (Faleide et al., 2002). The relatively calm, predictable periods covering the Cenozoic are Pliocene and Pleistocene, mainly affected by post-glacial uplift with coarse-grained clays (Isaksen & Tonstad, 1989). The coarse-grained clays of Pliocene and Pleistocene age contain immature mineralogy (Thyberg et al., 2000).

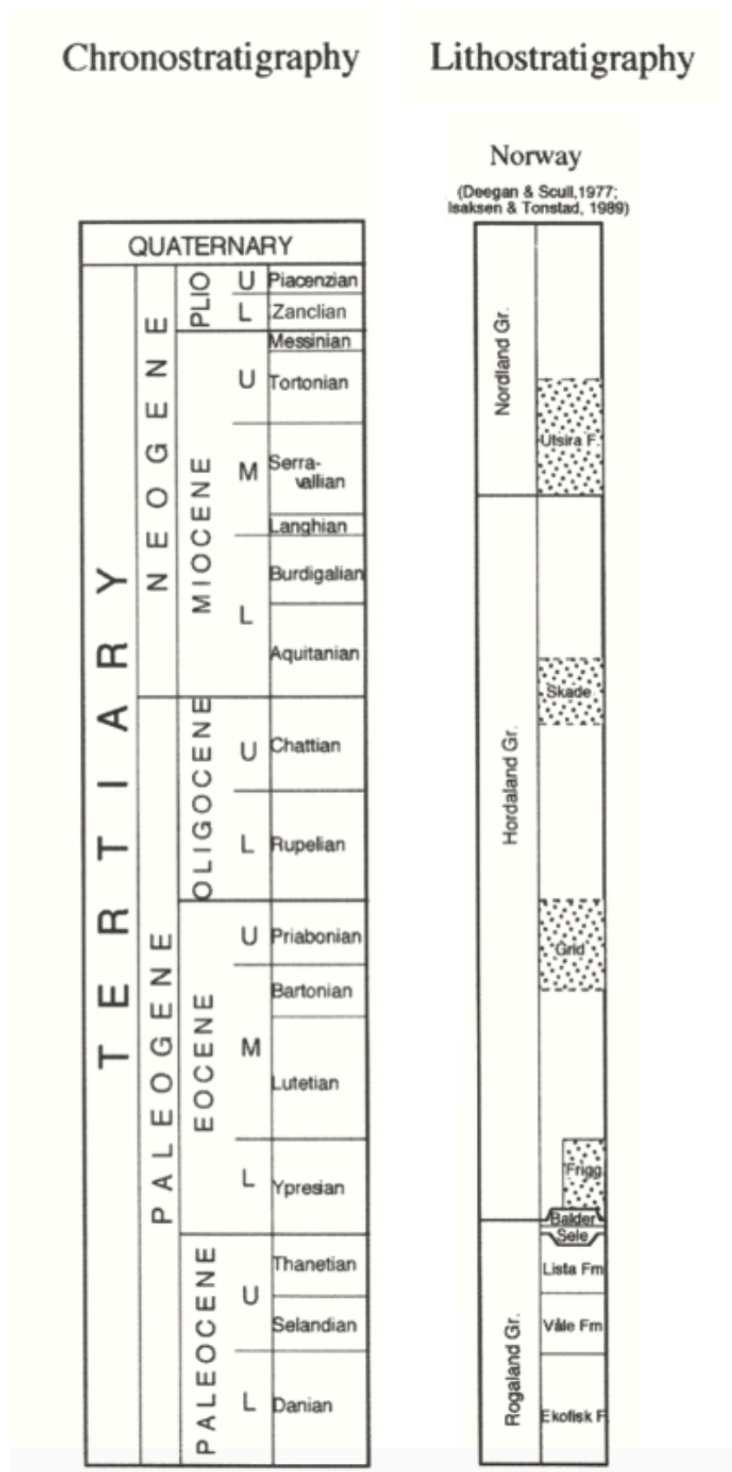


Figure 2-4: Chronostratigraphic and lithostratigraphic columns from the period of Cenozoic modified of Jordt et al. (2000). The lithostratigraphic column display key formations deposited during the Cenozoic.

3. Theoretical background

This chapter aims to give a brief overview of processes and terminology relevant for data collection and discussion of polygonal faults, which are commonly referred to in this study.

3.1 Polygonal faults

This section reviews the knowledge of basinal settings favorable for polygonal fault development, lithology facies relevant for formation, and potential trigger mechanisms. It also includes a description of diagenesis in the Cenozoic sediments and polygonal fault geometries, and seismic identification.

A polygonal pattern is not only restricted to marine geological processes and can develop from desiccation cracks and permafrost thawing (Dewhurst et al., 1999; NASA, 2021). The observation of polygonal patterned cracks formed from thawing of permafrost results from contraction (figure 3-1B). As permafrost melts, remaining ice comprises a lower density than the melted water that forms an active dense layer and generates contraction of the ice and forms polygonal patterned cracks (figure 3-1A) (NASA, 2021). Permafrost polygonal cracks and desiccation cracks are associated with a subaerial process. In addition to these processes are the pattern observed to form under the water column by contraction and shrinkage of water-filled clays, resulting in polygonal faults (Dewhurst et al., 1999).

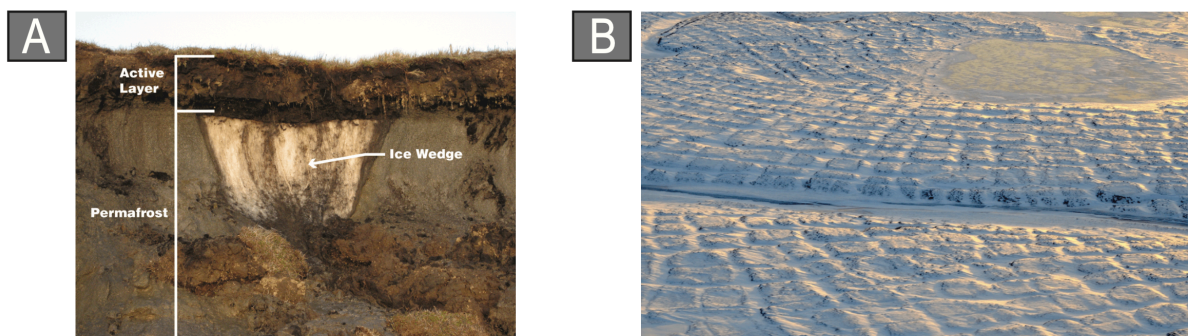


Figure 3-1: A) Cross-section display frozen soil in arctic environments, and how the interaction of an active layer of meltwater on top of the frozen soil form a distinct wedge shape, B) polygonal patterned cracks developed from thawing of permafrost in the Arctic. A distinct polygonal pattern is displayed from plan view. Lack of scale from images modified of Nasa (2021).

3.1.1 Occurrence

Polygonal faults are restricted to sedimentary basins on passive margins and cratonic basins and are broadly studied through 2D and 3D seismic. The fault systems are closely related to fine-grained sedimentary successions and cover areas of $>1.000.000 \text{ km}^2$ in a total of over 200 sedimentary basins (figure 3-2) (Cartwright & Dewhurst, 1998; Dewhurst et al., 1999; Stuevold et al., 2003; Davies & Ireland, 2011). The polygonal fault systems are rarely observed in coarse-grained sedimentary successions worldwide but have been observed in coarse-grained successions, with interbedded fine-grained sediment intervals (Cartwright et al., 2003).

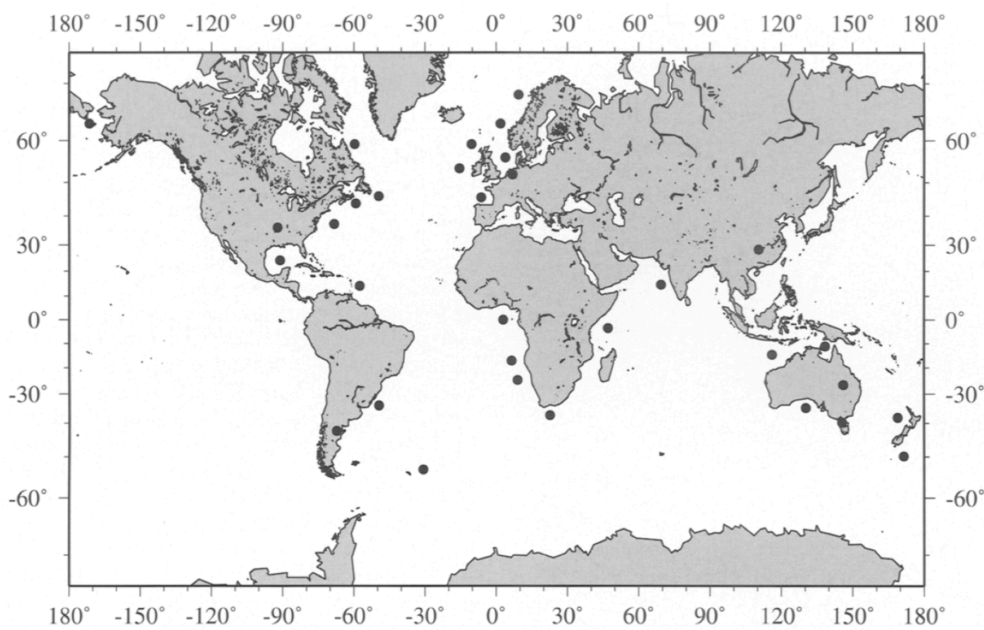


Figure 3-2: The global distribution of polygonal fault system, marked as black dots, as recognized from seismic data. The polygonal fault systems are located at passive margins or cratonic basins. The global distribution map is retrieved from Cartwright et al. (2003).

Polygonal faults form evenly distributed within restricted sedimentary basins and are discovered at the basin center, slope, and flank settings (Dewhurst et al., 1999; Lonergan & Cartwright, 1999). In the northern North Sea are the polygonal faults mainly situated in the Early Eocene to Mid-Miocene sediments, deposited in deep marine environments. From the studies of Cartwright et al. (2003), they emphasized how important it is not to make any judgments on the polygonality of the faults on a small area, which will not be correct due to broadly occurrence and varied geometry.

3.1.2 Lithologies

Polygonal faults develop in clay lithologies with high smectite or biogenic silica contents and have been exposed from partly drilled successions of the Ormen Lange field (Cartwright et al., 2003; Stuevold et al., 2003). Biogen silica is amorphous silica (opal A), one of the most abundant siliceous sediments in the deep sea, produced by planktonic organisms (Ireland et al., 2011). Smectite is the most mentioned sediment in combination with polygonal faults in the North Sea. It is related to its non-thermodynamically stable state in soils and sediments in ambient conditions, in addition to half the strength as of other clays at given stress levels (Wang & Schmugge, 1980; Kloprogge et al., 1999). The lithology of smectite is structured with layers of polymeric sheets of SiO_4 tetrahedra, resulting in extremely fine-grained sediments with low permeability, that compact very slowly (Thyberg et al., 2000). The high smectite content of clays originates from volcanic ash as an erosional product (Vrolijk, 1990; Løseth et al., 2003).

The polygonal faults of the Early Eocene-Mid-Miocene sediments exhibit successions of clays with a high smectite content that has contributed significantly to the depositional of the periods (Dewhurst et al., 1999; Thyberg et al., 2000; Marcussen et al., 2009; Wrona et al., 2017). The high smectite content originated from volcanic ash transported from Iceland to the North Atlantic during the period (Dewhurst et al., 1999; Løseth et al., 2003).

3.1.3 Trigger mechanisms

The formation of polygonal faults is unclear, and authors debate several potential trigger mechanisms of polygonal fault systems. A trigger mechanism is a determinant factor for developing a polygonal fault system, in the sediment successions and basinal settings, polygonal faults favor. Cartwright et al. (2003) and Sun et al. (2009) listed suggested trigger mechanisms for developing of the polygonal fault systems. Based on the broad distribution and pattern of the faults, multiple trigger mechanisms can be reliable. A rejected trigger mechanism is tectonic activity because of anisotropic orientation, combined with low displacement (<100 m) of faults. However, tectonic imprints are suggested to possibly affect polygonal faults with a slightly preferred orientation (Sun et al., 2009; Wrona et al., 2017). A review of suggested trigger mechanisms of polygonal faults is listed below.

Density inversion

Density inversion is the process of compaction between two viscous fluids in an arrangement where the dense fluid is overlying the less dense fluid (Henriet et al., 1988; Cartwright, 1994; Watterson et al., 2000; Wrona et al., 2017). The arrangement generates a state where the less dense fluid moves upward, and the dense fluid will sink to the base (Henriet et al., 1988).

Water-filled clays can behave as viscous fluids and be affected by the process of density inversion. They can be influenced by a compactional state resulted from the loading of denser sediments upon which the underlying clays lose porosity. Dewatering results from compaction where water between grains is released from the underlying sediments (figure 3-3) (Sun et al., 2009). The compactional state generated by density inversion is argued to easily disrupt clay successions with an increased pore pressure (Henriet et al., 1988).

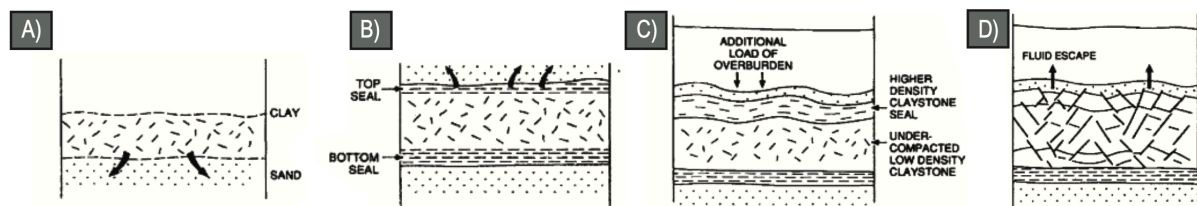


Figure 3-3: A step-by-step model displaying Taylor-Rayleigh instabilities in clays, modified of Cartwright (2003) and Henriet et al. (1989). **A)** deposition of clays, **B)** overpressure build-up from additional sediment load, forming top and bottom seals, **C)** additional load generate density inversion folds of the strata, and finally **D)** fluid escape and faulting from pore pressure collapse.

Density inversion is related to the concept of Rayleigh-Taylor instabilities, that is a process that occurs at an unstable interface, developing sinusoidal instabilities and upwelled pattern, where structures are spread into overlying sediments, generating a failure in host succession (figure 3-3) (Henriet et al., 1988). The result of Rayleigh-Taylor instabilities are anticlinal, and synclinal folds are acting as density inversion folds and upward fault growth because of fluid escape (Watterson et al., 2000). Polygonal faults are proposed to form from a viscous drag under a mobile clay unit, combined with Andersonian faults and collapse structures. Andersonian faults clarify stress regimes and quantitative parameters as the shape and orientation of faults (Simpson, 1997). Density inversion combined with gravitational instabilities is an essential

contributor to the formation of polygonal faults (Henriet et al., 1988). Anticlinal and synclinal folds appear as graben/horst structures between polygonal faults in seismic cross-sections, related to density inversion (Watterson et al., 2000). As suggested in studies done by Henriet et al. (1988), this relationship should be more or less universal. Cartwright et al. (2003) discussed the weaknesses of the density inversion model, and if it is applicable, the relationship between polygonal faults and density inversion folds should be universal. Polygonal faults display deformational fold structures in some areas; still, the folds are far from well represented in all polygonal fault systems. The lack of density inversion folds the model requires is seen as a significant weakness.

Gravitational sliding

Gravity processes downslope provide necessary conditions for extension and initiate extensional faulting (Higgs & McClay, 1993; Clausen et al., 1999; Cartwright et al., 2003). An analog sandbox experiment demonstrates extensional faulting, where a sliding box filled with altering colored sand reflects an anisotropic model (Higgs & McClay, 1993). The experiment demonstrated a non-rigid block rotation and extensional faults associated with gravity collapse by moving the box relative to a static end wall. The analog sandbox model can be compared to fault development on the basin slope and results in a uniform dip towards the shelf, which is an anticipated from fault development downslope (Cartwright et al., 2003). Additional results from the sandbox model experiment of Higgs and McClay (1993) reveal a transition from planar fault planes to gently listric with increased extension. Similar sandbox experiments have been conducted by Ellis and Dryden (1987) and Vendeville et al. (1987), which based their models on extension from tilting. The outcome clarified a uniform dip direction of the faults.

Sediments located in slope settings could, in addition to gravity, be triggered by the resistance of the downslope displayed by a basal detachment, which is crucial at the base for isolation of sliding (Hesthammer & Fossen, 1999; Cartwright et al., 2003; Fossen, 2016). A basal detachment acts as a separation of a faulted sequence from a non-faulted sequence and preserves faulted sequence. Cartwright et al. (2003) argued that the slope gradient might influence fault orientations based on gravitational forces of submarine fans, turbidites, or gravity flows. If this is the case, it is expected to observe a strong relationship between fault strikes running parallel to the slope. When exposed to a high extension of gravity sliding, fault blocks tend to rotate, and the degree of deformation within sediments tend to increase in the direction of sliding (Hesthammer & Fossen, 1999; Fossen, 2016). Submarine slides resulting from sliding and mass

transport deposits (MTD), displaying characteristics of blocks. The geometry of blocks fit well as a jigsaw puzzle and display traces of bidirectional sliding, which might be influenced by tilting and rejuvenation (Cox et al., 2020). Another suggestion for visible orientation trends is the propagation of faults in underlying sediments. However, as the polygonal faults are distributed with a wide range of orientations, not only restricted to slope settings, but gravitational sliding is also most likely not the only controlling factor for polygonal fault development.

Syneresis

Syneresis is a chemical reaction influenced by the sediment's colloidal nature that initiates a sudden imbalance of molecules as a liquid is extracted (Walstra, 1993; Dewhurst et al., 1999). Syneresis is a suggested trigger mechanism for polygonal faults in smectite-rich marine clays during early compaction (Dewhurst et al., 1999). The lithology of marine clays holds a high ratio of salt minerals, which is an essential element in the process of syneresis as liquids are extracted from seawater, acting as an electrochemical force (White, 1961; Cartwright & Dewhurst, 1998). The salt concentrations of the clays are essential as it generates several structures through flocculation, shrinkage, and clay breakage. Structures that occur are among syneresis cracks, craters, fissures, and mounds. Fractures have been documented to form in clays under the conditions of syneresis in the North Sea, with electrochemical environment and marine clay mineralogy as the two most important factors influencing the process (White, 1961; Dewhurst et al., 1999).

The mechanism of syneresis describes pore fluids escaping from a clay-water system, and a realignment and new bonds form within the clay. Dewhurst et al. (1999) argued how syneresis results in extensional structures as an outcome of contraction, similarly, as previously described polygonal cracks originating desiccation and ice melting (section 3.1). Faults form by syneresis display inconsistent fault displacement linked to physical property variations within sediments. A general link between syneresis and grain size explains the vertical and lateral variation of polygonal fault distribution (Walstra, 1993; Dewhurst et al., 1999; Cartwright et al., 2003). Syneresis is proposed to generate planar faults to form at shallow depths (<100 m) in close communication with the electrochemical force of seawater, where listric faults form at deeper depths (Dewhurst et al., 1999).

Goultly (2002) and Cartwright et al. (2003) argued for weaknesses of the syneresis model. Syneresis is well recognized in chemical engineering but is poorly understood regarding polygonal fault formation in clays. Polygonal faults are known to develop in various marine clays. Still, the physical and chemical properties required for syneresis in clays are poorly documented. The main weakness of syneresis is that the fault systems are expected to be constrained to a specific marine clay and do not hold any seismic characteristics. However, as polygonal faults develop broadly in various marine clays, that may cause disruption and hinder of the syneresis process.

Gravitational loading

Gravitational loading is a mechanism of sediment failure generated by weak sediments that induce failure, instead of consolidation, from confined, vertical loading (Cartwright et al., 2003). Weak sediments exhibit low friction coefficients, resulting in fluidization and normal faults from an increased pore pressure when the in-situ stresses are too big to sustain (Jolly & Lonergan, 2002).

A low friction coefficient can be central to the growth and development of polygonal systems in clays. However, it cannot be the only contributor triggering the development of the faults as an additional mechanism for nucleation is needed (Goultly, 2008). An additional mechanism of volume reduction and shear stress support gravitational loading and triggering of polygonal faults. Goultly (2002) argued how syneresis and density inversion are potential mechanisms of polygonal fault formed under the condition of zero horizontal strain. Cartwright et al. (2003) argued how the confined weak sediments is affected by this mechanism are a potential weakness.

Particle dissolution

As a process of diagenesis, particle dissolution has been suggested as a formation mechanism of polygonal faults. Diagenesis is described as a chemical change in mineralogy linked to consolidation, where mineral dissolution describes a loss of granular volume in sediments potentially triggering polygonal fault formation (Shin et al., 2008; Cartwright, 2011).

Experimental work by Shin et al. (2008) demonstrated the importance of failure conditions in uncemented sediments under a deformational regime influenced by grain dissolution. The uncemented sediments performed in this experiment were volcanic ash. Cartwright (2011)

described that the experiment of Shin et al. (2008) was conducted to reconstruct a deformational regime. The configuration of the experiment contained instrumented oedometer, measuring strains and ratio of horizontal to vertical stresses. The stresses were measured from a uniaxial compression test. As the experiment ran, proportions of table salt and glass beads were combined to trigger particle dissolution. Cartwright (2011) summarized the key outcomes of the experiment. Contraction of particles can result in stresses at the macro scale, caused by a drop from the initial vertical effective stress to an active pressure condition, leading to failure. Failure caused by stress changes is called contraction-driven shear failure. Contraction-driven shear failure could result from gravitational stress and strictly relate to diagenetic processes. Potential diagenetic reactions that can result in contraction-driven shear failure are: 1) dissolution of detrital calcite/aragonite, 2) dissolution of minor amounts of cementing phase (calcite, opal, quartz), and 3) remineralization of organic matter (Shin et al., 2008). In the work of Davies and Ireland (2011), they argued how polygonal faults could be triggered and linked to the process of diagenesis. Cartwright (2011) argued that contraction and contraction-driven shear failure due to diagenesis could explain potential changes in nucleation and the growth of fractures. Based on this, the suggestion of diagenetically induced shear-failure is a valid candidate for a trigger mechanism of polygonal fault systems, argued by Cartwright (2011). The polygonal faults can be triggered by the potential reactions is listed above by Shin et al. (2008).

How reliable this mechanism is for the development of polygonal systems is further debated. Cartwright (2011) argued that polygonal systems are distributed in fine-grained successions, often found in chemically unstable clays (Kloprogge et al., 1999). The widely distributed polygonal fault systems can be affected by several reactions, where particle dissolution is a valid candidate. It exhibits physical property changes that can induce contraction-driven shear failure. Polygonal faulted areas from the North Sea are observed in areas of the opal transformation and areas with no knowledge of particle dissolution (Olobayo, 2015). In addition to this, it is hard to state particle dissolution from seismic images with a lack of mineralogy data or recognizable seismic characteristics. Based on this, polygonal faults may develop regardless of particle dissolution.

3.1.3 Diagenesis in the Cenozoic successions

Diagenetic processes of clay minerals are crucial to understand, as they determine the mechanical and chemical compaction of sediments (Bjørlykke, 1998). Opal A/CT and smectite/illite are two diagenetic processes central in the biogenic silica and smectite-rich clay successions in the study area. The chemical change of diagenesis leads to a transformation of grains within a rock and can occur at various temperatures, pressures, and chemical property gradients (Blatt, 1979; Higgins et al., 2018).

Opal transformation

The opal transformation is present as a diagenetic event in the study area and includes the transformation from biogenic silica (opal A) to crystalline silica (opal CT) to cryptocrystalline quartz (chert) (Kastner et al., 1977; Rundberg & Eidvin, 2005). The transformation is a maturation concept of biogenic silica, introduced by Bramlette (1946), where conversion rate depends on the host sediment's time, temperature, and composition, combined with the pore fluid (Ireland et al., 2011). At even higher temperatures and a greater burial depth, crystalline silica transforms to quartz.

The opal transformation results in increased density and reduced porosity at a narrow interval generating a diagenetic reflection event, revealing a large acoustic impedance contrast (Cartwright, 2011; Ireland et al., 2011; Hermanrud & Undertun, 2019). The diagenetic reflection event is observable through seismic cross-sections in narrow intervals of < 20 m, as a cross-cutting, flat positive polarity event (Lynne et al., 2005; Davies & Ireland, 2011). The porosity reduction is supported by Davies and Clark (2006) and is related to a dehydration reaction, causing rapid compaction resulting in shear fractures and faults with an additional overpressure mechanism of sediments buried at depths of 300-880 m reducing the sediments shear strength. An overpressure mechanism can lead to subsidence and circular depressions, which can assist the formation of polygonal faults (Davies et al., 2009). Similarly, Davies and Clark (2006) did observations where compaction from the transformation led to failure and fissured fault blocks. The sediment failures originate from expelled sediment fluids intruding the overburden stratigraphy, with approximately 200-400 m.

To summarize, the critical factors of failure from opal transformation are porosity reduction in the reaction front and lower shear strength of biogenic silica (Davies & Clark, 2006). The opal

transformation displays significant volume changes over narrow temperature intervals due to porosity reduction and fluidization, leading to shrinkage and potentially polygonal faulting (Davies & Clark, 2006; Cartwright, 2011).

Smectite transformation

An additional, noteworthy diagenetic process present in the sediments of the northern North Sea is the smectite transformation. As previously discussed in chapter 2, the Eocene and Oligocene sediments hold significant high smectite content lithologies. The high smectite content of sediments is a dominant factor for compaction, as it holds a large amount of water, generating a low matrix density when deposited, in addition to low permeability, high porosity, and high-water content (Marcussen et al., 2009; Hermanrud & Undertun, 2019).

Gibbs (1977) explained how composition and physical sorting of sediments by size change laterally. The responsible mechanisms behind this are related to relative sea-level and the system tracts for the lateral variations in clay compositions. Smectite and illite are clay minerals resulting from high stand periods, where kaolinite occurs close to the sediment source as a proximal facies (Thyberg et al., 2000). Smectite has low density, low permeability, and compact very slowly, in addition to the unique property of a high shrink-potential (Weaver, 1989; Thyberg et al., 2000).

Water is released during smectite diagenesis due to the dissolution of smectite and precipitation of illite and quartz, leading to 30% dewatering, generating a potential overpressure in clays (Burst, 1969; Środoń, 1999; Marcussen et al., 2009). The dissolution of smectite occurs at burial depths greater than 2000 m and temperatures above 60-80° and has been suggested to occur at a depth interval of several kilometers (Marcussen et al., 2009). As the transformation occurs within such a considerable depth interval, the smectite/illite transformation will not display any abrupt physical property changes visible from seismic reflection within the mudstones of the North Sea (Hermanrud & Undertun, 2019).

3.1.4 Geometries and seismic identification

Polygonal faults display a characteristic, recognizable pattern from seismic cross-sections and plan view, arranged in multidirectional polygonal networks (Dewhurst et al., 1999). Polygonal faults are commonly identified in constrained tiers, with coarse-grained units as detachments acting as correlateable stratigraphic units (Cartwright et al., 2003; Stuevold et al., 2003).

Constrained tiers can be represented by sequences that display distinct seismic signatures and geometries influenced by various strains.

Polygonal faults display a plan form pattern from plan view with a variable geometry of the faults of highly polygonal, curved to rectangular patterns with length scales of 2-3 km (figure 3-4) (Cartwright, 2011). The distinct plan form patterns display significant variations of the polygonal faults spacing, orientation, and intersection relationship. Cartwright (2011) suggested that the variations in plan form patterns of polygonal faults can result from topography, fault density, and tectonic context. However, are the various plan form patterns associated with the uniform strike polygonal faults display (Lonergan & Cartwright, 1999; Sun et al., 2009; Wrona et al., 2017). The plan form pattern is generally well-defined, with high amplitude reflections, but data quality and geological processes can decrease the visibility and pattern of the plan form patterns.

The variety of geometries and plan form patterns of polygonal faults is associated with lithology. However, as important as the lithology of the host rock is the lithology of the adjacent lateral tiers. The lithology of adjacent tiers can determine the propagation and growth of polygonal faults (Cartwright et al., 2003).

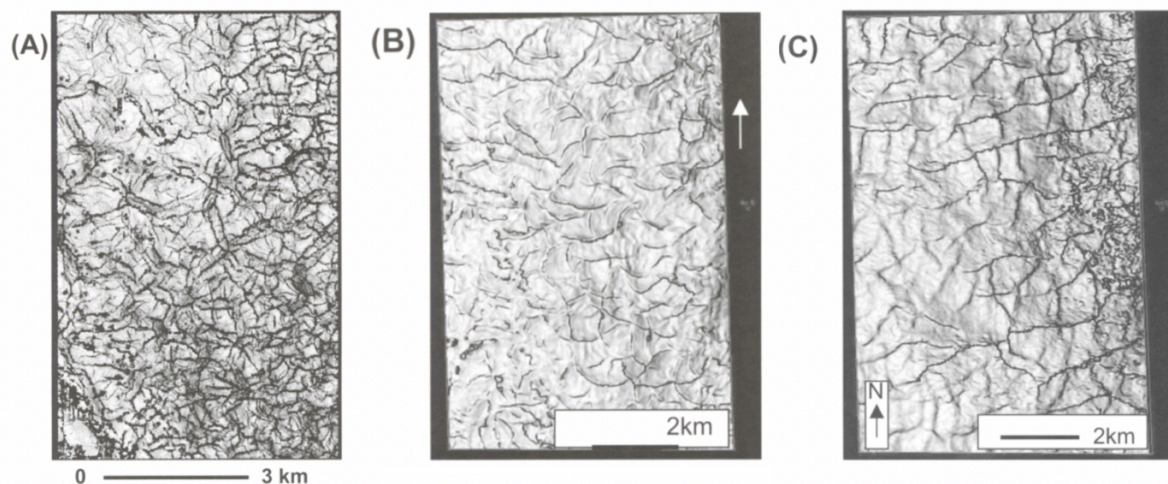


Figure 3-4: Variance attribute map displaying three types of various plan form patterns of polygonal fault systems in plan view. **A)** Highly polygonal plan form pattern, **B)** curved plan form pattern, and **C)** rectangular plan form pattern. Figure retrieved from Cartwright (2003).

3.2 Soft sediment remobilization

Soft sediment remobilization displaces unconsolidated sediments after deposition and creates common deformational structures as sand injections, mud volcanoes, pipes, pockmarks, and authigenic carbonates (Briedis et al., 2007; Huuse et al., 2010). The deformational structures involve various geometric expressions such as dikes, sills, flame structures, irregular networks, and water escape structures. Remobilized sediments displace sedimentary succession closely connected to slope instabilities resulting from slumping, sliding, and creep, which result in features ranging from centimeters to hundreds of meters and can significantly impact the sediment distribution in a reservoir (Lonergan et al., 2000).

The formation of soft sediment remobilization is generally an outcome of rapid overpressure. It requires a parent body (unconsolidated), an overpressure gradient, excess fluids, and a low-permeable seal (Hermanrud et al., 2019). Several potential trigger mechanisms are suggested, where Huuse et al. (2010) and Hurst et al. (2011) mention potential overpressure mechanisms by rapid loading, earthquake activity, tectonic stress, and rapid fluid migration.

The Oligocene sequences in the northern North Sea display evidence of soft sediment remobilization and are suggested influenced by rapid differential loading (Andresen & Clausen, 2014). A common deformational structure in the Oligocene sequences is sand injections resulting from overpressure of the source sand. The source sand is influenced by fluids from deeper successions that facilitated suitable conditions for sediment remobilization of sediments. The remobilized sediments from the Oligocene sediment are related to periods of flank uplift leading to disturbance and loading from additional sediment input (Hermanrud et al., 2019).

3.3 Network topology

Polygonal faults develop in networks, and topology is a method that can be applied to describe the characteristics and arrangement of fault networks (Nixon et al., 2012; Morley & Nixon, 2016; Duffy et al., 2017). The topology of fault networks describes the arrangement and geometrical relationships between the faults (Sanderson & Nixon, 2015). Polygonal faults are categorized as small-scale faults. To fully comprehend complex fault networks such as polygonal fault systems, knowledge of spatial variation, geometry (orientation, length), and topology (arrangement, connectivity) are central.

The topology of polygonal faults as a two-dimensional fracture network consists of a graph of nodes and branches between nodes (figure 3-5) (Sanderson & Nixon, 2015; Morley & Nixon, 2016; Duffy et al., 2017; Nixon et al., 2020). A node represents one point where faults intersect, splay, abut or terminate. Three types of nodes are recognized and are classified: I-nodes represent isolated tips, Y-nodes represent splays/abutments, and X-nodes represent crossing fractures. The classes of nodes display isolated nodes as I-nodes and connected nodes as Y- and X-nodes (Sanderson & Nixon, 2015). Therefore, the branches between the nodes can also be classified into three topological groups depending on their degree of connectivity: I-I branches represented by two I-nodes, I-C partly connected branches represented with one I-node, and one Y/X-node and C-C doubly connected branches represented by two Y/X-nodes (figure 3-5). The proportion of the different nodes and branches can be plotted in ternary diagrams, enlightening a relationship of faults in a network (Ortega & Marrett, 2000; Manzocchi, 2002; Sanderson & Nixon, 2015; Duffy et al., 2017; Nixon et al., 2020).

Topological data of polygonal faults in this thesis is crucial to characterizing different fault networks. The ability to separate networks into different nodes and branches quantifies their degree of connectivity, thus relating the geometry (length, orientation) with their connectivity which is essential for flow (Manzocchi, 2002; Sanderson & Nixon, 2015). How this was used in this thesis is further explained in the following chapter of data and methodology (chapter 4).

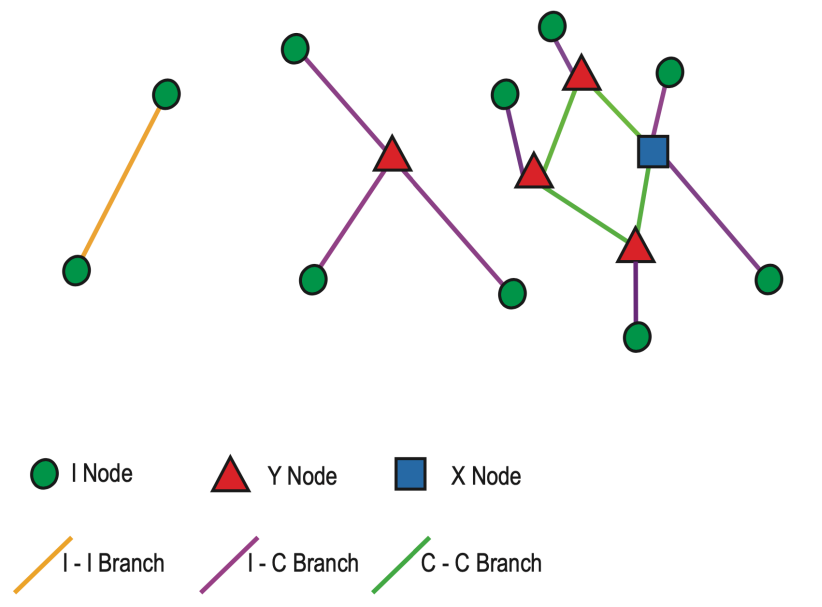


Figure 3-5: Simplified sketch of nodes and branches in a fracture network. Three types of nodes are represented by isolated (I-nodes) and connecting (Y- and X-nodes) nodes. Three types of branches are represented by I-I branches (fully isolated), I-Y (partly connected), and C-C (fully connected).

3.5 Seismic attributes

A seismic attribute is a quantitative measure of a given seismic characteristic (Chopra & Marfurt, 2005). Seismic attributes were extracted from Petrel in this thesis to identify geological features of interest. A wide range of seismic attributes develop in line with computer technology, which are useable to interpret structures, stratigraphy, and fluid properties within seismic interpretation studies. Two types of attributes were extracted from Petrel: variance and ant-tracking.

Variance attribute displays a sharp edge method that measures differences from a mean value (Pigott et al., 2013). Variance maps can image structural and sedimentological features like channels and faults as sharp and highlighted features. Low variance features reveal a dark color. Variance maps can either be generated from an interpreted surface or directly from a variance cube. Ant-tracking is an algorithm that increases features visual continuity by skeletonizing an image (Mai et al., 2009). The algorithm is used for interpretation improvements and can reveal an improved visualization of structures from a variance map. An ant-track map can be generated from a variance cube or directly from an interpreted surface.

4. Data and methodology

This chapter covers an overview of seismic and well data, in addition to methods of seismic interpretation, topology, and workflows conducted in this study.

4.1 Seismic and well data

This study was examined through a 3D regional seismic dataset covering the larger parts of the northern North Sea, an area of approximately 26.000 km². The 3D broadband seismic dataset (TWT_NVG_PDSM) was provided by CGG and represents the North Viking Graben (NVG) high-resolution seismic dataset (figure 4-1).

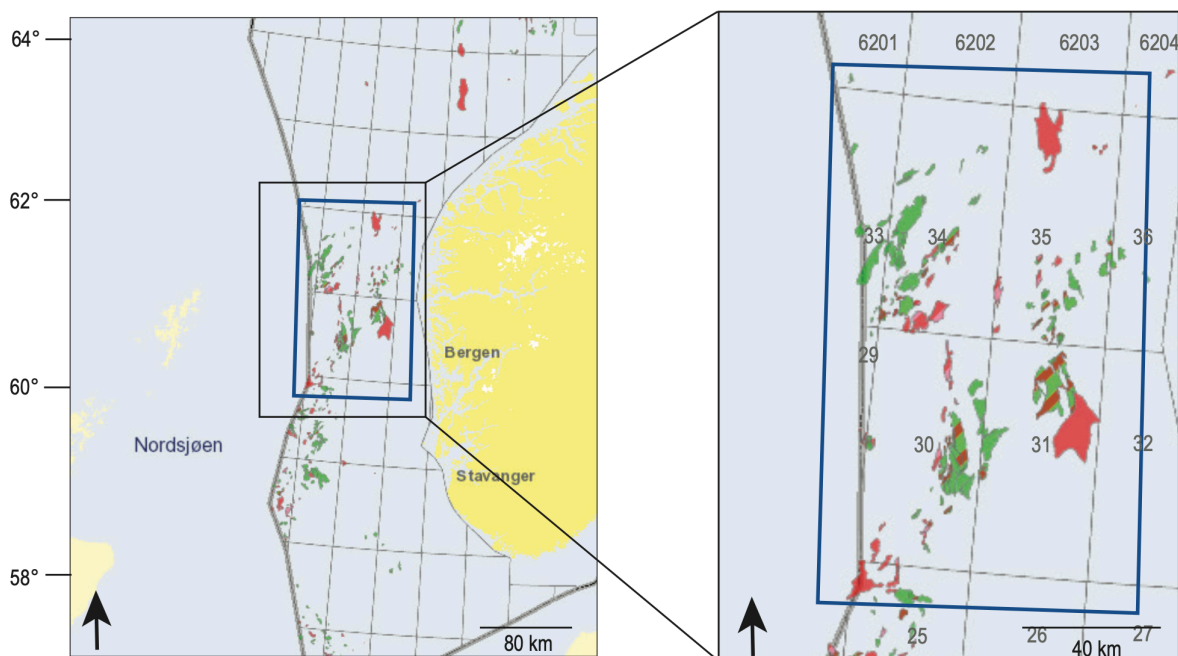


Figure 4-1: Location of the seismic survey (TWT_NVG_PDSM) in the northern North Sea. The seismic survey is marked in the blue box. The map is retrieved from the Norwegian Petroleum Directorate's FactMaps (04.05.2021).

The seismic dataset surrounds quadrants 29, 30, 31, 33, 34, and 35, were only limited parts of quadrants 25, 26, 27, 32, 36, 6201, 6202, 6203, and 6204 were covered. The inlines and crosslines of the seismic are oriented N-S and E-W and a horizontal spacing of the seismic lines within the seismic survey of 12, 5 m. The seismic dataset has a normal American polarity, defining a positive polarity event linked to a peak and is zero-phased processed (figure 4-2). A peak represents a positive amplitude and an increase in acoustic impedance contrast. A positive amplitude is associated with a soft event, and a negative amplitude is associated with a hard

event (Simm & White, 2002). The 3D seismic dataset was used to interpret continuous sequence boundaries at various stratigraphic levels. The high resolution of the dataset made it possible to extract satisfying surface and seismic attribute maps.

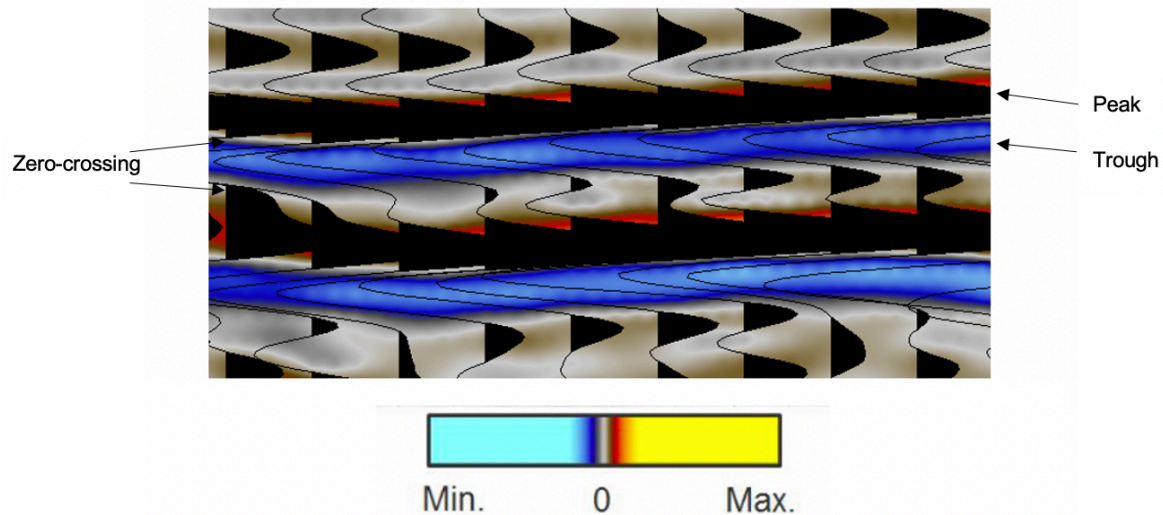


Figure 4-2: Seismic image displaying the seismic polarity of the seismic survey (TWT_NVG_PDSM). Maximum reflection amplitude is displayed by yellow, and minimum reflection amplitude by blue. The zero-crossing display amplitudes of zero and show the color of grey.

In the study, 16 wells were successfully used as ties in the seismic horizon interpretation (figure 4-3). The wells were imported from NPD's database, Diskos (Diskos, 2021). The wells are randomly distributed within the study area and are provided with available well tops, retrieved from NPD FactPages ("NPD FactPages," 2021). Well ties have been substantial for the correlation of seismic interpretations of horizon reflections. The extent and abundance of horizons of interest are deviating throughout the study area. Hence, some well ties at stratigraphic levels are missing (table 4-1).

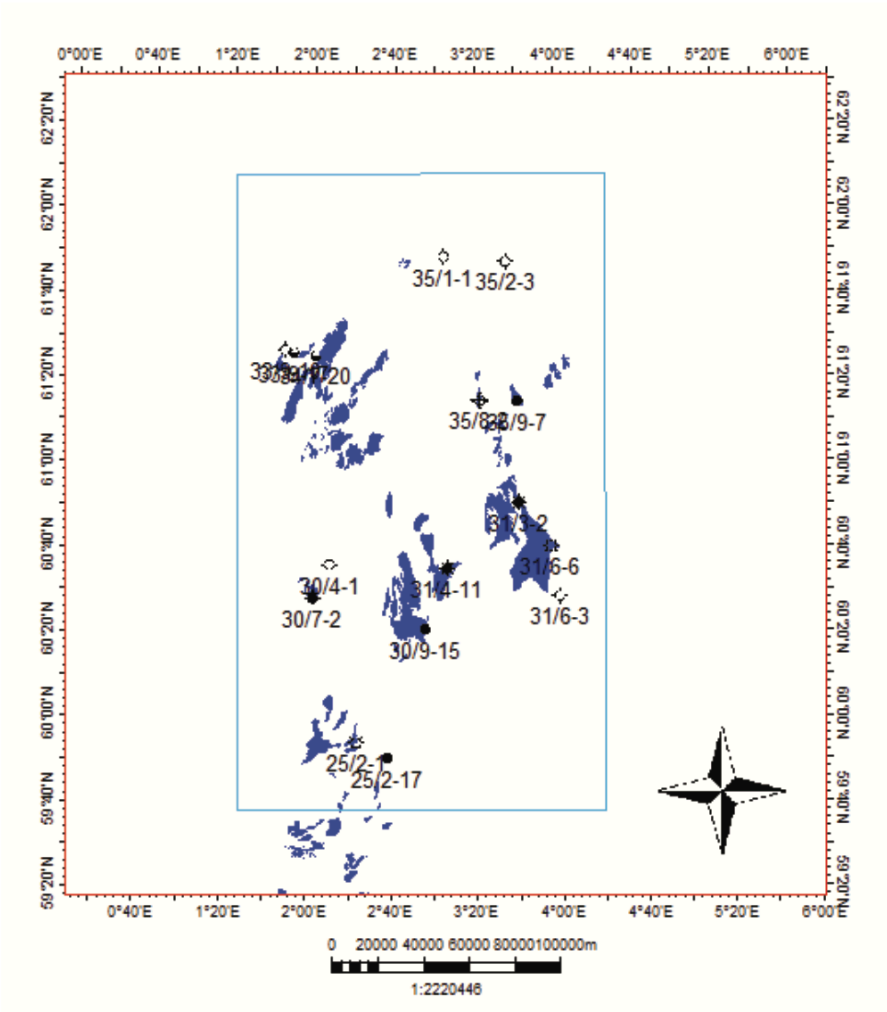


Figure 4-3: Location of wells used for correlation in the seismic interpretation work. The well locations are located within the seismic survey marked in blue and the shape of nearby fields is illustrated as blue polygons.

Table 4-1: Table of wells applied for correlation in the seismic interpretation of sequence boundaries. The first column in the table displays wells that contributed to the seismic correlation. The remaining columns display which stratigraphic horizons the wells were successfully applied for in the correlation work.

Wells	Correlation for CSS sequence boundaries	Top CSS-0	Top CSS-1	Top CSS-2	Top CSS-3	Top CSS-4	Top CSS-5/6	Top CSS-7
25/2-1	x	x	x	x				
25/2-17	x		x	x		x	x	x
30/4-1	x	x	x	x		x	x	
30/7-2	x	x	x	x		x	x	x
30/9-15	x	x	x	x				x
31/3-2	x	x	x	x		x	x	
31/4-11	x	x	x	x			x	x
31/6-3	x	x	x					
31/6-6	x	x	x	x			x	
33/9-10	x	x	x	x		x	x	x
33/9-17	x	x	x	x		x	x	x
34/7-20	x	x	x	x		x	x	x
35/1-1	x	x	x	x		x	x	x
35/2-3	x	x	x	x		x	x	x
35/8-2	x	x	x	x		x	x	x
35/9-7	x	x	x	x		x	x	x

4.2 Seismic interpretation

The seismic interpretation in this study was carried out by the seismic interpretation software Petrel 2019, developed by Schlumberger. The interpretation target for the thesis was the Cenozoic successions of the northern North Sea (figure 4-4). Jordt et al. (1995) described the sedimentary successions of the Cenozoic and distributed them into a “Cenozoic Sequence Stratigraphic framework (CSS)”. The framework contains ten seismic sequences (CSS-1 to CSS-10), based on biostratigraphy and correlating well logs from more than 30 central wells (figure 4-4).

The Cenozoic sequences (CSS) exhibit various lithologies of mainly sands and mudrocks, and the polygonal fault systems are primarily situated within the Hordaland Group (Wrona et al., 2017). The main interpretation target of this thesis is six sequences (CSS-1 to CSS-7) covering succession of Paleocene, Eocene, Oligocene, and Miocene (figures 4-4 and 4-6). The successions of Pliocene and Pleistocene were left out of this study based on the increase in glacial, immature lithologies, and coarsening upward trend from ice-rafted materials that do not hold polygonal fault systems (Thyberg et al., 1999; Eidvin et al., 2000).

Age (Ma)	Chronostratigraphy	Group	CSS sequences according to Jordt et al. (1995)	Interpreted reflectors in the northern North Sea	Lithostratigraphy	Polygonal fault appearance from Wrona et al. (2017)
2.58	Pleistocene	Nordland	CSS-10			
5.33			CSS-9			
	Pliocene		CSS-8	Top Miocene	Utsira	
	Miocene	Hordaland	CSS-7	Top Hordaland		
			CSS-6			
23.03			CSS-5	Top Oligocene	Skade	Isolated polygonal fault traces
	Oligocene	Hordaland	CSS-4	Diagenetic reflector Intra Oligocene		
33.9			CSS-3	Top Eocene		
	Eocene	Hordaland	CSS-2		Grid	
56.0	Paleocene	Rogaland	CSS-1	Top Paleocene	Frigg	
						Balder Sele Lista Våle
66.0				Base Paleocene		

Figure 4-4: Stratigraphic table of the Cenozoic period of sediments in the northern North Sea. The stratigraphic table has been adapted and modified from Hermanrud et al. (2019). The Cenozoic sequence stratigraphic (CSS) framework is based on work by Jordt et al. (1995) and polygonal fault occurrence by Wrona et al. (2017). The table displays time periods, Chronostratigraphy, groups, CSS framework, interpreted horizon reflections, lithostratigraphy, and polygonal fault appearance.

Interpolated interpretations from Faleide et al. (2002) and the University of Oslo were used as guidelines in the seismic interpretations of the Cenozoic sequences. The previous interpretations were based on 2D seismic data with a considerable poorer resolution than what was used in this study. However, they were suitable and beneficial as guidelines in the seismic interpretation work, pointing out the approximate location of each sequence boundary in the seismic data (figure 4-5). As the interpretations were interpolated, they did not reveal any detailed off-sets and onlaps of the reflections. The lower sequences of the Paleocene and Eocene periods were displayed well from the interpolated interpretations of Faleide et al. (2002) due to the large sequence thickness and uniform extent throughout the entire study area. The upper sequences of Oligocene and Miocene displayed less correlation due to various thicknesses and onlapping of sequences. In combination with the retrieved interpretations, own, detailed seismic interpretations were conducted of the whole study area (figure 4-5). Below is a description of the seven interpreted sequence boundaries (table 4-2).

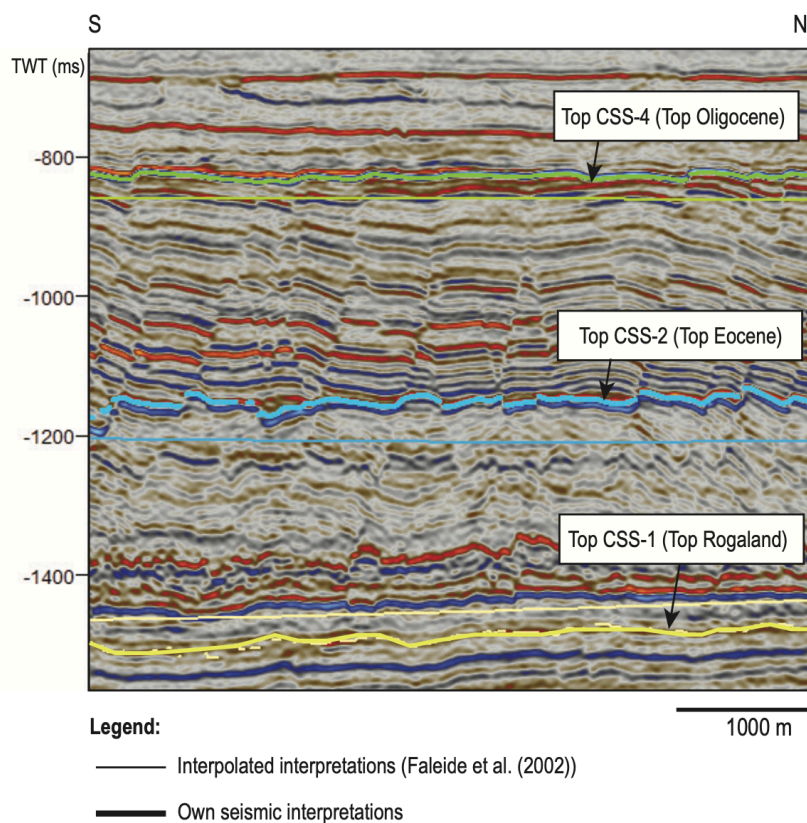


Figure 4-5: Seismic cross-section displaying interpolated interpretations retrieved from Faleide et al. (2002) and the University of Oslo as narrow interpretation lines, compared to own seismic interpretation work as wide interpretation lines. The cross-section displays the importance of own seismic interpretations for detailed surface and variance maps.

4.2.1 Interpreted sequence boundaries

Top CSS-0: The top of the CSS-0 sequence is represented by a seismic reflection that marks the base of the Paleocene sequence (Jordt et al., 1995). A positive seismic phase represents the surface (table 4-2). The horizon reflection is undisturbed, continuous through the study area, and easily interpretable with seeded 3D autotracking tool. The continuous surface is present in the entire area.

Top CSS-1: The top of the CSS-1 sequence is represented by a seismic reflection that marks the top of the Intra Paleocene-Early Eocene sequence (Jordt et al., 1995). Top CSS-1 represents the surface reflection of the Earliest Eocene and display a positive seismic phase, representing the top Balder tuffs and top Rogaland with a high to medium amplitude and is continuous throughout the study area (table 4-2) (Faleide et al., 2002). The extensive occurrence of top CSS-1 surface was interpreted with seeded 3D autotracking tool and was present in the entire area.

Top CSS-2: The top of the CSS-2 sequence is represented by a seismic reflection that marks the top Eocene sequence and the Eocene-Oligocene transition (Faleide et al., 2002). This transition boundary separates a relatively continuous interval with an overlying transparent and chaotic interval. A positive seismic phase represents top CSS-1, where the amplitude strength varies from high to medium (table 4-2). The surface is continuous in large areas but is observed as discontinuous west of the study area. The horizon was interpreted by seeded 2D autotracking tool and was not interpretable in certain areas (figure 5-13).

Top CSS-3: The top of the CSS-3 sequence is represented by a seismic reflection that marks the top of the Lower Oligocene sequence (Rundberg & Eidvin, 2005). Top CSS-3 appears as a minor surface on the eastern basin flank and display a positive seismic phase with a high amplitude which is continuous through the narrow area (table 4-2). The surface was interpreted with seeded 2D autotracking tool and manual interpretations that were needed of down lap onto underlying surface.

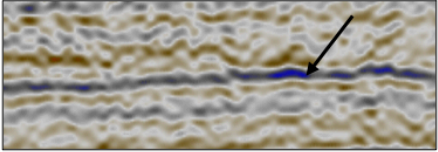
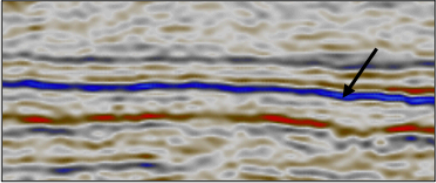
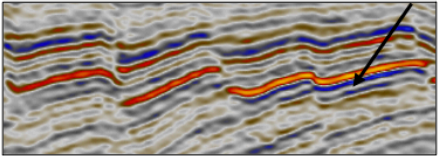
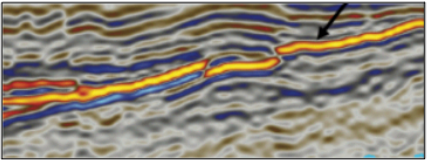
Top CSS-4: The top of the CSS-4 sequence is represented by a seismic reflection that marks the top of the Upper Oligocene sequence (Jordt et al., 1995). Top CSS-4 displays a negative seismic phase with a high to low amplitude reflection (table 4-2). The surface is polygonal

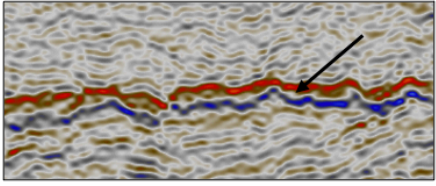
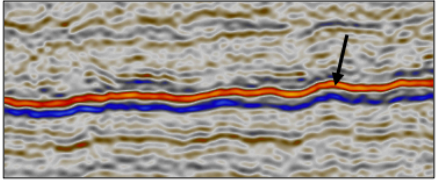
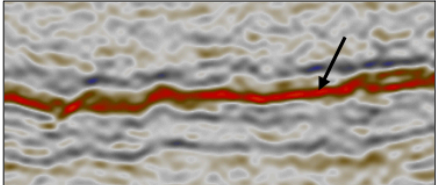
faulted in significant areas and appears continuous to discontinuous. Top CSS-4 is affected by sediment remobilization, making the horizon relatively discontinuous in certain areas. The horizon was interpreted with seeded 2D autotracking tool and manual interpretation of the onlap onto the underlying surface.

Top CSS-5/6: The top of the CSS-5/6 sequence is represented by a seismic reflection that marks the top of the Lower Miocene sequence and the Mid-Miocene unconformity (Løseth & Henriksen, 2005). Top CSS-5/6 is a merged horizon of top CSS-5 and CSS-6, where – was based on the interpretation of Tjensvold (2018) and supported by Faleide et al. (2002). The surface represents Mid-Miocene unconformity and displays a negative seismic phase with a high to medium amplitude (table 4-2). Top CSS-5/6 is continuous in the central parts of the area but are observed as discontinuous towards the basin flank in the west and east. The horizon was interpreted with seeded 2D autotracking tool and manual interpretation of the onlap onto the underlying surface.

Top CSS-7: The top of the CSS-7 sequence is represented by a seismic reflection that marks the top of the Upper Miocene sequence (Jordt et al., 1995). Top CSS-7 represents the surface reflection of Top Miocene, which in some areas coincides with the Utsira formation (Faleide et al., 2002). Top CSS-7 is represented by a negative seismic phase and displays a high to medium amplitude (table 4-2). The surface is continuous throughout the entire area and was easily interpretable with seeded 2D autotracking tool and manual interpretation of onlap onto the underlying surface.

Table 4-2: Reflection description of the seven interpreted sequence boundary reflections in this study: the table display seismic phase, reflection characteristics, and seismic expression.

Cenozoic sequence	Horizon name	Seismic phase	Reflection characteristics	Seismic expression
Top CSS-7	Top Miocene <i>(Intra Nordland group)</i>	Trough	High to medium amplitude. Continuous reflection.	
Top CSS-5/6	Mid Miocene <i>(Top Hordaland group)</i>	Trough	High to medium amplitude. Continuous to discontinuous reflection.	
Top CSS-4	Top Oligocene <i>(Intra Hordaland group)</i>	Trough	High to low amplitude. Continuous to discontinuous reflection.	
Top CSS-3	Early Oligocene <i>(Intra Hordaland group)</i>	Peak	High amplitude. Continuous to discontinuous reflection.	

Top CSS-2	Top Eocene <i>(Intra Hordaland group)</i>	Peak	High to low amplitude. Continuous to discontinuous reflection.	
Top CSS-1	Early Eocene <i>(Top Rogaland group)</i>	Peak	High to medium amplitude. Continuous reflection.	
Top CSS-0	Base Paleocene <i>(Intra Hordaland group)</i>	Peak	High to medium amplitude. Continuous reflection.	

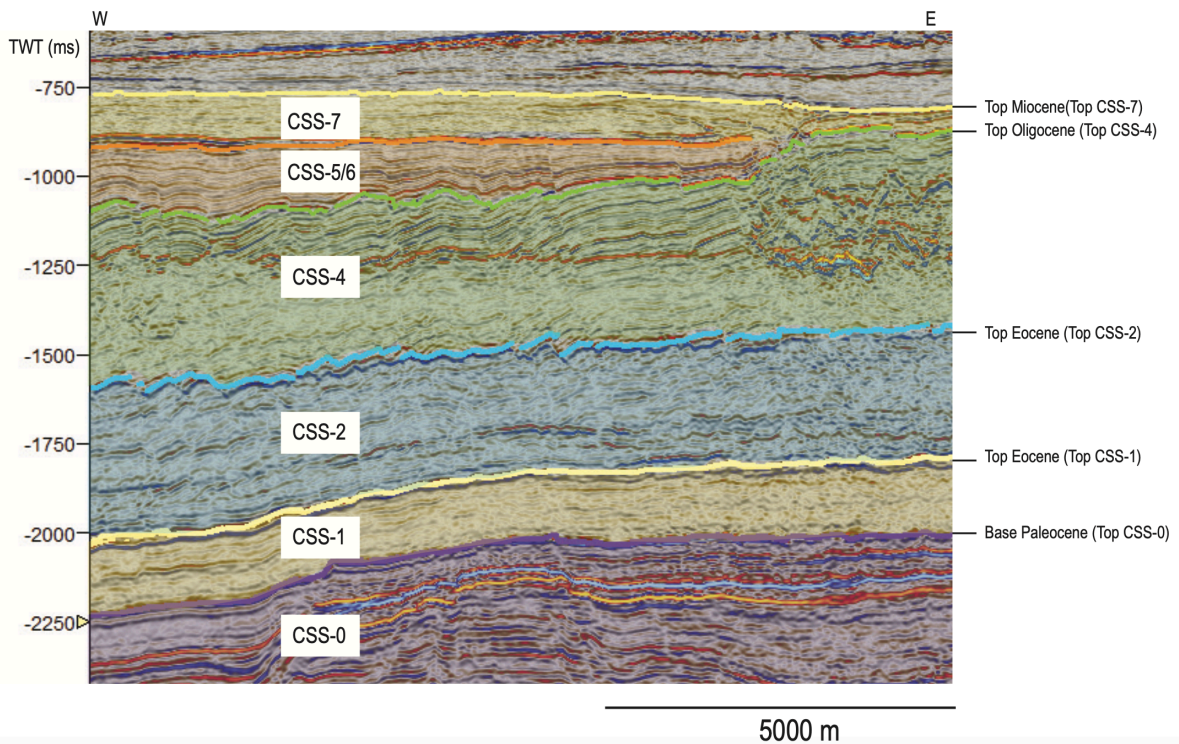


Figure 4-6: Seismic cross-section display seven interpreted sequence boundary reflections. The interpreted reflections are represented by six sequences. The reflection of Top CSS-3 is absent in this cross-section due to its restricted location in the basin. The vertical scale of the cross-section is in milliseconds (TWT). The sequences display various thicknesses, amplitude reflectivity, and structural features.

4.2.2 Seismic expression of sequences

The seismic signatures of the stratigraphic sequences form an important basis for the interpretation of polygonal faults. These signatures result from the lithological composition, which is again results of the depositional history. These relationships are covered here (in the methodology chapter of the thesis) to maintain a clear focus on the main topic of this thesis (polygonal faults) in the result and discussion chapters.

CSS-1 represents the Paleocene-Early Eocene sequence and the seismic signature is characterized by a westward prograding wedge, indicating outbuilding from the East Shetland Platform and the areas of southern Norway (Faleide et al., 2002). The sequence covers lithologies of smectite-rich clays and turbiditic sand displayed with an irregular reflectivity (Thyberg et al., 2000; Løseth et al., 2003). The top and base of the sequence display powerful positive amplitude reflections associated with a soft event of high density sand lithologies (table 4-2) (Isaksen & Tonstad, 1989; Simm & White, 2002). Two main depocenters are located in the Viking Graben and outside Sognefjord based on the sediment distribution (Jordt et al., 1995). The seismic expression of the sequence is relatively uniform, with minor variations throughout the basin (figure 5-6). The thickness of the sequence varies and appear thickest towards the basin margins, and thin with gain higher amplitude reflections northward.

CSS-2 represents the sequence of largely Eocene and consists of mainly mudrocks with a high smectite content from alternations of volcanic ash (Thyberg et al., 2000; Marcussen et al., 2009). Traces of alternations of sand and thin clay intervals are observed north of the Horda Platform and display an alternating reflectivity near the top and base of the sequence, recognized as the Frigg sand at the base, consisting of thick, immature sand with thin intervals of clay and siltstone (figure 5-13) (Jordt et al., 1995). The reflectivity in the middle of the sequence appears constant, indicating minor lithology changes. CSS-2 is bound at the top and base by powerful positive amplitude reflections associated with a soft event of high density sand lithologies (table 4-2) (Isaksen & Tonstad, 1989; Simm & White, 2002). The seismic expression of the sequence is observed to thin eastward and consist of depocenters along the Viking and central graben in the basin center. Faleide et al. (2002) proposed that CSS-2 was deposited from the uplifted East Shetland Platform, with signatures suggesting deposition through gravity processes, resulted in turbidity currents in deep water.

CSS-3 represents the lower Oligocene wedge and is only present on the eastern basin flank (figure 5-19). The top of the sequence has previously been mapped as a continuous surface extending from the eastern margin to the basin center referred to as an unconformity (Jackson, 2007). However, based on present seismic data the sequence observed is restricted to the eastern flank with an outbuilding pattern that indicates deposition from the Norwegian margin (Rundberg & Eidvin, 2005). The sequence displays similarly lithologies as underlying sequences, with smectite-rich clays, originated from volcanic components, and display a relatively uniform reflectivity throughout the sequence (Thyberg et al., 2000). Both sequence boundaries of CSS-3 display powerful positive amplitude reflections related to a soft event with high density sand lithologies (table 4-2) (Simm & White, 2002). The seismic expression of the sequence is weakly defined in the basin center and appears with an elongated geometry along the N-S axis on the eastern basin flank. CSS-3 downlaps onto underlying CSS-2, characterizing a prominent sequence boundary.

CSS-4 represents the upper Oligocene sequence and exhibits lithologies of smectite and kaolinite, with high biogenic silica content in the basal parts of the sequence (Thyberg et al., 2000). CSS-4 displays similar outbuilding pattern and thickness variations as the CSS-2 from the East Shetland Platform (Jordt et al., 1995). The thickness variation is suggested to occur from sediment remobilization, represented by sand injections, mounds, and polygonal faults. The base of the sequence displays a powerful positive amplitude reflection associated with a soft event of high-density sand lithology and the top of the sequence displays a powerful negative amplitude reflection associated with a hard event of low-density clay lithology (table 4-2) (Simm & White, 2002). The seismic expression of the sequence is relatively uniform in the lowermost unit of the sequence but displays a more alternating reflectivity in the upper unit. A diagenetic reflection is present in the sequence and is located on the eastern half of the study area, cross-cutting reflections and appear with a positive polarity event (figure 5-26) (Lynne et al., 2005). CSS-4 is generally underlain by CSS-2, especially near the Atlantic continental margin, where CSS-3 is not present. On the eastern basin flank is CSS-4 onlapping into CSS-3.

CSS-5/6 represents the lower Miocene sequence and exhibits lithologies of smectite, but significantly less than underlying sequences. The smectite content of CSS-5/6 is according, to Thyberg et al. (2000) decreasing, upward in the sequence with a coarsening upward trend. Both sequence boundaries display powerful negative amplitude reflections, indicating a hard event

of low density clays (table 4-2) (Simm & White, 2002). The sequence displays an alternating reflectivity with variations of clays and sands deposited from the eastern basin margins and occur as a fully defined sequence (figure 5-37) (Jordt et al., 1995; Faleide et al., 2002). The seismic expression of the sequence appears as a prograding wedge, outbuilt from the East Shetland Platform into the basin center near the central Viking Graben (Jordt et al., 1995). The sequence thin and transpire below seismic resolution northward in area.

CSS-7 represents the upper Miocene sequence and is located above the Mid-Miocene unconformity bound by powerful negative amplitude reflections as sequence boundaries, associated with hard events of low density clays (figure 5-40 and table 4-2) (Simm & White, 2002). Parts of CSS-7 correlates to the Utsira formation (Faleide et al., 2002), and are deposited under a relative fall in the sea-level, which resulted in shallow marine deposits. The seismic expression of the sequence is well defined in the basin center of the study area, with a prograding signature indicating the Norwegian margin as the main provenance area.

4.2.3 Uncertainties

As the study was carried out using seismic interpretation, there may be some uncertainties and deviations compared to previous author's interpretations of the sequences within the study area of the northern North Sea:

- Manually seismic interpretation of Cenozoic sequences may come with uncertainties based on the level of seismic interpretation experience and point of view.
- Areas in the western part of the Eocene unit were not interpreted in this study because of disturbances in the seismic data from sediment remobilization.
- CSS-5/6 combined seismic unit may not be consistent horizon reflection. CSS-5/6 thin below seismic resolution in northern parts of the study area.

4.3 Topology and Geometry Analysis

A topological and geometric analysis of the polygonal faults was conducted in QGIS (version 13), using the toolbox Network GT. Network GT is a bespoke toolbox that can be used for sampling and extracting the geometric and topological characteristics of two-dimensional

fracture networks (Nyberg et al., 2018). Generated ant-tracked attribute maps retrieved from a variance cube in Petrel were imported into QGIS. The attribute maps were scaled based on a threshold ant-track value where the fault traces were imaged satisfactory. The polygonal faults were digitized by manually interpreting fault traces with polylines in QGIS. When all faults were interpreted, an interpretation boundary and sample area were generated as polygons. The polyline and polygons provide the inputs for the geometry and topological tools within the Network GT toolbox.

A variety of geometrical and topological data were retrieved and visualized from the analysis in Network GT. These include the number counts and proportions of the different node (I-nodes = N_I , Y-nodes = N_Y , and X-nodes = N_X) and branch types (I-I, I-C, and C-C branches), as well as an array of network parameters including fault intensity, connecting node frequency and average connections per branch. The intensity (m^{-1}) is described by total trace length (m) divided by the sample area (m^2) (Mauldon et al., 2001; Sanderson & Nixon, 2015). The total trace lengths represent the total sum of the length of all branches (Mauldon et al., 2001). The intensity is often mentioned as fracture density in the literature (Sanderson & Nixon, 2015). The connecting node frequency (N_c , m^{-2}) is described by the division of the number of connecting nodes ($N_C = N_Y + N_X$) per sample area (m^2) (Sanderson & Nixon, 2015). The average connections per branch (C_B) quantifies the degree of connectivity divided by the number of branches (N_B) in figure 4-7.

A

$$N_B = \frac{1}{2}(N_I + 3N_Y + 4N_X)$$

B

$$C_B = \frac{3N_Y + 4N_X}{N_B}$$

Figure 4-7: **A)** Equation display number of branches in a fracture network. N_B = number of branches, N_I = number of I-nodes, N_Y = number of Y-nodes, N_X = number of X-nodes. **B)** Equation display connections per branch (C_B).

As a branch can have a maximum of two connecting nodes, the average number of connections per branch (C_B) results in a dimensionless number of 0-2. A value of 0 represents a branch with two isolated nodes, whereas a value of 2 represents a branch with two connecting nodes. As the connections per branch (C_B) is derived from the node counts, it can be contoured onto the ternary diagrams of both nodes and branches (figure 4-8). In general, networks with a high proportion of I-I branches and I-nodes exhibit a low level of connectivity ($C_B \approx 0$) and plot near the top corner of the ternary diagrams (figure 4-8). Whereas networks with a high proportion of C-C branches, Y-nodes, and X-nodes exhibit a high level of connectivity ($C_B \approx 2$) and plot near the lower corners of the ternary diagrams (figure 4-8).

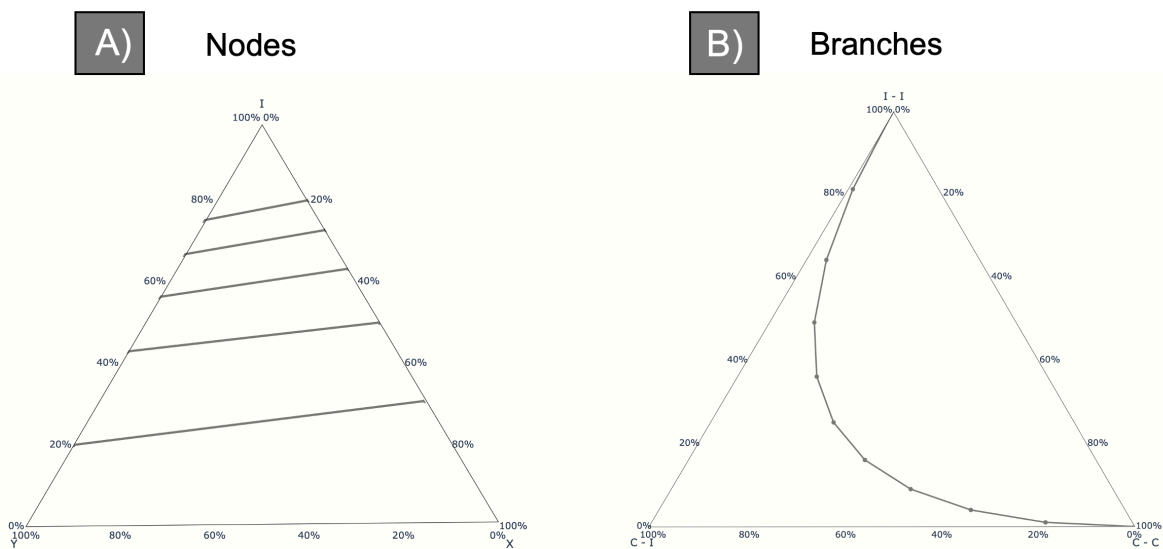


Figure 4-8: Ternary diagrams display the connectivity of nodes and branches in a fracture network. **A)** Ternary diagram displaying connectivity of nodes, and **B)** ternary diagram displaying connectivity of branches. Nodes and branches in a fracture network tend to plot close to the general markers within the ternary diagrams.

4.3.1 Spatial visualization of fracture networks

Contour grids of the different network parameters provide an effective way to visualize the spatial variation of the fault network properties. Contour grids divide the interpreted network into rows and columns of grid cells, with each grid cell representing a circular sample area that overlaps with adjacent grid cells. Thus, each grid cell provides a moving circular sample window. Connecting node frequency, fault intensity and connections per branch are some of

the parameters that were calculated for each grid cell. A color scale bar can then be applied to the contour grid to represent different values of a given parameter providing a powerful tool for visualizing spatial variations within the network.

4.3.3 Uncertainties

The topological analysis may come with some uncertainties:

- The interpreters experience plays a significant role in the accuracy of the interpretations.
- The identification of nodes and fault linkage can become subjective due to data resolution.
- Data quality and resolution of seismic images imported from Petrel may cause loss of some structures and cut-offs from fault segments (Morley & Nixon, 2016).
- Scaling of colors of the attribute maps may cause loss of structural features.

4.4 Workflow

The workflow conducted in this thesis is listed in figure 4-9. Seismic research was crucial to gain an overview of the polygonal faults' extensive distribution within the study area. The seismic research led to the interpretation of seven sequence boundary reflections. Spacing with an interval of 265 was first performed in the seismic interpretation, where later more detailed interpretations with intervals of 64-128 were performed. The finalized interpretation of the sequence boundary reflections was used to create surface and attribute maps.

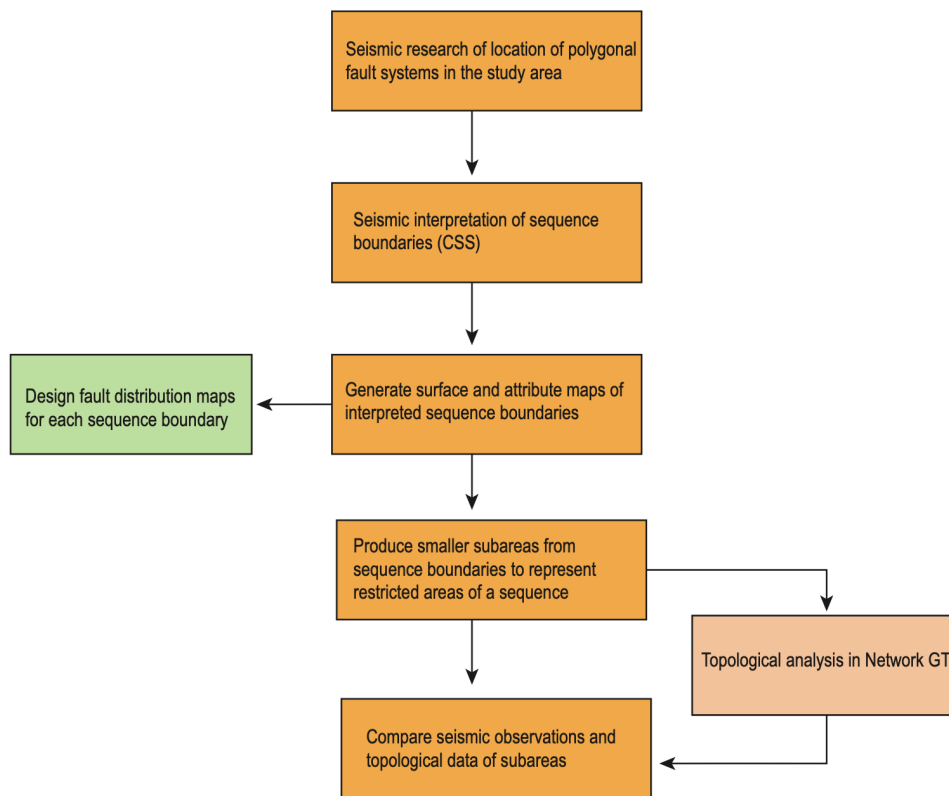


Figure 4-9: Workflow described step by step of the work conducted in this thesis.

4.4.1 Fault distribution maps

The surface maps created are displayed as fault distribution maps. The fault distribution maps display faulted areas of sequences from interpreted sequence boundaries (figure 4-11). The maps are subdivided by three types of color-coded polygons representing faulting, non-faulting, and uncertainty (figure 4-10 and table 4-3). This division was carried out by investigation of variance maps and seismic cross-sections.

Areas located within a red polygon suggest non-faulting and are characterized with continuous, undisturbed reflections. Areas located within a yellow polygon suggest faulting and are characterized by a clear offset of the seismic reflections. Areas located within a black polygon suggest uncertainty and are characterized with low seismic resolution or disturbed horizon reflections, causing discontinuous reflections (figure 4-10).

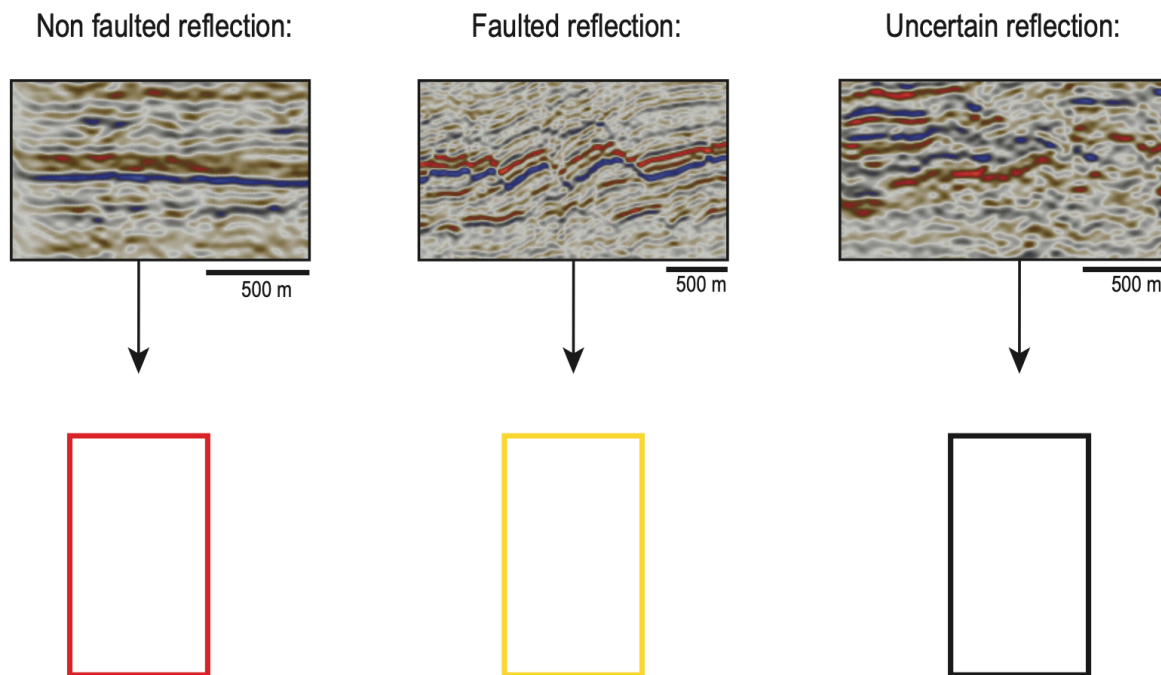


Figure 4-10: Seismic images displaying the seismic signature of interpreted reflection horizons divided into color-coded areas. A non-faulted reflection horizon is represented by a red polygon, a faulted reflection horizon is represented by a yellow polygon, and an uncertain reflection horizon is represented by a black polygon. Finalized surface maps with polygons are displayed in figure 4-9.

4.4.2 Subareas

The fault distribution maps display the areas of faulting in the sequences. Minor subareas were designed to get an overview of faulting at different sequences (table 4-3). One subarea covers approximately an area of 56 km² of a sequence and display a well-defined fault network. The number of subareas representing one sequence is determined on fault appearance at that stratigraphic level (figure 4-11).

The Cenozoic sequences are extensive and cover most of the study area, including deposits from both basin slope and basin center positions. The position of the basin slope and basin center changed through time. Observations of thickness variations and literature can be used. Inferences of the position of the basin centers were made from observations of thickness variations within each sequence and examination of past research on basin development in the area.

The East Shetland Platform is the main provenance area of CSS-2, CSS-4, and CSS-5/6. The main provenance area of CSS-1, CSS-3, and CSS-7 is the East Shetland Platform and southern Norway (section 4.2.2) (Faleide et al., 2002). The frequent uplift events shifted the location of the basin center and basin slope over the Cenozoic period. Locations referred to in chapter 5 (table 4-3) are the present positions observed from seismic images, where the original location under deposition is interpreted and discussed in chapter 6.

Table 4-3: Division of subareas within stratigraphic sequences displayed in a table. The table display sequences holding subareas, epoch, base, and top sequence boundary, and present basin location.

CSS	Epoch	Base sequence boundary	Top sequence boundary	Subarea	Present basin location
CSS-0	Upper Mesozoic	-	Top CSS-0	0A	Basin flank
				0B	Basin flank
				0C	Basin floor
CSS-1	Paleocene- Early Eocene	Top CSS-0	Top CSS-1	1A	Basin floor
				1B	Basin floor
				1C	Basin flank
CSS-2	Largely Eocene	Top CSS-1	Top CSS-2	2A	Basin flank
				2B	Basin flank
CSS-3	Lower Oligocene	Top CSS-2	Top CSS-3	3A	Basin flank
				3B	Basin flank
				3C	Basin flank
CSS-4	Upper Oligocene	Top CSS-3	Top CSS-4	4A	Basin floor
				4B	Basin flank
				4C	Basin flank

CSS-5/6	Lower Miocene	Top CSS-4	Top CSS-5/6	5/6A	Basin flank
CSS-7	Upper Miocene	Top CSS-5/6	Top CSS-7	7A	Basin flank

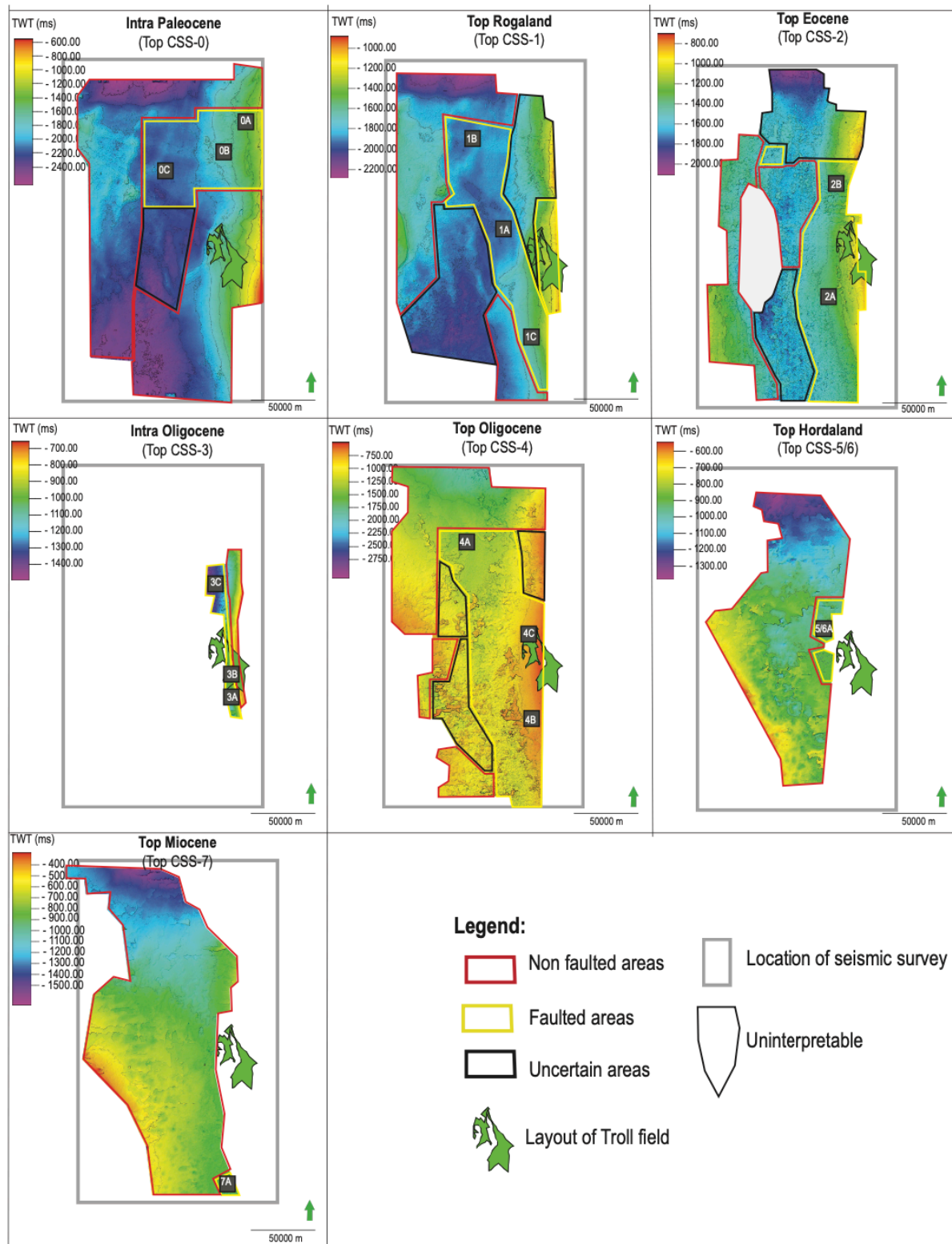


Figure 4-11: Surface maps representing all seven interpreted sequence boundaries of six sequences. Each surface map holds color-coded polygons that display areas of faulting, non-faulting, and uncertainty, where each faulted area is represented by a set of subareas (56 km²) which is further studied.

5. Seismic observations and topological characteristics of polygonal faults

This chapter covers a description of the seismic observations and the topological analysis of polygonal fault discovered in the northern North Sea. The presence of polygonal fault systems in the Hordaland Group has previously been demonstrated, where this study proceeds further with the investigation through 3D seismic data examining and mapping fault distribution and behavior in the sedimentary basin. The chapter contains observations from sequences of the Cenozoic sequence stratigraphic framework (figure 4-3). Each sequence is presented with the geological evolution of the sequence. Further, are seismic and topological observations for subarea within the sequences presented.

5.1 CSS-0 (Upper Mesozoic sequence)

The sequence corresponds to the upper Mesozoic sequence and is bound by top CSS-0 (figure 5-1). Top CSS-0 represents the top Shetland Group and base of the Cenozoic sediments. Successions situated below this sequence boundary are of Upper Mesozoic (Cretaceous) age and are not included in the CSS framework (Jordt et al., 1995). Based on the presence of polygonal faults situated below this sequence boundary, the faults were included as results. No interpreted base of these polygonal faults has been defined, and the faults are mainly described ~200 ms below top CSS-0. The succession of Upper Mesozoic was investigated to gain a broad overview of the pattern and behavior of the polygonal faults below the Cenozoic sediments.

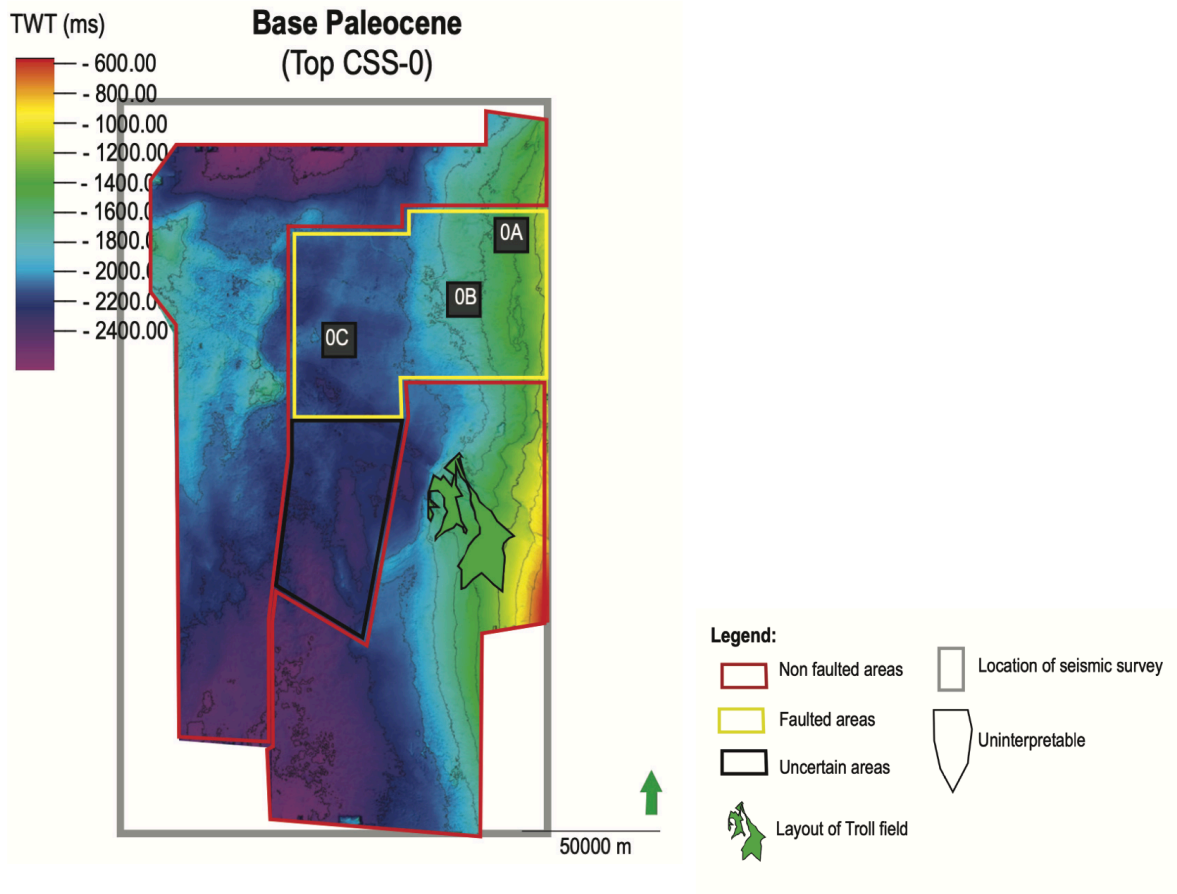


Figure 5-1: Top CSS-0 (Intra Paleocene) surface map displaying three subareas within the faulted area of the horizon. Remaining areas of the surface map display non-faulted and uncertain areas. The layout of the Troll field is used as an indicator for approximate location.

Subarea 0A

The area is located on the northeastern basin slope, where the sediment successions are characterized by medium amplitude reflections (figure 5-2). Top CSS-0 displays a bright amplitude reflection with a sharp offset of minor normal faults associated with polygonal faults. The fault offsets are observed in underlying reflections at ~150 ms depths below top CSS-0. Below this level are the reflections transparent, disturbed, and hard to track. Any faults below this level cannot be identified from the seismic data (figure 5-2C).

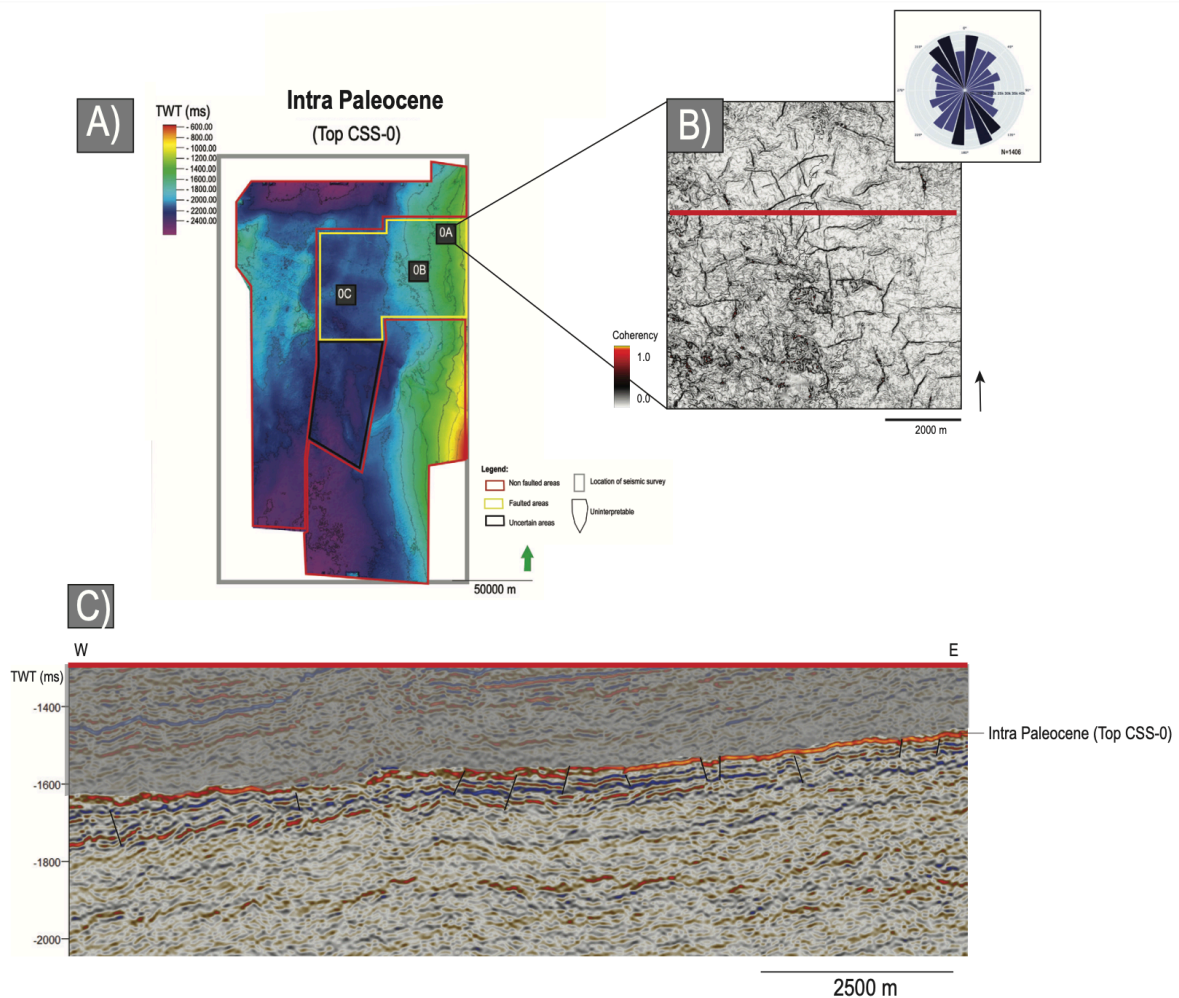


Figure 5-2: *A) Intra Paleocene surface map displaying three subareas within the faulted area of the horizon. B) Variance attribute map of subarea 0A displaying plan form pattern of the polygonal faults. The red line represents the seismic cross-section. The variance map is combined with a rose diagram displaying orientation trends of the subarea, where orientation trends are marked in dark blue. C) Seismic cross-section of polygonal faults situated in sediments below Top CSS-0 (Intra Paleocene).*

The fault displacement is hard to state based on the low seismic resolution downward in the successions. However, the visible faults display planar fault planes. Variance maps display a polygonal geometry of the faults with an isolated to rectangular plan form pattern, denser obliquely through the area (figure 5-2B). A rose diagram shows a dominant orientation (NNW-SSE) of the polygonal faults (figure 5-2B). The polygonal faults display connectivity of $0.99 C_b$, with faults less connected on the eastern half of the subarea (figure 5-3). This observation is evident through contour maps of 2D intensity and connecting node frequency displaying a higher composition of connections and intensity towards the west.

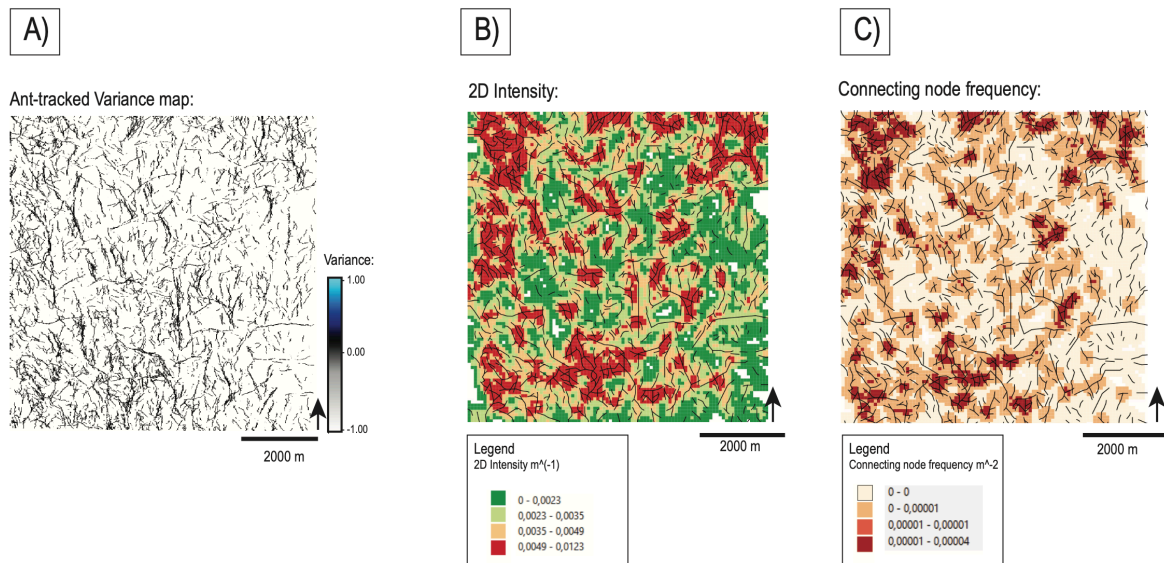


Figure 5-3: Map views of polygonal fault patterns of subarea 0A. **A)** Ant-tracked variance map used for manual fault interpretation and foundation for contour maps, **B)** 2D intensity map (m^{-1}) displaying intensity variations, and **C)** connecting node frequency map (m^{-2}). The combination of map views shows increased connectivity and intensity on the western half of the area.

Subarea 0B

The area is comparable to the previous subarea, located on the eastern basin slope, further southwest (figure 5-4A). The sequence displays several parallels to the previous subarea with blurry amplitude reflections. In addition, are both subareas observed with minor normal faults present ~ 100 - 150 ms below top CSS-0 (figure 5-4C). The sediments situated below this interval appear transparent and chaotic with low seismic amplitude reflections. Any polygonal faults below this interval are hard to observe based on seismic resolution. The maximum fault displacement of the polygonal faults is observed at 100 ms below top CSS-0, holding a higher amplitude reflection than underlying and overlying reflections (figure 5-4C).

Seismic cross-sections display planar to listric fault plane of the faults, with a polygonal geometry of rectangular to curved plan form pattern observed from variance map (figure 5-4B). This subarea displays a dominant orientation trend of the polygonal faults (NNW-SSE, NNE-SSW) that hold moderate-high connectivity of $1.15 C_b$ (figure 5-4B).

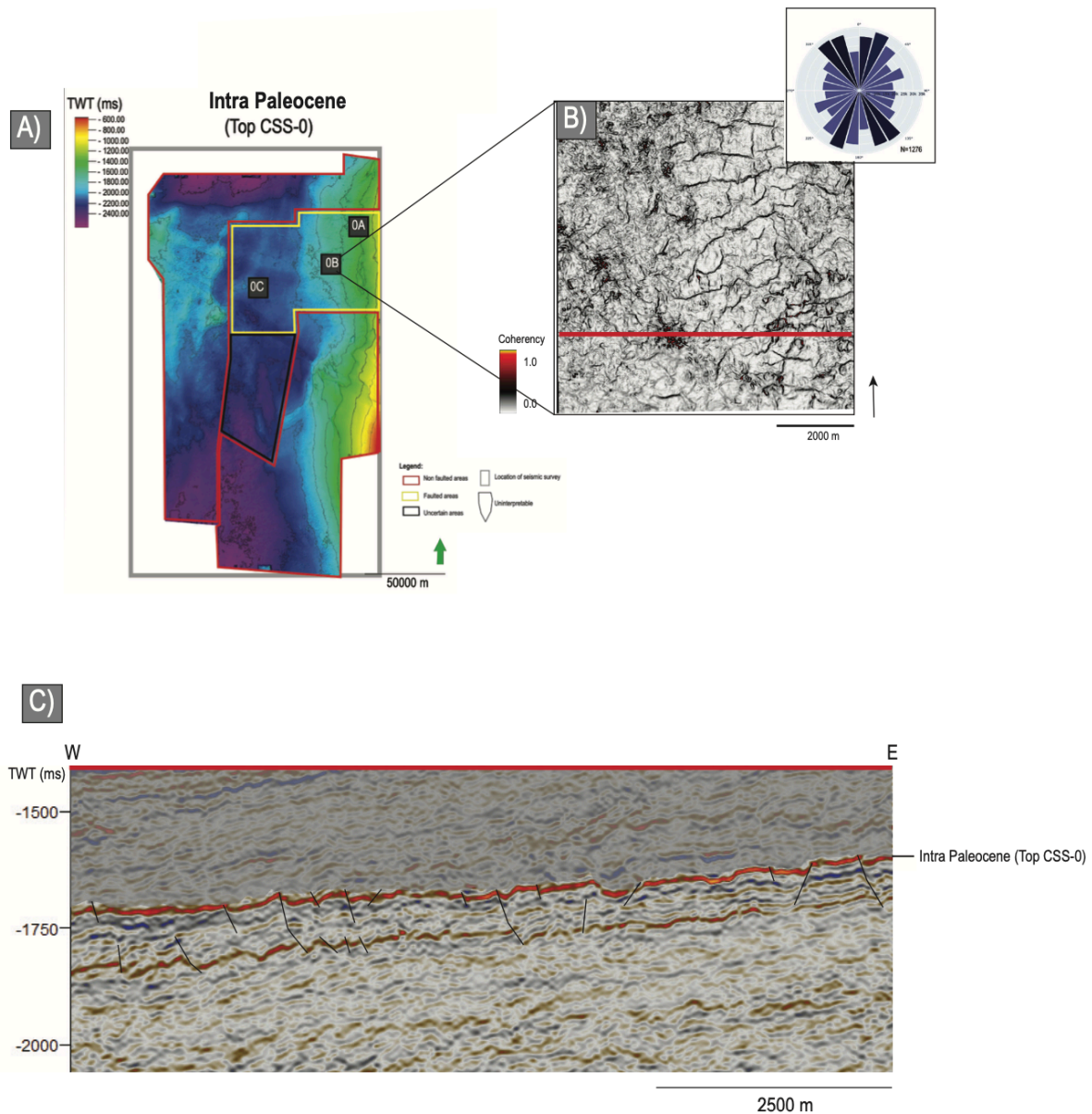


Figure 5-4: A) Intra Paleocene surface map displaying three subareas within the faulted area of the horizon. B) Variance attribute map of subarea 0B displaying plan form pattern of the polygonal faults. The red line represents the seismic cross-section. The variance map is combined with a rose diagram displaying orientation trends of the subarea, where orientation trends are marked in dark blue. C) Seismic cross-section of polygonal faults situated in sediments below Top CSS-0 (Intra Paleocene).

Subarea 0C

The area is situated on the northern basin floor of the study area (figure 5-5A). This subarea stands out from previous subareas of the sequence as the reflections appear with continuous, medium amplitudes. The reflections display visible, distinct normal faults associated with polygonal fault patterns ~500 ms below the top horizon (figure 5-5C). Like previous areas of Intra Paleocene, orientation trends are observed (NNW-SSW) detected through the rose diagram with low-moderate connectivity of 0.90 C_b (figure 5-5B).

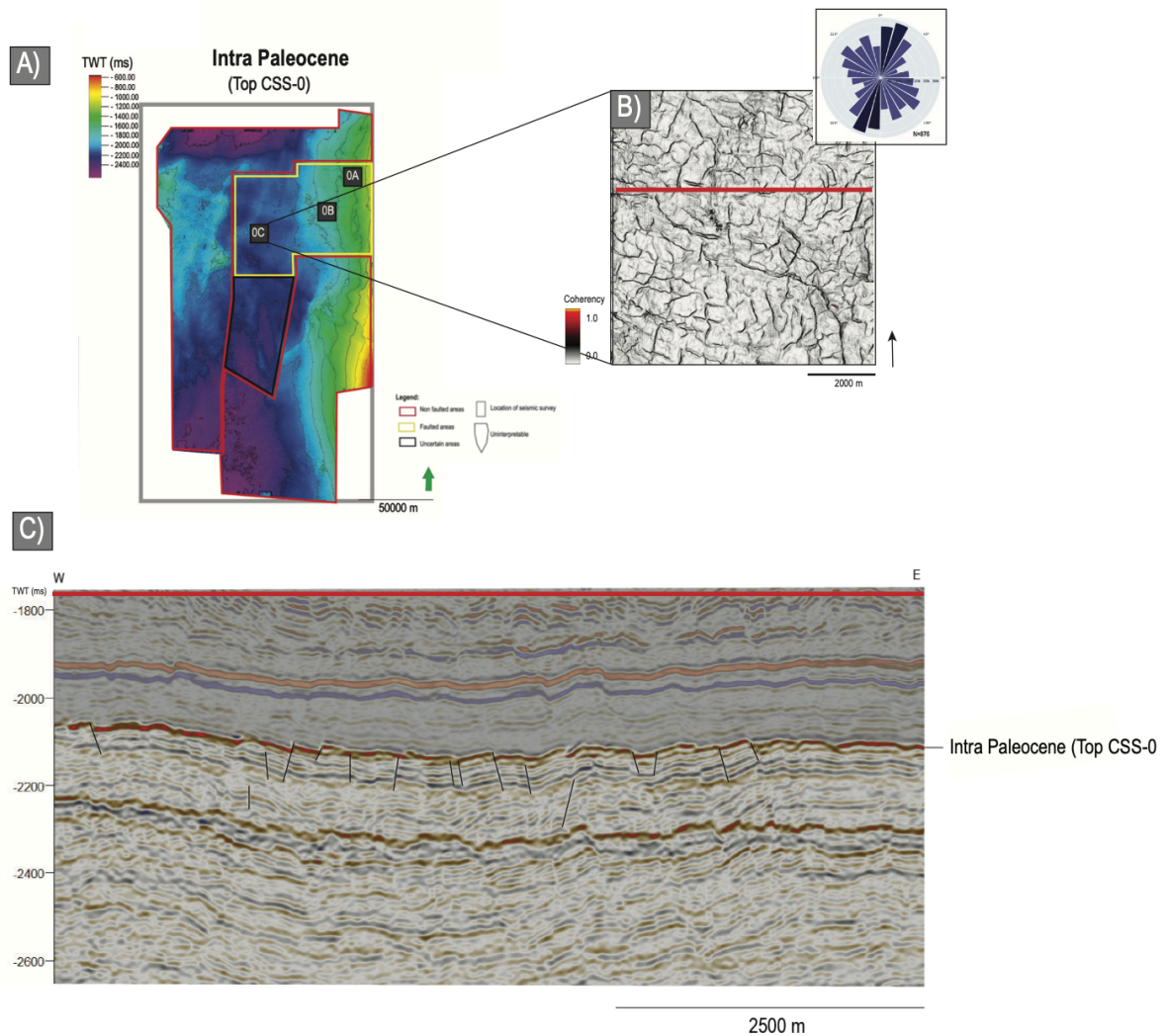


Figure 5-5: **A)** Intra Paleocene surface map displaying three subareas within the faulted area of the horizon. **B)** Variance attribute map of subarea 0C displaying plan form pattern of the polygonal faults. The red line represents the seismic cross-section. The variance map is combined with a rose diagram displaying orientation trends of the subarea, where orientation trends are marked in dark blue. **C)** Seismic cross-section of polygonal faults situated in sediments below Top CSS-0 (Intra Paleocene).

The polygonal faults are layer-bound, with planar fault planes showing no distinct fault displacement trends. The faults are more abundant and continuous near top CSS-0. Observations from the variance map display a polygonal geometry of isolated to rectangular plan form patterns of the polygonal faults (figure 5-5B).

5.2 CSS-1 (Paleocene-Early Eocene sequence)

The sequence corresponds to the Paleocene and Early Eocene sediments and is bound by top CSS-0 and top CSS-1, representing the Top Balder surface. The sequence appears with a

modest thickness near the basin center. It reaches a thickness of ~ 270 ms and gradually increases in thickness towards the basin flanks reaching maximum thickness of ~ 515 ms (figure 5-6) (section 4.2.2). The seismic signature of the sequence is uniform, holding continuous medium amplitude reflections. Minor variations are observed within the sequence with the occasionally appearance of higher amplitude reflections. The sequence appears extensive and is present further north and south in the study area combined with appearance on both basin flanks (figure 5-6).

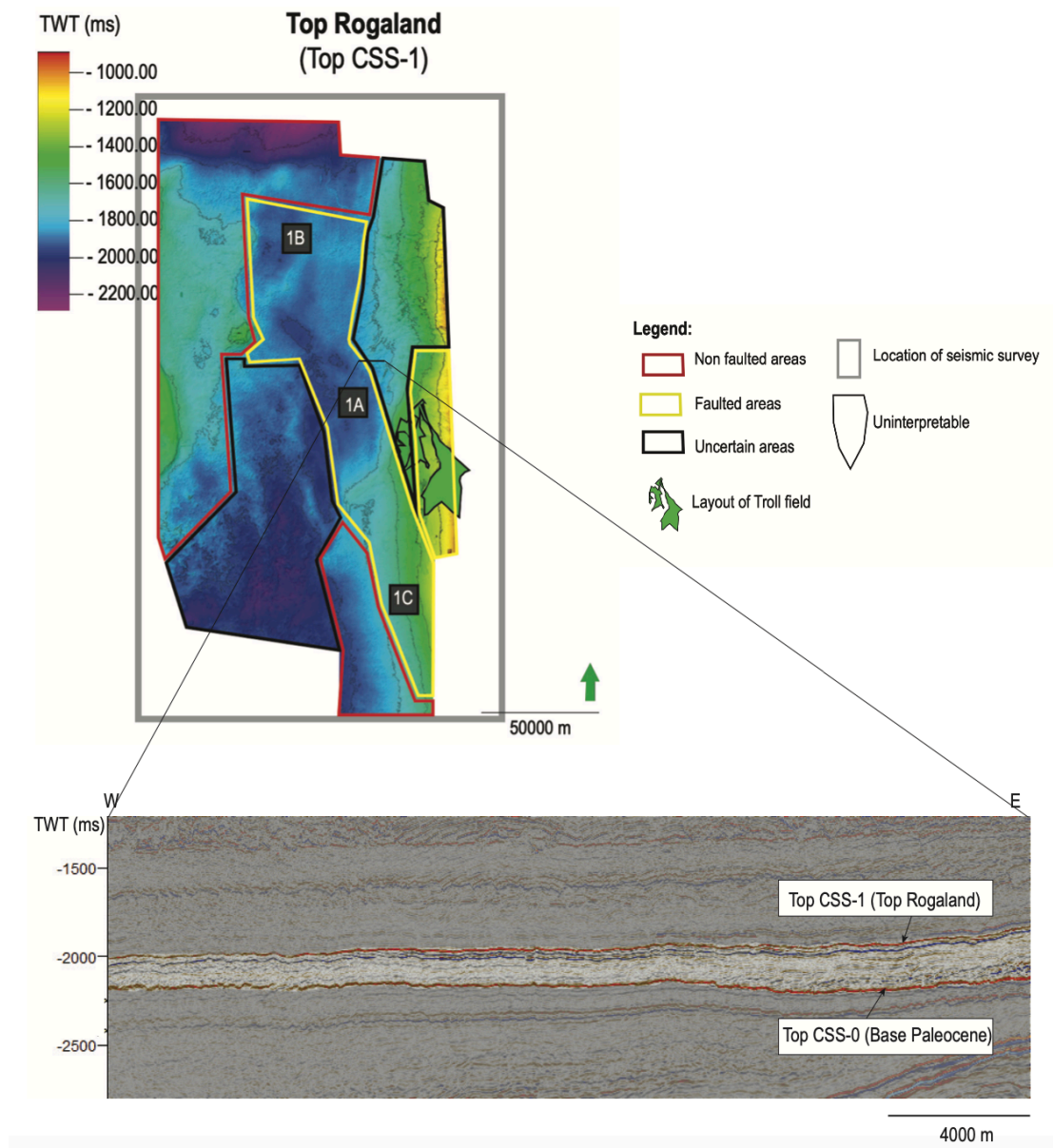


Figure 5-6: Top CSS-1 (Top Rogaland) surface map displaying three subareas within the faulted area of the horizon. The seismic section displays the uniform thickness of CSS-1. Remaining areas of the surface map display non-faulted and uncertain areas. The layout of the Troll field is used as an indicator for approximate location.

Subarea 1A

The area is in the middle of the basin floor, and the sequence is characterized by medium amplitude reflections displaced by minor normal faults (figure 5-7). The variance map of top CSS-1 displays isolated to rectangular fault traces with a polygonal geometry (figure 5-7B). Isolated fault traces displayed from the variance map consist of a significant portion of minor NNW-SSE trending faults, combined with a few more prominent faults. The average branch length of all polygonal fault traces is 370 m, minor faults with lengths of ~50-100 m, and more prominent faults with lengths of <1000 m. The combination of more prominent and minor faults in the area results in isolated fault traces showing low connectivity of 0.50 C_b . The preferred NNW-SSE orientation is supported by observations from the rose diagram. The more prominent faults exhibit a more randomly distributed orientation than the minor faults (figure 5-7B). The polygonal faults appear as generally spaced within the with various fault displacement through the sequence. Seismic cross-sections display fault plane geometries of planar to gently listric shape, displaying a more faulted lower unit (figure 5-7C). Top CSS-0 is commonly displaced by faults and appears as a high amplitude reflection.

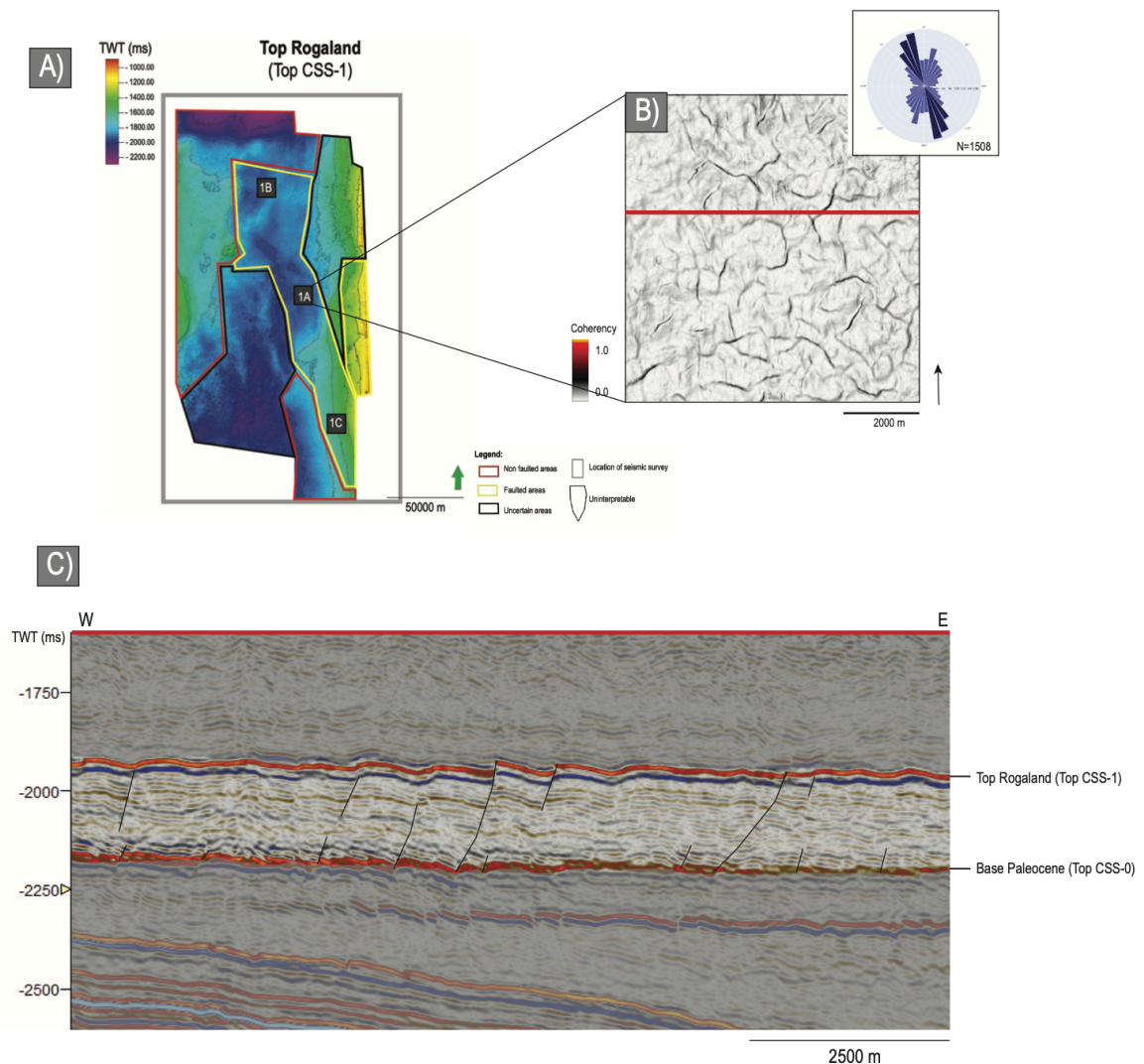


Figure 5-7: **A)** Top Rogaland surface map displaying three subareas within the faulted area of the horizon. **B)** Variance attribute map of subarea 1A displaying plan form pattern of the polygonal faults. The red line represents the seismic cross-section. The variance map is combined with a rose diagram displaying orientation trends of the subarea, where orientation trends are marked in dark blue. **C)** Seismic cross-section of polygonal faults situated in CSS-1 (Paleocene sequence).

Subarea 1B

The area is located on the northern basin floor, and the sequence is not dominated by the structures of faulting, as they appear infrequent through the sequence with minor fault displacement of the reflections (figures 5-8A and 5-8C). The observation of infrequent fault traces is supported by a low fault density of 17.8 per km² measured from fault traces at top CSS-1. Combined with a low fault density, display the interpreted polygonal faults a low connectivity 0.59 C_b .

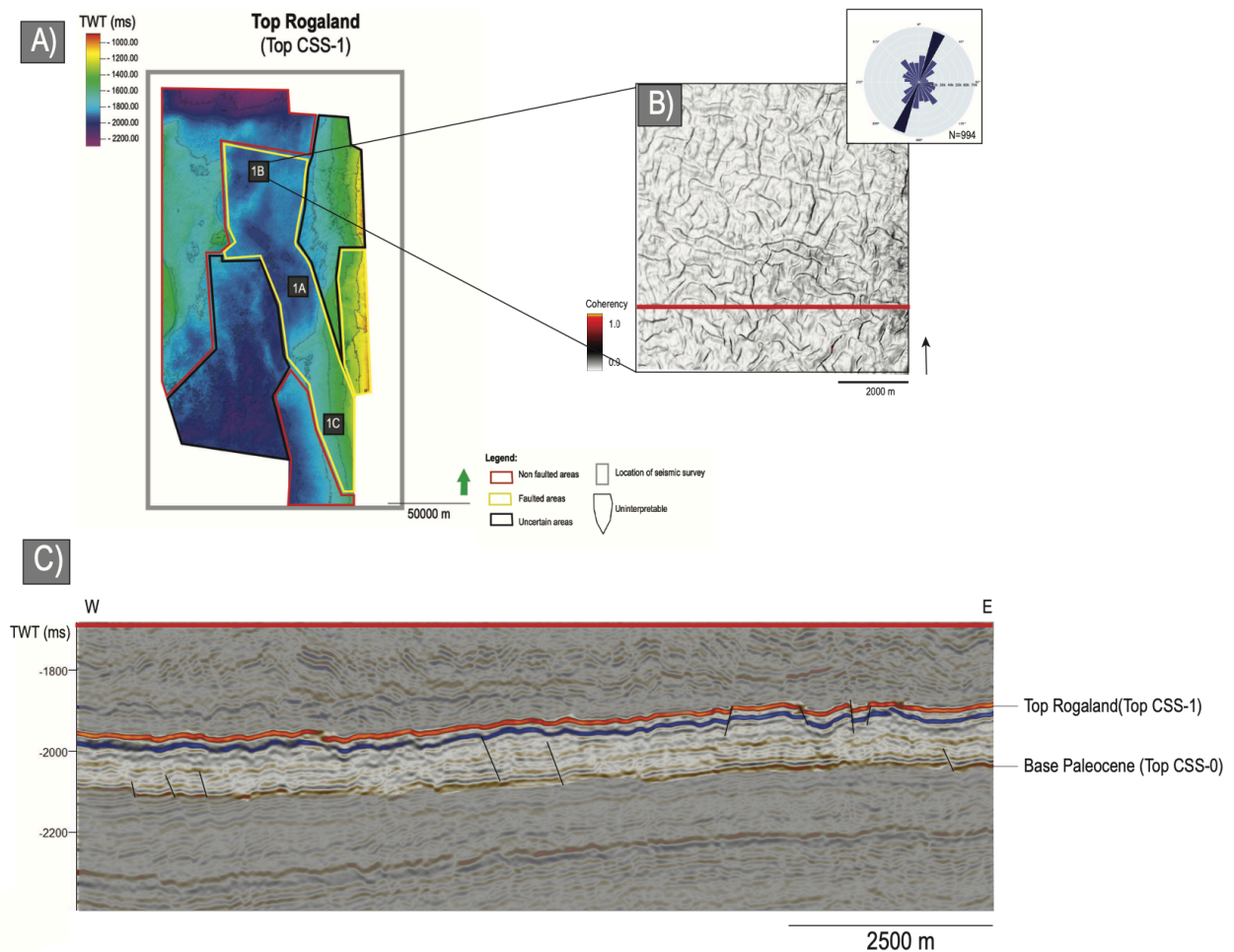


Figure 5-8: **A)** Top Rogaland surface map displaying three subareas within the faulted area of the horizon. **B)** Variance attribute map of subarea 1B displaying plan form pattern of the polygonal faults. The red line represents the seismic cross-section. The variance map is combined with a rose diagram displaying orientation trends of the subarea, where orientation trends are marked in dark blue. **C)** Seismic cross-section of polygonal faults situated in CSS-1 (Paleocene sequence).

The fault displacement in the sequence appears minor throughout the area. Top CSS-1 appears more isolated and less disturbed by faulting than the remaining parts of the sequence. The fault planes are observed as more or less planar throughout the sequence (figure 5-8C). First recognized from map view is a superior proportion of polygonal faults developed on the eastern half of the area (figure 5-8B). This observation is supported by contour maps of 2D intensity and connecting node frequency displaying similar trends with relatively higher connectivity of fault traces on the eastern half (figure 5-9). The variance map displays a polygonal geometry of rectangular plan form patterns of the polygonal faults, which display a preferred orientation trend (NNE-SSW) (figure 5-8B). Top CSS-0 is displayed as disturbed by fault off-sets (figure 5-8C).

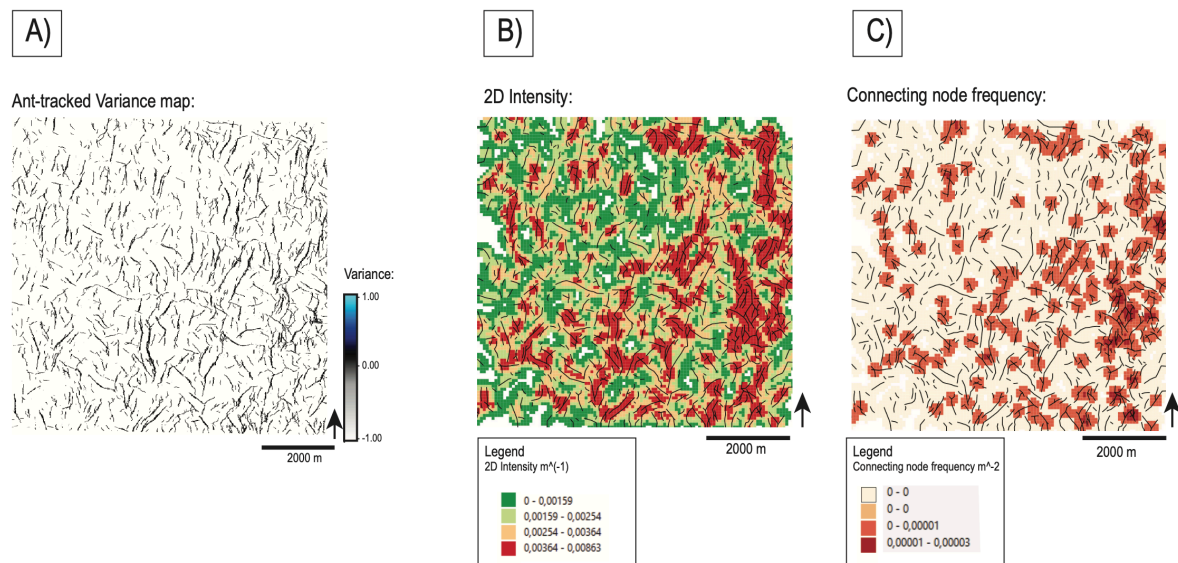


Figure 5-9: Map views of polygonal fault patterns of subarea 1B. **A)** Ant-tracked variance map used for manual fault interpretation and foundation for contour maps, **B)** 2D intensity map (m^{-1}) displaying intensity variations, and **C)** connecting node frequency map (m^{-2}). The combination of map views shows increased connectivity and intensity on the eastern half of the area.

Subarea 1C

The area is located on the southeastern basin flank, and the sequence is characterized by continuous to discontinuous, medium seismic amplitude reflections (figure 5-10A). The amplitude reflections located in the southern part of the sequence appear more visible and continuous than the remaining parts of the sequence. A contrasting observation of slightly dense connectivity of faults on the eastern half is identified from contour maps displaying 2D intensity and connecting node frequency (figure 5-11).

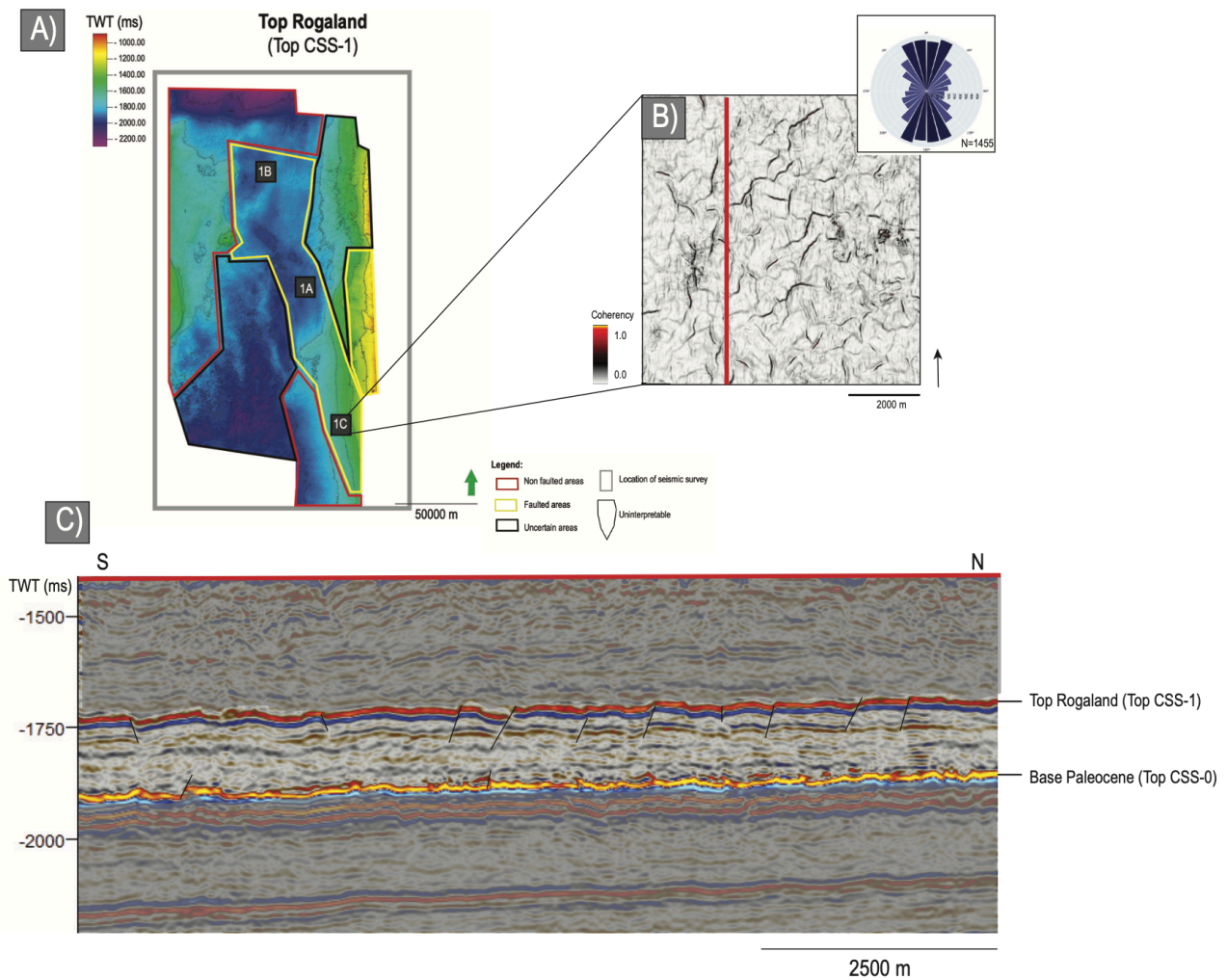


Figure 5-10: *A) Top Rogaland surface map displaying three subareas within the faulted area of the horizon. B) Variance attribute map of subarea 1C displaying plan form pattern of the polygonal faults. The red line represents the seismic cross-section. The variance map is combined with a rose diagram displaying orientation trends of the subarea, where orientation trends are marked in dark blue. C) Seismic cross-section of polygonal faults situated CSS-1 (Paleocene sequence).*

Observations from the variance map of top CSS-1 exhibit a polygonal geometry of isolated to rectangular plan form patterns of the faults (figure 5-10B). The plan form pattern identified from Top CSS-1 holds a relatively low connectivity of $0.82 C_b$. The fault planes are hard to interpret downward in the sequence based on loss of continuity in the seismic (figure 5-10C). In areas with high continuity are fault planes visible through the sequence, with the maximum fault displacement situated close to top CSS-1 (figure 5-10C). The fault plane of the polygonal faults displays close to a uniform planar geometry.

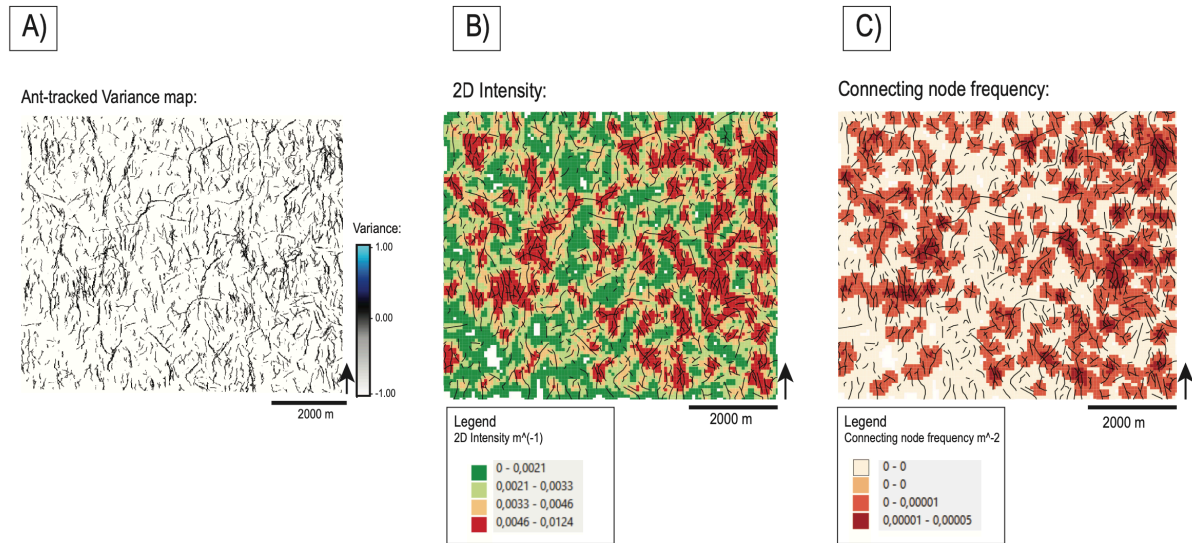


Figure 5-11: Map views of polygonal fault patterns of subarea 1C. **A)** Ant-tracked variance map used for manual fault interpretation and foundation for contour maps, **B)** 2D intensity map (m^{-1}) displaying intensity variations, and **C)** connecting node frequency map (m^{-2}). The combination of map views shows increased connectivity and intensity on the western half of the area.

Like previous areas of CSS-1, this area displays a slightly preferred orientation (N-S) (figure 5-10B). The orientation of the polygonal faults can be divided and visualized into two sets, where one set holds orientations of (0, 40) and (140, 180), while another set holds orientation of (40, 140) (figure 5-12). The first set displays faults slightly oriented N-S (NNW-SEE, NNE-SSW).

Polygonal Fault Trace Map:

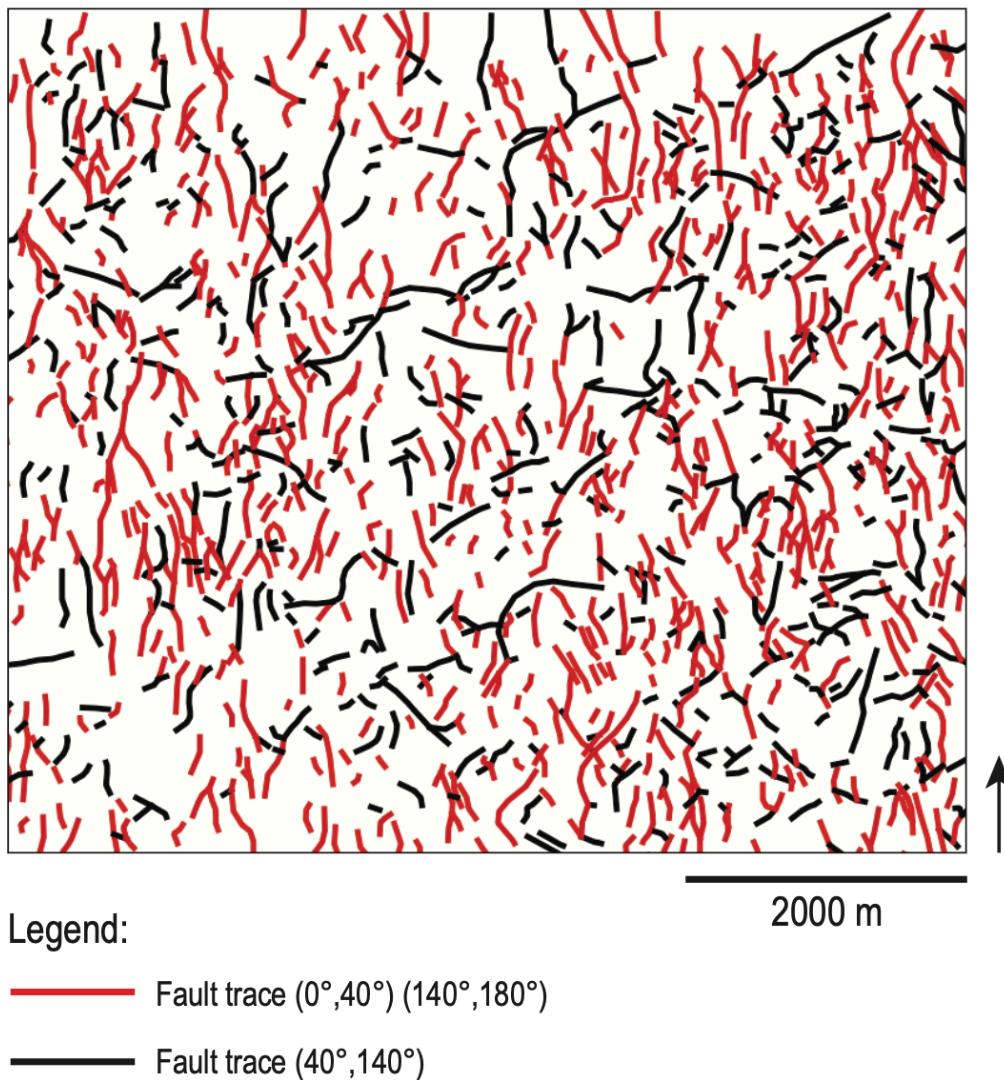


Figure 5-12: Interpreted fault traces from the topological analysis. The interpreted fault traces are visualized in two colors representing two sets. The polygonal faults colored in red hold the first set with orientations ranging ($0^\circ, 40^\circ$) and ($140^\circ, 180^\circ$), where the polygonal faults colored in black hold the second set with orientations ranging ($40^\circ, 140^\circ$). The red-colored fault traces display a roughly N-S trend of the polygonal faults.

5.3 CSS-2 (Largely Eocene sequence)

The sequence corresponds to the Largely Eocene sequence and is bound by top CSS-1 and top CSS-2. Compared to adjacent sequences, this sequence appears as a thick sequence reaching a maximum thickness of ~470 ms along the basin center (figure 5-13). The sequence decreases towards the basin flanks. The seismic character of the sequence is an alternation between continuous to discontinuous amplitude reflections. More extensive variations are observed in the sequence with blur, chaotic reflections, and high to low amplitude reflections (section 4.2.2) (5-16C). The sequence appears relatively extensive and is present further north and south in the study area.

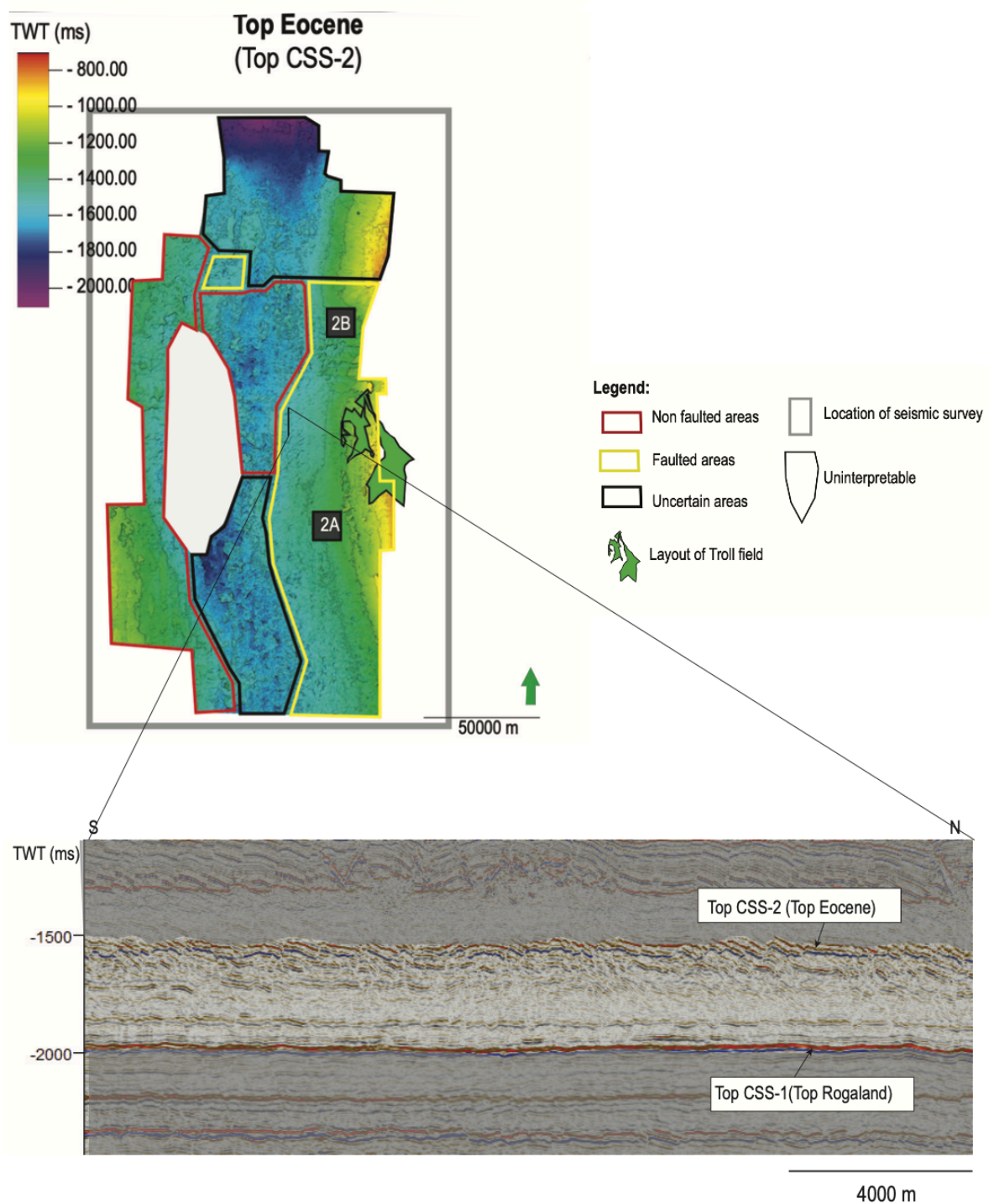


Figure 5-13: Top CSS-2 (Top Eocene) surface map displaying two subareas within the faulted area of the horizon. The seismic section displays uniform, thick CSS-1. Varying amplitude reflections are displayed within the sequence. Remaining areas of the surface map display non-faulted and uncertain areas. The layout of the Troll field is used as an indicator for approximate location.

Subarea 2A

Subarea 2A is located on the southeastern basin slope, and the sequence is characterized by medium to high amplitude reflections, where occasionally areas of blur occur (figures 5-14A and 5-14C). Top CSS-2 displays a rotated, high amplitude, polygonal faulted reflection (figure 5-14C). Polygonal faulted reflections are continuously observed ~50 ms below top CSS-2 and hold polygonal faults that exhibit a close to uniform planar fault plane (figure 5-14C). Minor polygonal faults appear close to top CSS-1, with a planar fault plane geometry (figure 5-14C). The maximum displacement of the faulting is most pronounced near top CSS-2 (figure 5-14C).

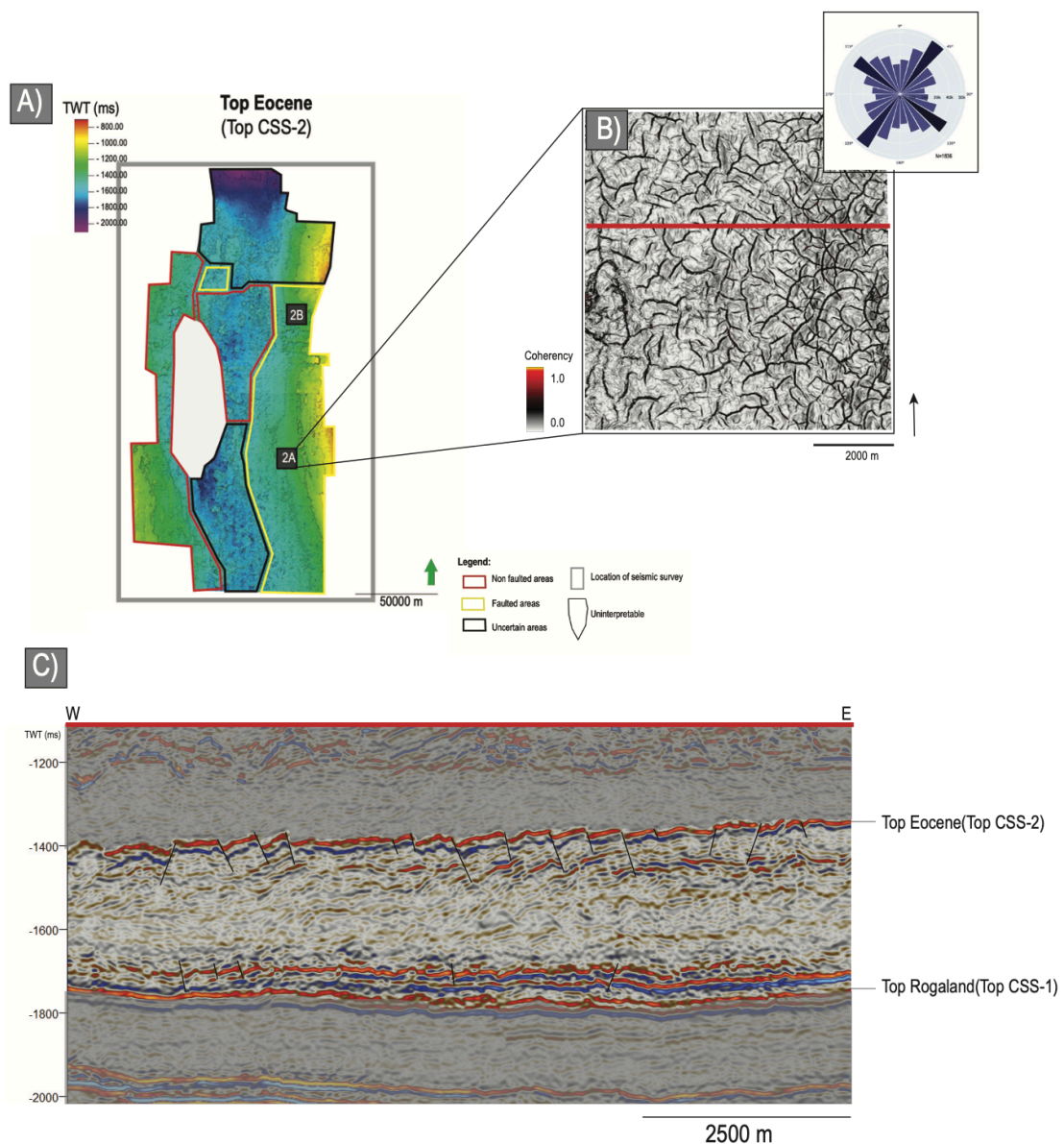


Figure 5-14: **A)** Top Eocene surface map displaying three subareas within the faulted area of the horizon. **B)** Variance attribute map of subarea 2A displaying plan form pattern of the polygonal faults. The red line represents the seismic cross-section. The variance map is combined with a rose diagram displaying orientation trends of the subarea, where orientation trends are marked in dark blue. **C)** Seismic cross-section of polygonal faults situated in CSS-2 (Eocene sequence).

Observations from the variance map display a polygonal geometry of rectangular to curved plan form pattern of the faults (figure 5-14B). The plan form pattern of the faults displays poorly connected polygonal faults in the southwestern part of the sequence, supported by observations from contour maps showing clusters of high connectivity on the eastern half of the sequence (figures 5-14B and 5-15). The overall connectivity of the polygonal faults is relatively high, with a value of $1.28 C_b$.

Seismic cross-sections display structures of graben/horst interacting with polygonal faults restricted to the northern part of the sequence. The orientation of the faults shows slightly preferred trends of NW-SW and NE-SW (figure 5-14B).

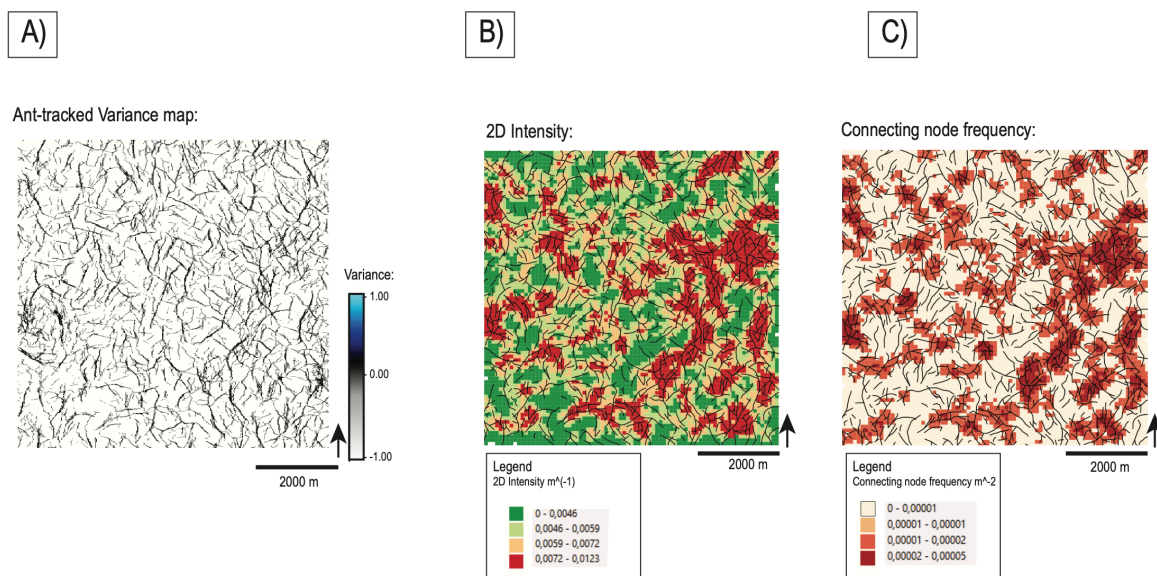


Figure 5-15: Map views of polygonal fault patterns of subarea 2A. **A)** Ant-tracked variance map used for manual fault interpretation and foundation for contour maps, **B)** 2D intensity map (m^{-1}) displaying intensity variations, and **C)** connecting node frequency map (m^{-2}). The combination of map views shows increased connectivity and intensity on the western half of the area.

Subarea 2B

The area is located on the eastern basin flank, further south of the previous area of the sequence (figure 5-16A). The amplitude reflections in the sequence display varying low to high amplitudes. Observations from the variance map of top CSS-2 display a polygonal geometry of

rectangular to curved fault patterns, with a relatively high connectivity of 1.13 C_b (figure 5-16B). The contour maps display increased connectivity on the southwestern half of the sequence, with decreasing intensity and connectivity obliquely through the sequence (figure 5-18). CSS-2 display three separate units, where unit 1 shows a low seismic resolution unit close to the base with planar reflections, unit 2 show high amplitude, chaotic reflections in the middle of the sequence, and unit 3 show a blurry unit close to the top (figure 5-16).

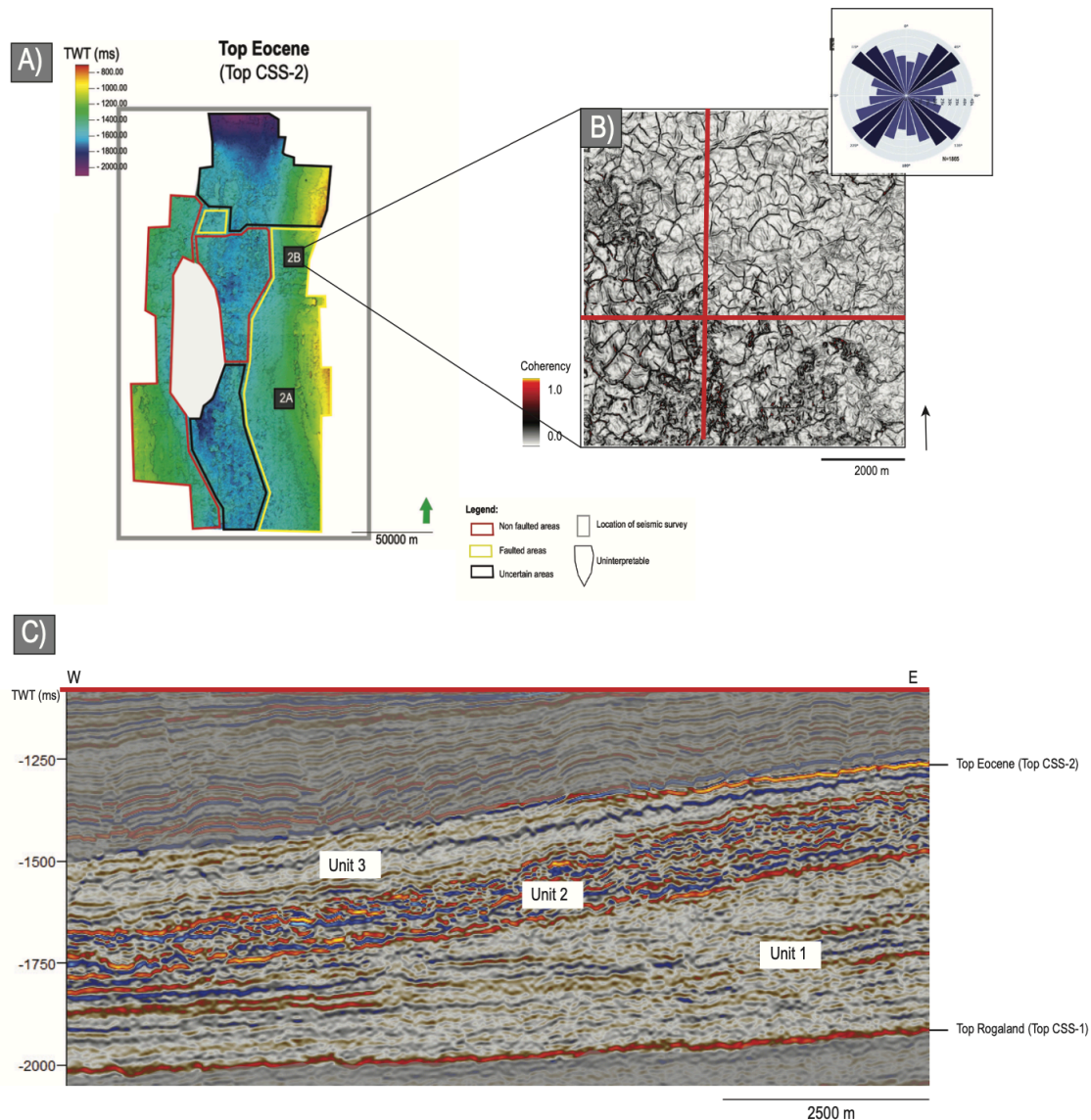


Figure 5-16: A) Top Eocene surface map displaying three subareas within the faulted area of the horizon. B) Variance attribute map of subarea 2B displaying plan form pattern of the polygonal faults. The red line represents the seismic cross-section. The variance map is combined with a rose diagram displaying orientation trends of the subarea, where orientation trends are marked in dark blue. C) Seismic cross-section of polygonal faults situated in CSS-2 (Eocene sequence).

The abundance of faults is mostly in unit 3, where the maximum fault displacement is found near top CSS-2. The fault plane is displayed with a planar fault plane geometry. Polygonal faults are generally not observed from seismic cross-sections in the lower units of 1 and 2 (figure 5-16). The high amplitude reflections displayed in unit 2 appear chaotic, challenging observations of polygonal faults, with structures of V-shaped 2-D geometries (figure 5-17).

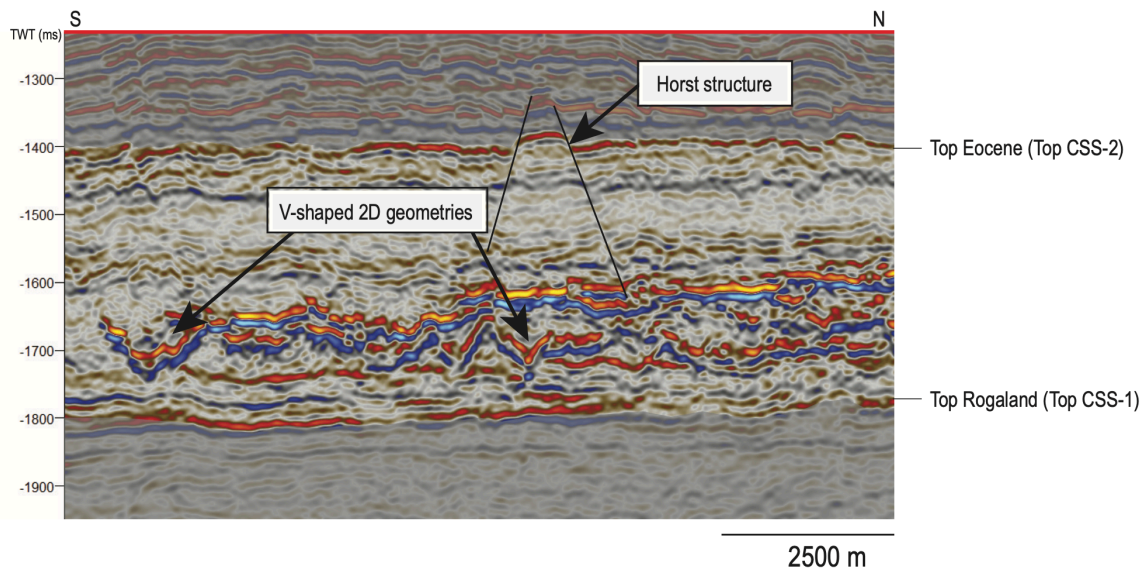


Figure 5-17: N-S seismic cross-section displaying V-shaped 2D geometries located near the base of subarea 2B (Eocene sequence). In addition, is graben/horst structures present in the upper unit of the sequence.

Unit 2 decreases in thickness and relocates from a depth from top CSS-2, from ~1500 ms to ~1720 ms towards the south in the sequence. In addition, is the unit observed as decreasing from the east towards the west. Unit 1 does not show any polygonal faults and is located close to top CSS-1, displaying an undisturbed sequence boundary (figures 5-16 and 5-17). Correspondingly, as previous areas of CSS-2 preferred orientation trends are observed (NW-SE and NE-SW) (figure 5-16B).

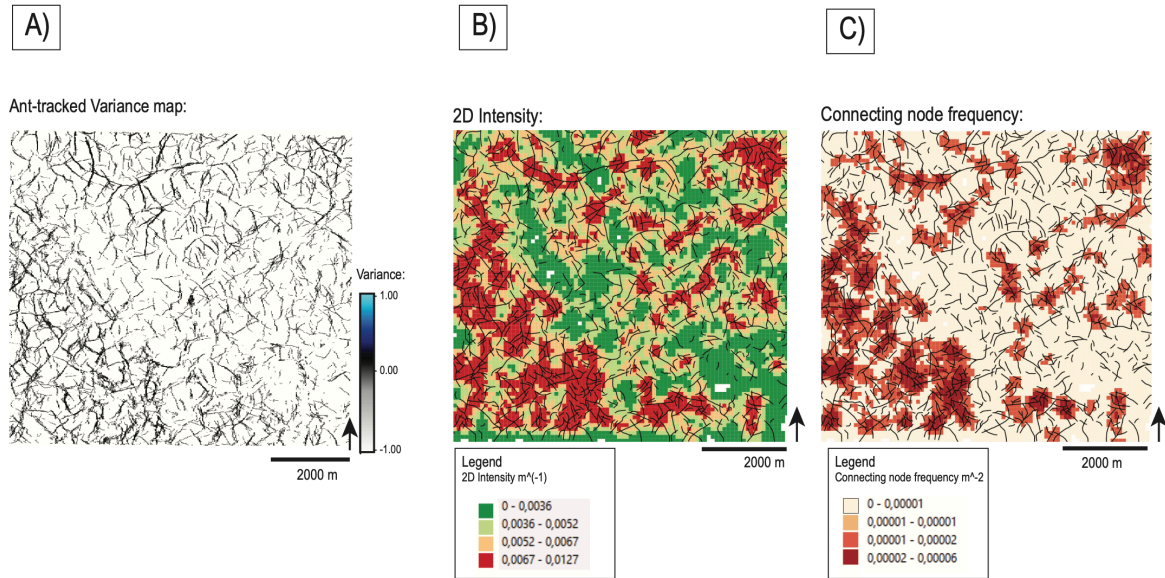


Figure 5-18: Map views of polygonal fault patterns of subarea 2B. **A)** Ant-tracked variance map used for manual fault interpretation and foundation for contour maps, **B)** 2D intensity map (m^{-1}) displaying intensity variations, and **C)** connecting node frequency map (m^{-2}). The combination of map views shows increased connectivity and intensity on the southeastern half of the area.

5.4 CSS-3 (Lower Oligocene sequence)

The sequence corresponds to the Lower Oligocene wedge sequence and is bound by top CSS-2 and top CSS-3. The sequence appears as a localized wedge unit pinching out from the eastern basin flank (section 4.2.2) (figure 5-19). CSS-3 has a prograding appearance towards the west and displays a decrease in thickness of the wedge sequence distal in the basin (figure 5-19). The seismic signature of the sequence is relatively uniform, holding medium amplitude reflections. The sequence onlaps onto top CSS-2 at the most distal part of the wedge. The sequence appears restricted to a minor area, reaching a maximum thickness of ~ 280 ms along the eastern basin flank.

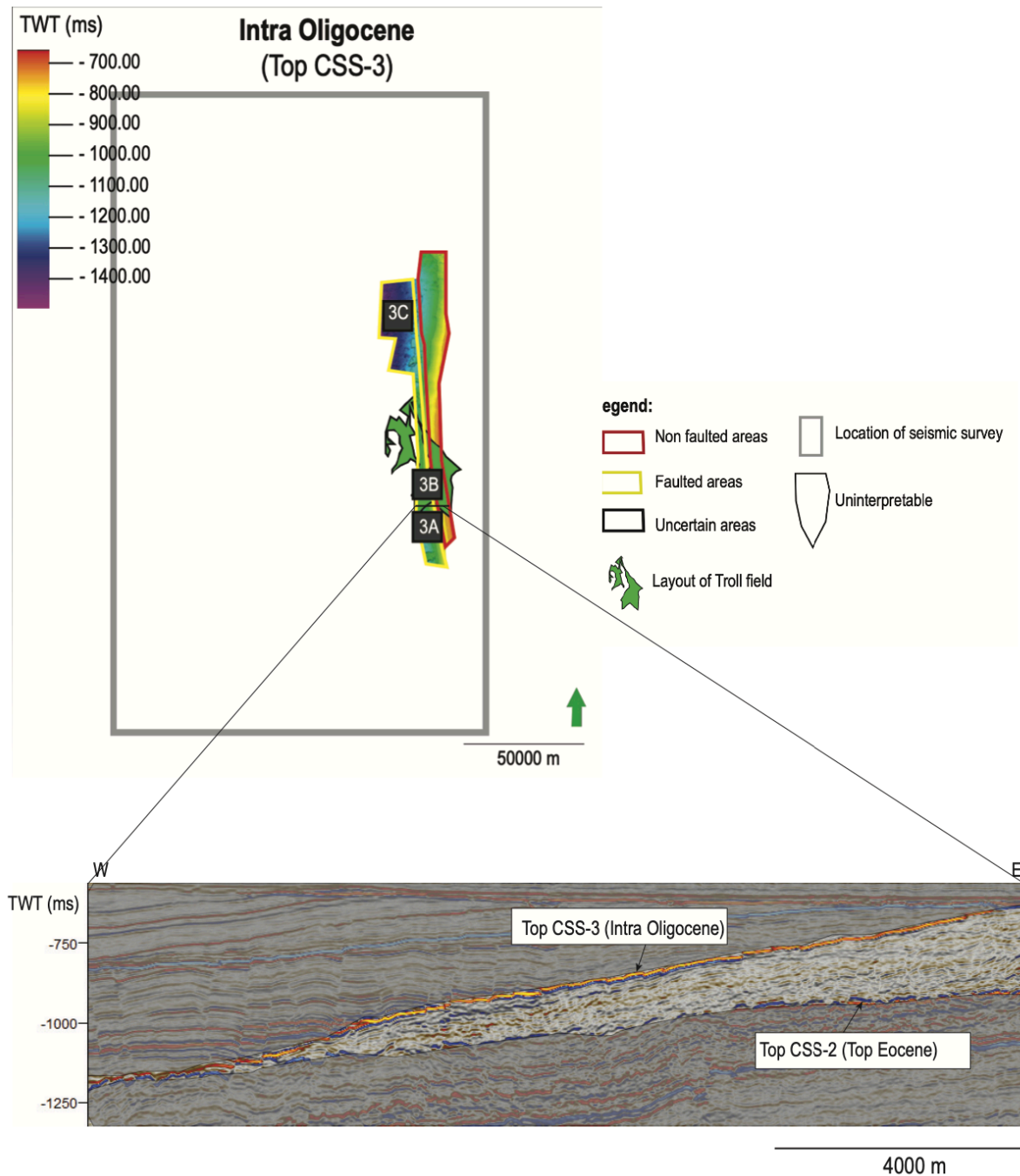


Figure 5-19: Top CSS-3 (Intra Oligocene) surface map displaying three subareas within the faulted area of the horizon. Remaining areas of the surface map display non-faulted and uncertain areas. The layout of the Troll field is used as an indicator for approximate location.

Subarea 3A

The area is located on the eastern basin flank, and the sequence displays low to medium amplitude reflections (figure 5-20A). The geometry of the fault planes is planar to gently listric, with the site of maximum fault displacement close to top CSS-2 (figure 5-20C).

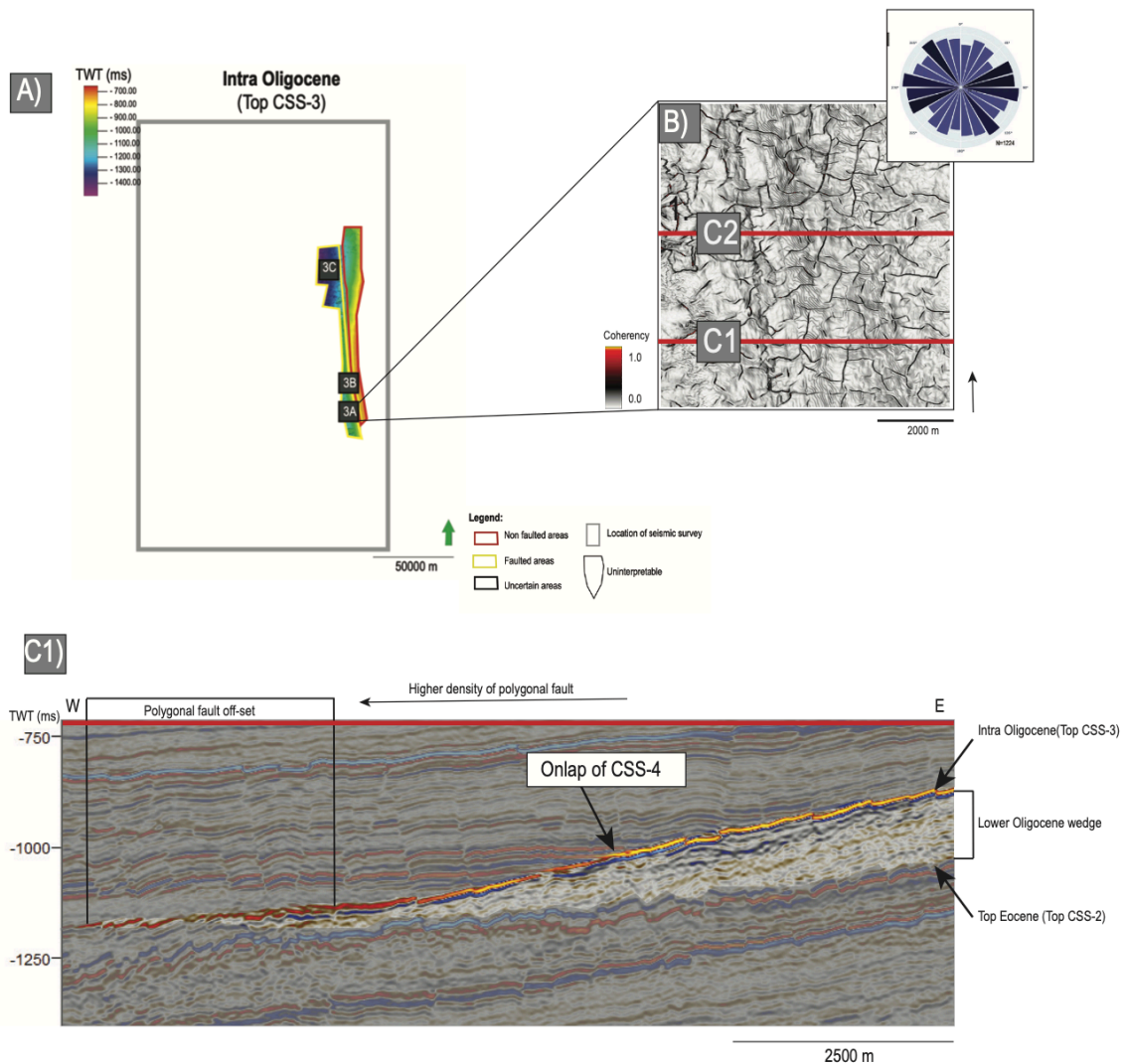


Figure 5-20: A) Intra Oligocene surface map displaying three subareas within the faulted area of the horizon. B) Variance attribute map of subarea 3A displaying plan form pattern of the polygonal faults. The red line represents the seismic cross-section. The variance map is combined with a rose diagram displaying orientation trends of the subarea, where orientation trends are marked in dark blue. C) Seismic cross-section of polygonal faults situated in CSS-3 (Lower Oligocene sequence).

First recognized from seismic cross-sections are more frequently developed faults on the western half of the sequence displaying propagated fault planes to adjacent sequences (figures 5-20A and 5-21). The opposite half of the sequence displays a set of more prominent normal faults that extend at a depth of ~750 ms from top CSS-5/6 to top CSS-0 (figure 5-21). Remaining faults on this half display minor normal faults (~ 50 ms) that appear close to the sequence boundaries. Observations from the variance map of top CSS-3 display a polygonal geometry of rectangular to curved plan form patterns of the faults, with relatively high

connectivity of $1.17 C_b$ (figure 5-20B). Seismic cross-sections show an alternation of fault planes intersecting into CSS-3 (figure 5-21). The polygonal faults display a slightly preferred E-W trend (figure 5-20B).

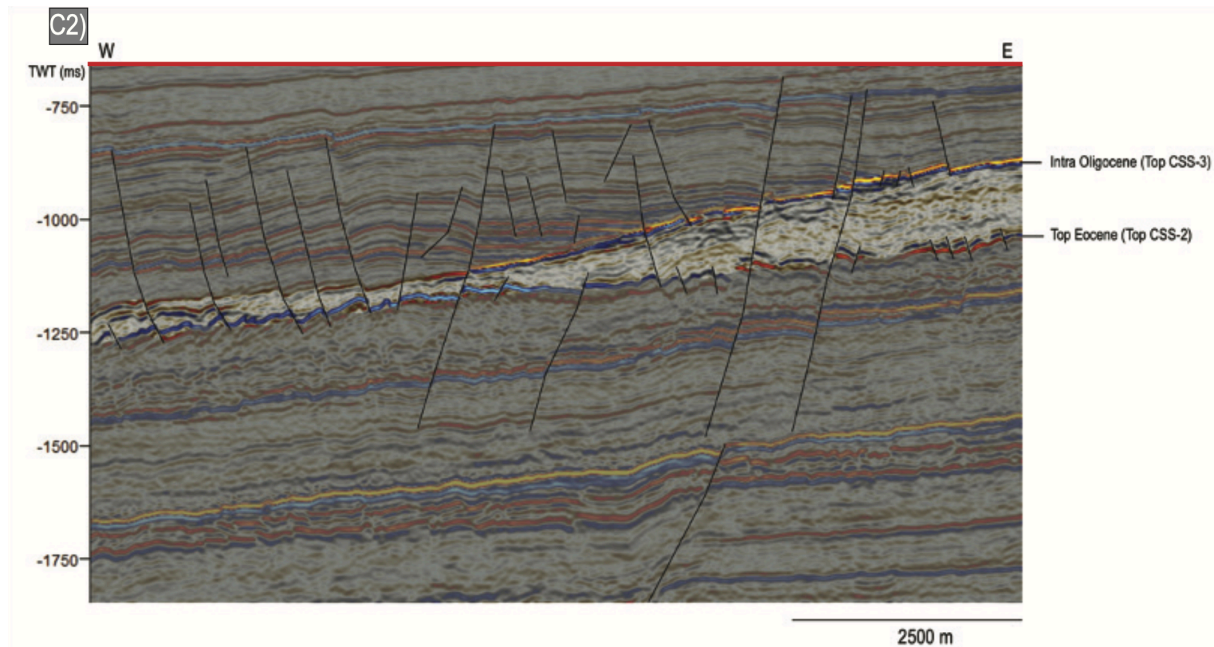


Figure 5-21: E-W seismic cross-section displaying interpreted fault planes of polygonal faults in subarea 3A. Faults tend to intersect more frequently on the western half compared to the eastern half. The sequence holds a set of larger and minor faults.

Subarea 3B

The area is located on the eastern basin flank, north of the previously described subarea (figure 5-22A). The sequence displays medium amplitude reflections with observed minor normal faults that show relatively high connectivity of $1.07 C_b$. The variance map of top CSS-3 displays a polygonal geometry of isolated to curved plan form patterns of the polygonal faults (figure 5-22B). However, do the variance map display denser polygonal fault traces on the western half of the sequence. The top and base reflections of the sequence display dissimilarities. Top CSS-3 shows a bright, high amplitude, polygonal faulted reflection, and top CSS-2 exhibits a rotated, lower amplitude reflection, with a higher density of polygonal faults (figure 5-22C). Polygonal faults are observed in narrow intervals close to the top and base of the sequence, with additional faults extending from top to base. The geometry of the fault planes is observed as planar and listric through seismic cross-sections (figure 5-22C). The maximum

fault displacement is located close to the rotated, displaced top CSS-2 (figure 5-22C). The reflections underlying top CSS-3 (~50 ms) exhibit low to medium amplitude reflections. Below is the unit more transparent with low amplitude reflections (figure 5-22C). The polygonal faults in CSS-3 appear connected to underlying and overlying sequences, where the propagated fault planes expose seismic signatures of alternating fault plane dip in underlying sequences.

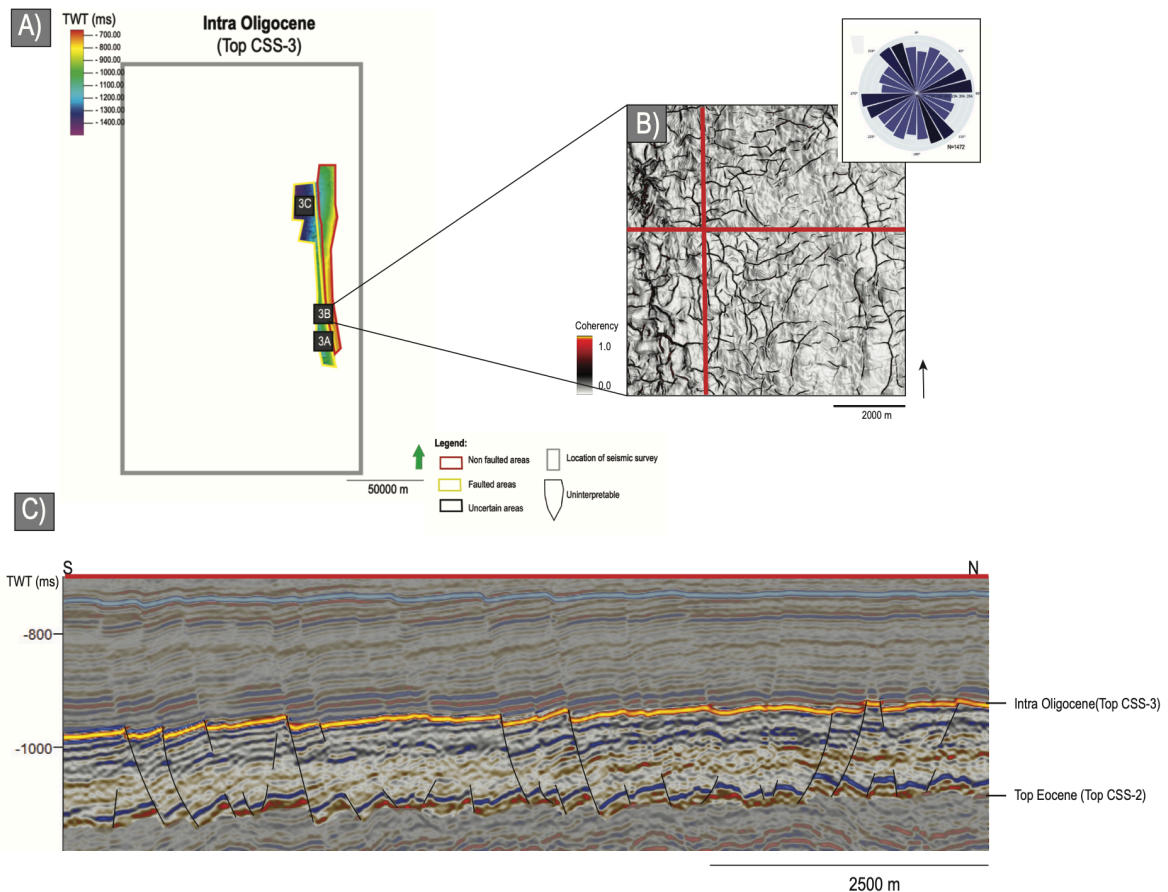


Figure 5-22: A) Intra Oligocene surface map displaying three subareas within the faulted area of the horizon. B) Variance attribute map of subarea 3B displaying plan form pattern of the polygonal faults. The red line represents the seismic cross-section. The variance map is combined with a rose diagram displaying orientation trends of the subarea, where orientation trends are marked in dark blue. C) Seismic cross-section of polygonal faults situated in CSS-3 (Lower Oligocene sequence).

Observations from seismic cross-sections display a prominent normal fault cross-cutting through nearby Cenozoic sequences on the eastern half of the sequence (figure 5-23). There are no observable structural features influenced by the major faulting event. The area exhibit slightly preferred NW-SE and NE-SW trends of the polygonal faults (figure 5-22B).

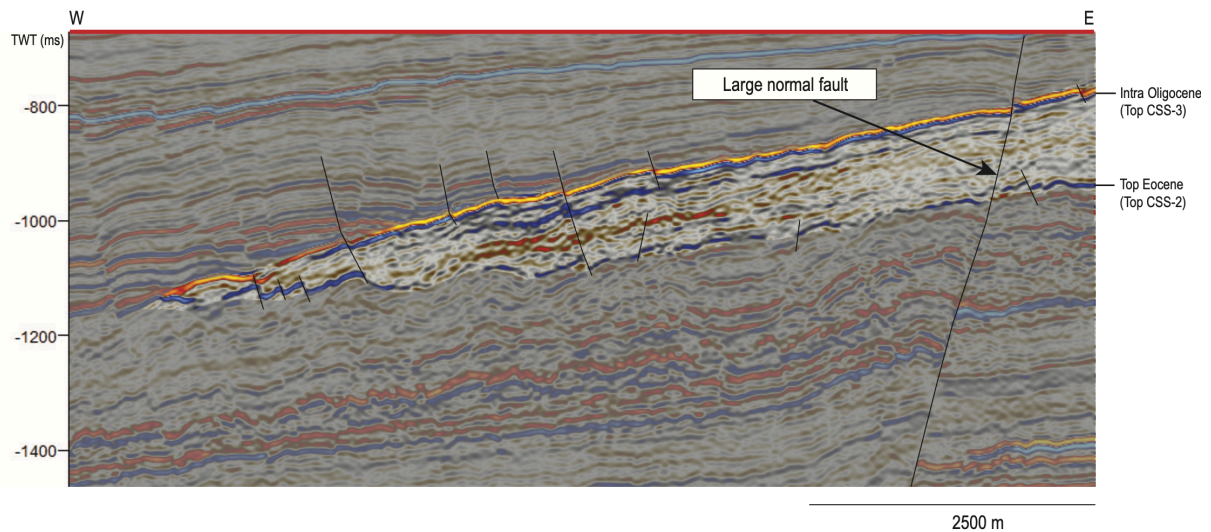


Figure 5-23: E-W seismic cross-section displaying polygonal faults in subarea 3B. The large normal fault intersecting present Cenozoic sequences does not impact the orientation of polygonal faults in the Lower Oligocene sequence (CSS-3).

Subarea 3C

The area is located north on the eastern basin flank, where the sequence is characterized by medium amplitude reflections observed with minor normal faults (figure 5-24A). The normal faults display a planar to listric fault plane geometry, and the site of maximum fault displacement is observed as a variable within the sequence. The variance map of Top CSS-3 displays curved plan form patterns of the faults that exhibit connectivity of 0.84 C_b and slightly preferred orientation trends (NW-SE and NE-SW) (figure 5-24B). The identified polygonal faults in the sequence are intersecting into overlying and underlying sequences (figure 5-24C).

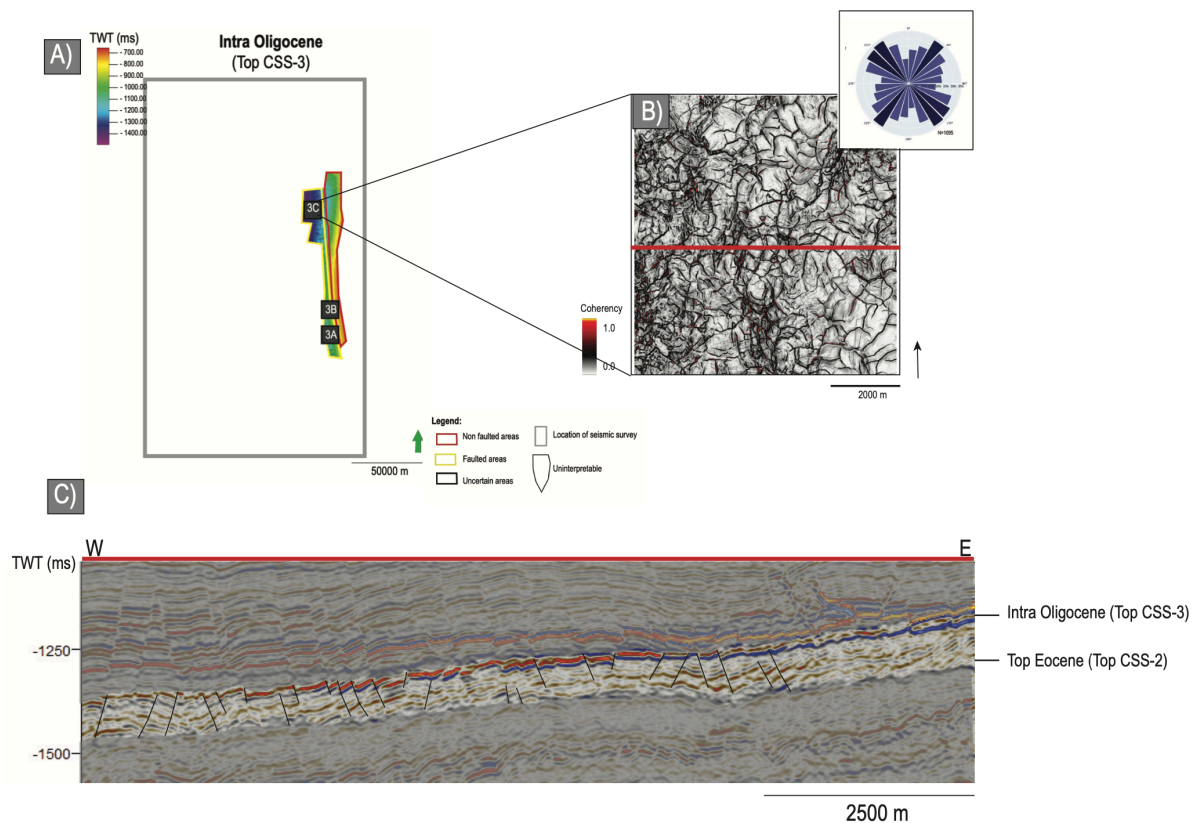


Figure 5-24: A) Intra Oligocene surface map displaying three subareas within the faulted area of the horizon. B) Variance attribute map of subarea 3C displaying plan form pattern of the polygonal faults. The red line represents the seismic cross-section. The variance map is combined with a rose diagram displaying orientation trends of the subarea, where orientation trends are marked in dark blue. C) Seismic cross-section of polygonal faults situated in CSS-3 (Lower Oligocene sequence).

5.5 CSS-4 (Upper Oligocene sequence)

The sequence corresponds to the Upper Oligocene sequence and is bound by top CSS-2, top CSS-3, and top CSS-4, representing the base Miocene surface. The sequence appears with a varied thickness and reaches a maximum thickness of ~630 ms near the North Viking Graben in the basin center (section 4.2.2). The sequence displays piles of chaotic seismic reflections near the transition of the basin flanks and basin center. Disregarding variations, the sequence holds medium to high amplitude reflections. The sequence appears extensive and is present further north and south in the study area (figure 5-25). On the eastern flank, the sequence is observed onlapping onto the wedge-shaped CSS-3. The abundance of the CSS-3 is poorly observed on the southern half, and CSS-4 appears underlain by CSS-2 in the remaining areas.

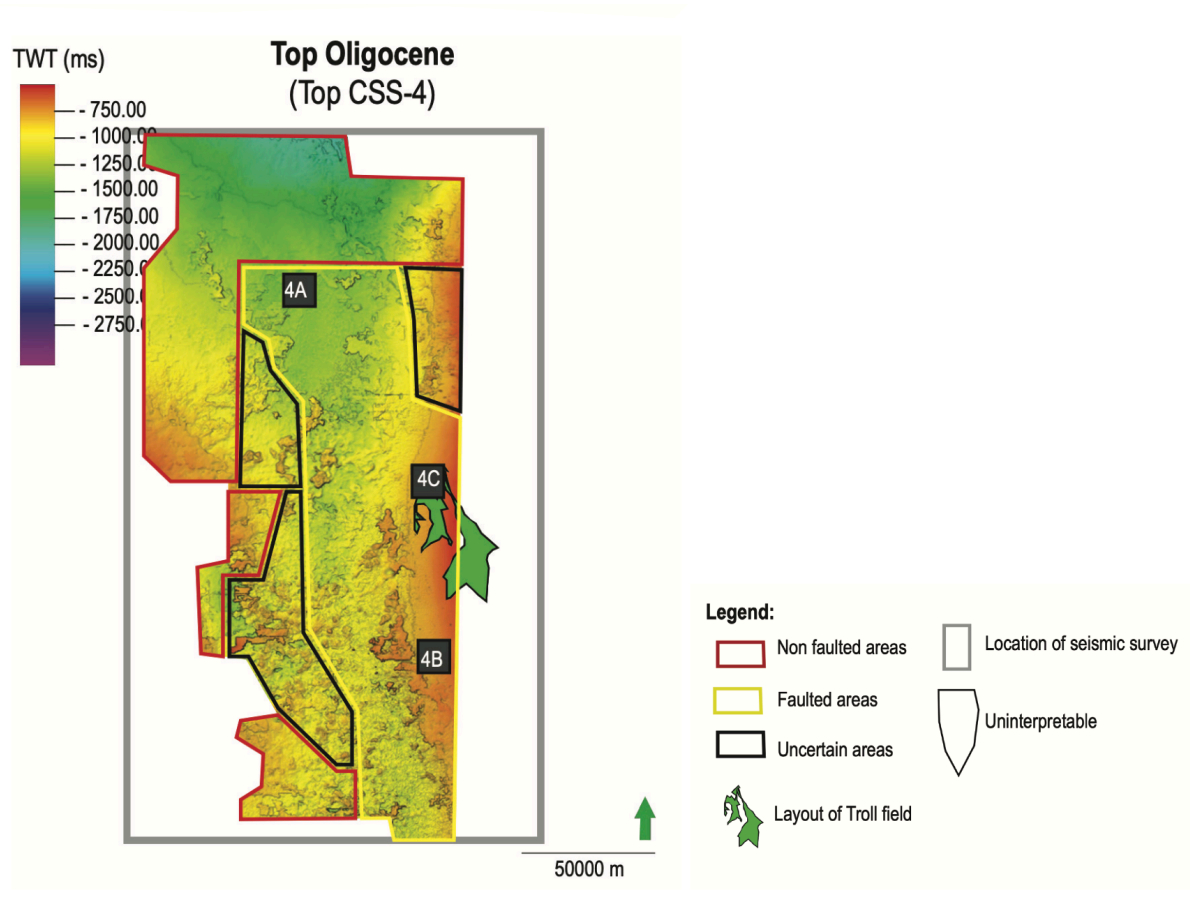


Figure 5-25: Top CSS-4 (Top Oligocene) surface map displaying three subareas within the faulted area of the horizon. Remaining areas of the surface map display non-faulted and uncertain areas. The layout of the Troll field is used as an indicator for approximate location.

Seismic reflection event

CSS-4 is divided as two separate units separated by a flat seismic reflection event (figure 5-26). The upper unit of the sequence exhibit layer-bound, high amplitude reflections, where the lower unit of the sequence exhibits low-medium amplitude reflection with more transparent characteristics (figure 5-26).

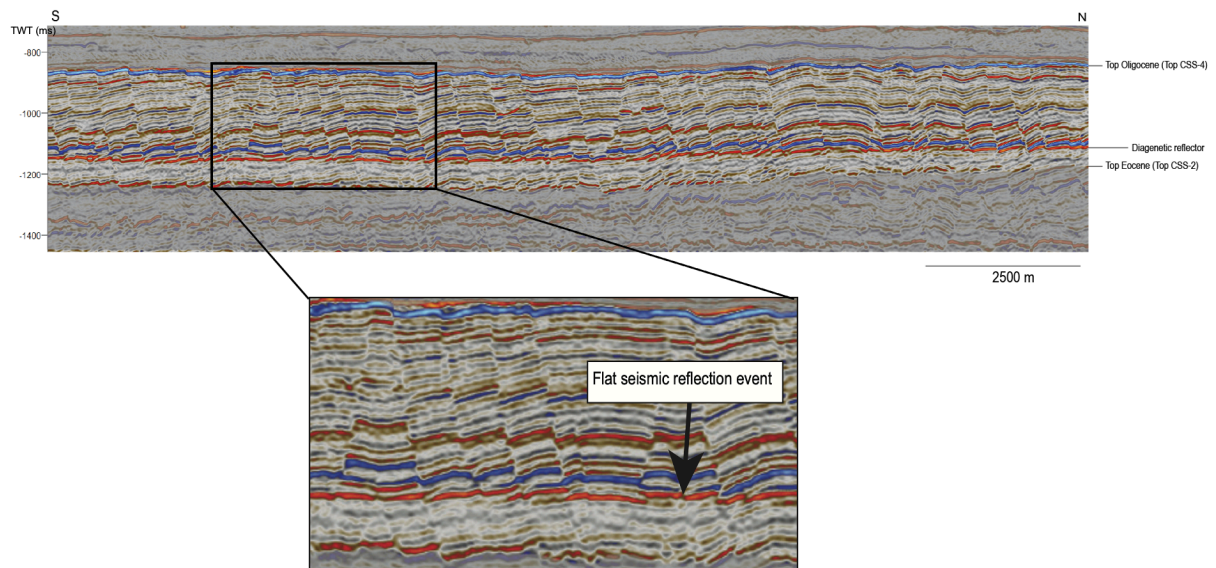


Figure 5-26: N-S seismic cross-section displaying the flat, seismic reflection event situated in the middle of CSS-4, dividing the sequence into two units with unlike reflectivity.

The two units separated by a flat reflection event are characterized by a positive seismic polarity and cross-cutting previous reflections (figure 5-26). The seismic reflection event is located on the eastern half of the study area, covering a region of 6446.25 km². As the reflection approach the western half of the study area, it gradually phases out into a low amplitude, chaotic and disturbed reflection (figure 5-27). The reflection event is observed with minor off-sets in communication with fault intersections (figure 5-26). The reflection event is located at depths ranging between ~1000-1200 ms.

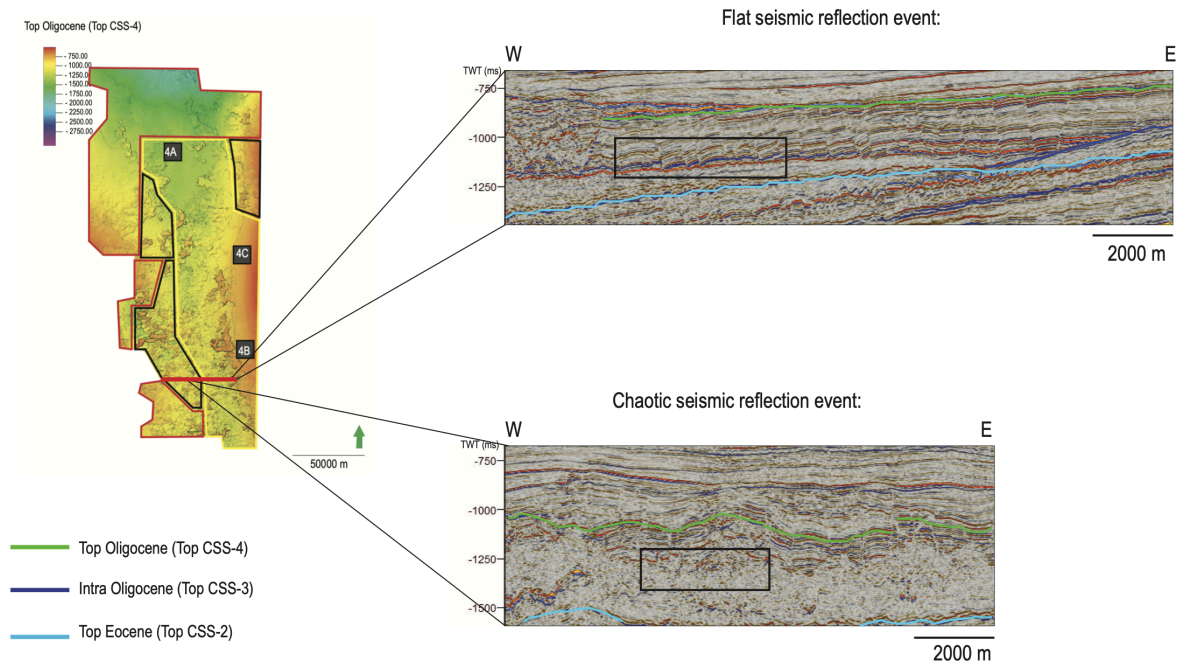


Figure 5-27: E-W seismic cross-section displaying the reflection event in the middle of CSS-4 altering from a flat seismic reflection event located on the eastern half that phases out into a more chaotic reflection that is hard to track further west in the basin.

Subarea 4A

The area is located on the northern basin floor, where the sequence is displayed with medium amplitude reflections (figure 5-28A). Seismic cross-sections display dense networks of normal faults in the sequence displaying relatively high connectivity of $1.24 C_b$ (figure 5-28C). The variance map of top CSS-4 displays a polygonal geometry of isolated to curved plan form patterns of the polygonal faults (figure 5-28B).

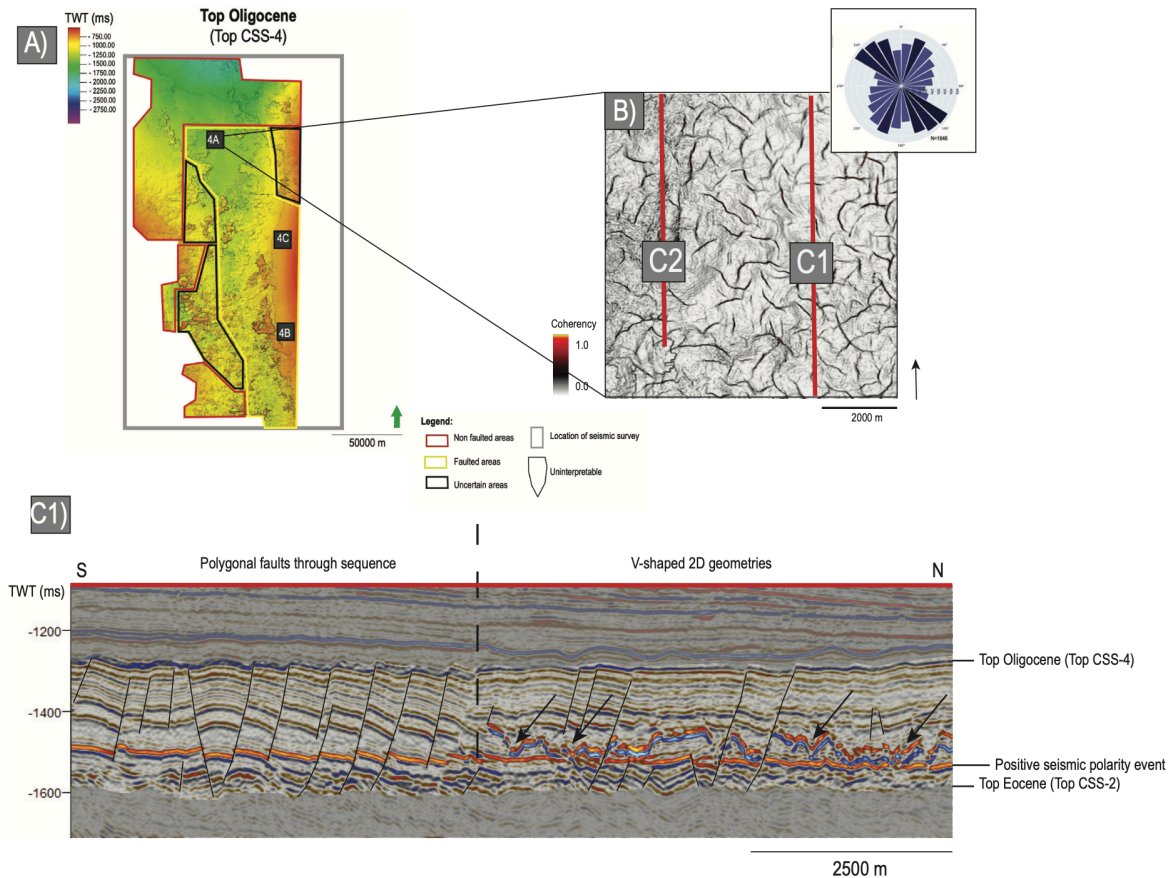


Figure 5-28: A) Top Oligocene surface map displaying three subareas within the faulted area of the horizon. B) Variance attribute map of subarea 4A displaying plan form pattern of the polygonal faults. The red line represents the seismic cross-section. The variance map is combined with a rose diagram displaying orientation trends of the subarea, where orientation trends are marked in dark blue. C) Seismic cross-section of polygonal faults situated in CSS-4 (Upper Oligocene sequence).

Top CSS-4 displays a displaced reflection that exhibits traces of the site of fault tip termination (figure 5-28C). The offsets of top CSS-4 are traced through the sequence and show the maximum fault displacement is in the upper unit (figure 5-28C). Features as graben/horst and bent reflections are also observed within the densely faulted upper unit of the sequence (figure 5-28C). In addition, is V-shaped 2D-geometries with high amplitude reflections observed above flat seismic reflection event (figure 5-29). In the western half of the sequence, it is possible to distinguish between a polygonal faulted upper unit in the south and V-shaped 2D geometries in the north (figure 5-28C). The transition is declining towards the eastern half of the sequence. The fault plane geometries of the polygonal faults are observed as planar to gently listric, alternating to a gentler dip below the flat reflection event. Observations of polygonal faults in the lower unit display intersecting into the underlying sequence.

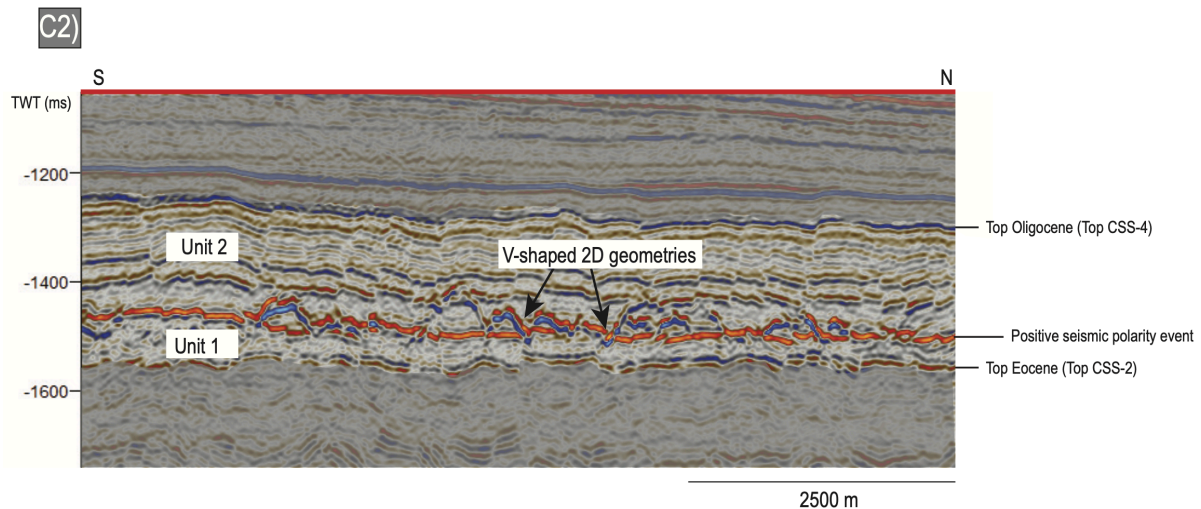


Figure 5-29: N-S seismic cross-section displaying CSS-4 divided into two separate units by a seismic reflection event. V-shaped 2D geometries are observed close to the reflection event in the middle of the sequence.

First recognized from the variance map view, a more frequent polygonal fault pattern in the southern part of the area coincides well with the previously described transition trend between polygonal faults and V-shaped geometries (figures 5-28B and 5-28C1). This observation is in addition supported by a contour map of 2D intensity and connecting node frequency. The contour map exhibit relatively well-connected fault traces except for the northeastern part of the area (figure 5-30). The polygonal faults display a slightly preferred orientation (NW-SE and NE-SW) (figure 5-28B).

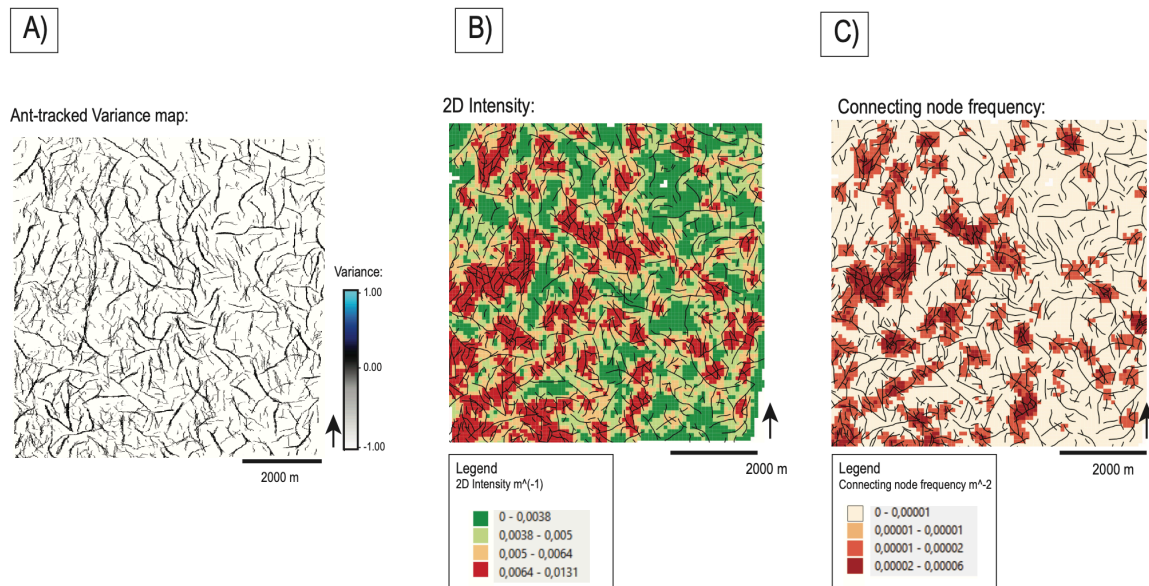


Figure 5-30: Map views of polygonal fault patterns of subarea 4A. **A)** Ant-tracked variance map used for manual fault interpretation and foundation for contour maps, **B)** 2D intensity map (m^{-1}) displaying intensity variations, and **C)** connecting node frequency map (m^{-2}). The combination of map views shows increased connectivity and intensity on the eastern half of the area.

Subarea 4B

The area is located on the southeastern basin flank, where the sequence is characterized by medium amplitude reflections displaying minor normal faults (figures 5-31A and 5-31C). The minor normal faults are situated close to top CSS-4, and the faults show overall connectivity of $0.93 C_b$. The fault planes are observed as planar to gently listric, displaying the site of maximum fault displacement in the upper unit (figure 5-31C). The flat seismic event shows a minor offset compared to the upper- and lower-unit faults intersecting the sequence (figure 5-31C). The variance map of top CSS-4 displays a polygonal geometry of curved plan form patterns of the polygonal faults that shows a vaguely favored orientation trend (E-W and NW-SE) (figure 5-31B).

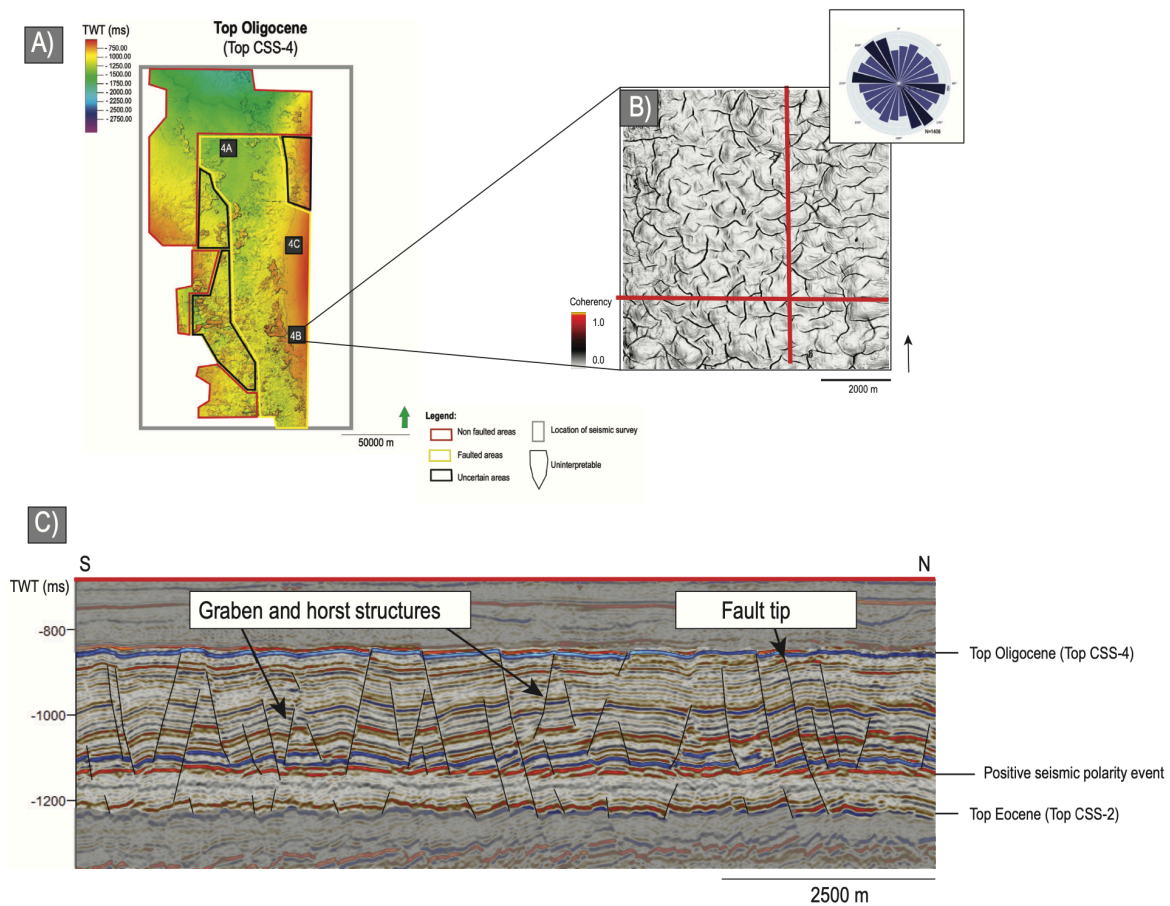


Figure 5-31: A) Top Oligocene surface map displaying three subareas within the faulted area of the horizon. B) Variance attribute map of subarea 4B displaying plan form pattern of the polygonal faults. The red line represents the seismic cross-section. The variance map is combined with a rose diagram displaying orientation trends of the subarea, where orientation trends are marked in dark blue. C) Seismic cross-section of polygonal faults situated in CSS-4 (Upper Oligocene sequence).

The polygonal faults intersecting through the sequence display commonly a gentler dip in the lower unit (figure 5-31C). In addition, display the lower unit a set of minor polygonal faults (lengths of ~ 50 ms) located close to top CSS-2, which appear close to uniform planar fault plane and intersects into the underlying sequence (figure 5-31C). Seismic cross-sections display structures of graben/horsts and bent reflections in the upper unit above the flat seismic event (figure 5-31C). Observations from seismic cross-sections display a mounded feature within the upper unit of the area. In addition, mounded features appear with chaotic and disturbing reflections, combined with V-shaped 2D geometries and reverse faults directly above the flat seismic event (figure 5-32). The mounded features act as a disturbance in the polygonal faulted unit, and a sharp boundary separates the mounded feature from the parallel, layer-bound

polygonal faults. Observations from the surface and variance map display an N-S orientation of the mounded feature, located perpendicular to the basin slope (figure 5-33).

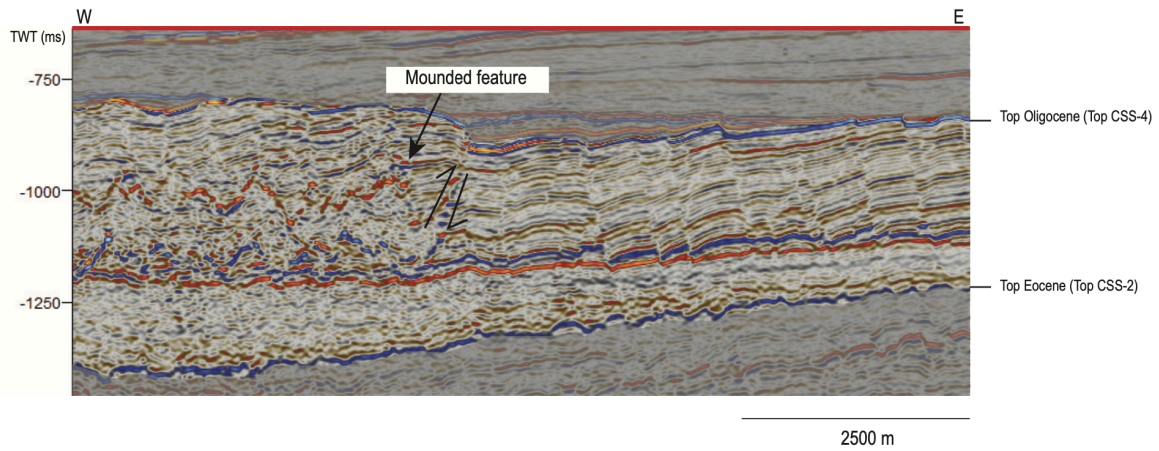


Figure 5-32: E-W seismic cross-section displaying mounded feature in the upper unit of CSS-4. The mounded feature displays traces of V-shaped 2D geometries directly above the flat seismic event. The sharp boundary between the polygonal faulted unit and the mounded unit shows reverse faulting.

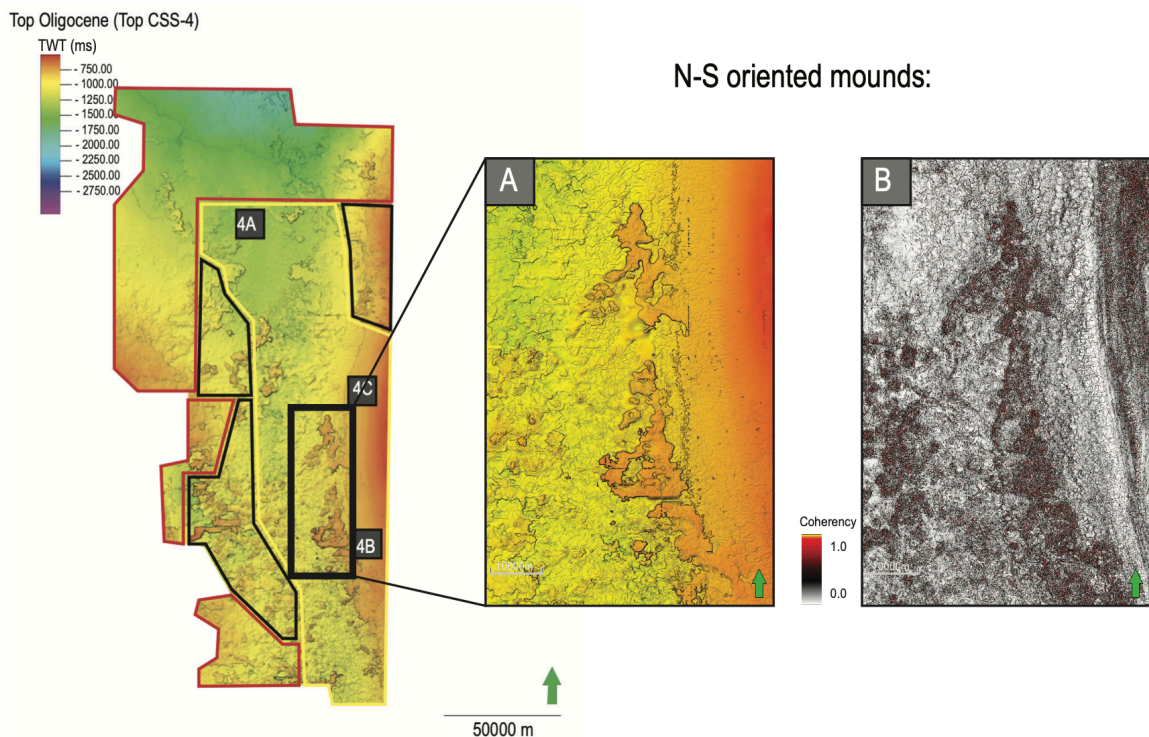


Figure 5-33: Distribution of mounded feature displayed from Top Oligocene surface map. **A)** Zoomed in surface map of the mounds situated near the base of the eastern basin slope, and **B)** variance attribute map of the same area displays a clear N-S oriented mounded feature.

Subarea 4C

The area is located on the eastern basin flank, where the sequence is characterized with medium amplitude reflections (figures 5-34A and 5-34C). The variance map of top CSS-4 displays a polygonal geometry of isolated to curved plan form patterns of the polygonal faults that show relatively low connectivity ($C_b = 0.90$) (figure 5-34B).

The two units of CSS-4 display different amplitude strengths, where the upper unit exhibit medium amplitude reflections, while the lower unit exhibit high amplitude reflections (figure 5-34C). The upper fault tips are observed in the upper unit and terminate close to top CSS-4. Faults are observed intersecting through the sequence with a fault plane that displays planar to gently listric geometries. The site of maximum fault displacement is in the lower unit close to top CSS-2 that shows a bright polygonal faulted reflection (figure 5-34C). Observations of graben/horst and bent reflections are repetitive structures in the sequence and occur as structures among the polygonal faults (figure 5-34C). Seismic cross-sections and variance maps display an E-W trend where polygonal faults are more developed towards the west in the sequence (figure 5-34B). The polygonal faults display a vaguely preferred orientation trend (N-S) (figure 5-34B).

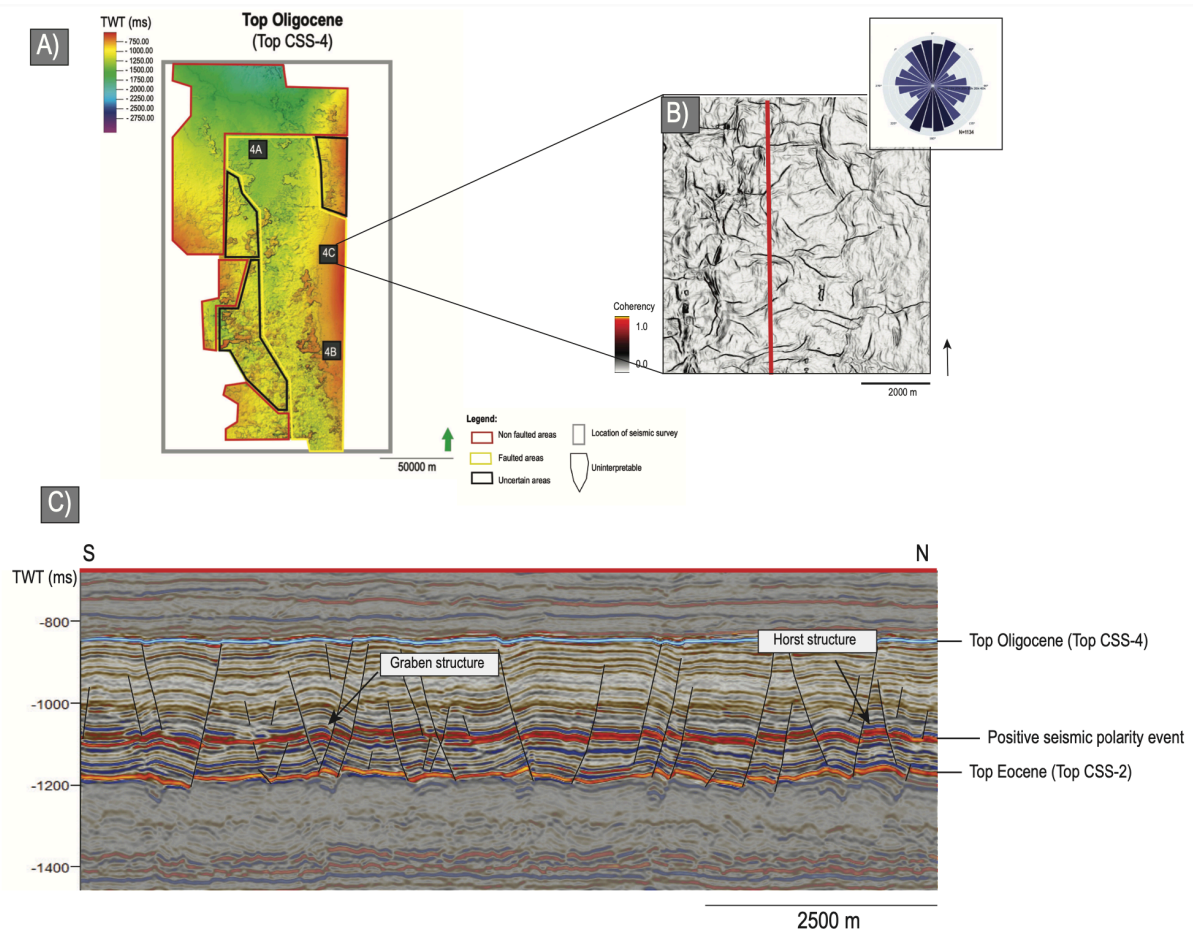


Figure 5-34: A) Top Oligocene surface map displaying three subareas within the faulted area of the horizon. B) Variance attribute map of subarea 4C displaying plan form pattern of the polygonal faults. The red line represents the seismic cross-section. The variance map is combined with a rose diagram displaying orientation trends of the subarea, where orientation trends are marked in dark blue. C) Seismic cross-section of polygonal faults situated in CSS-4 (Upper Oligocene sequence).

The plan form pattern of faults appreciated from the variance map displays different geometries through the sequence (figure 5-35B). It appears that fault patterns become more visible and distinct towards the top of the sequence and intersect into the overlying sequence (figure 5-35A).

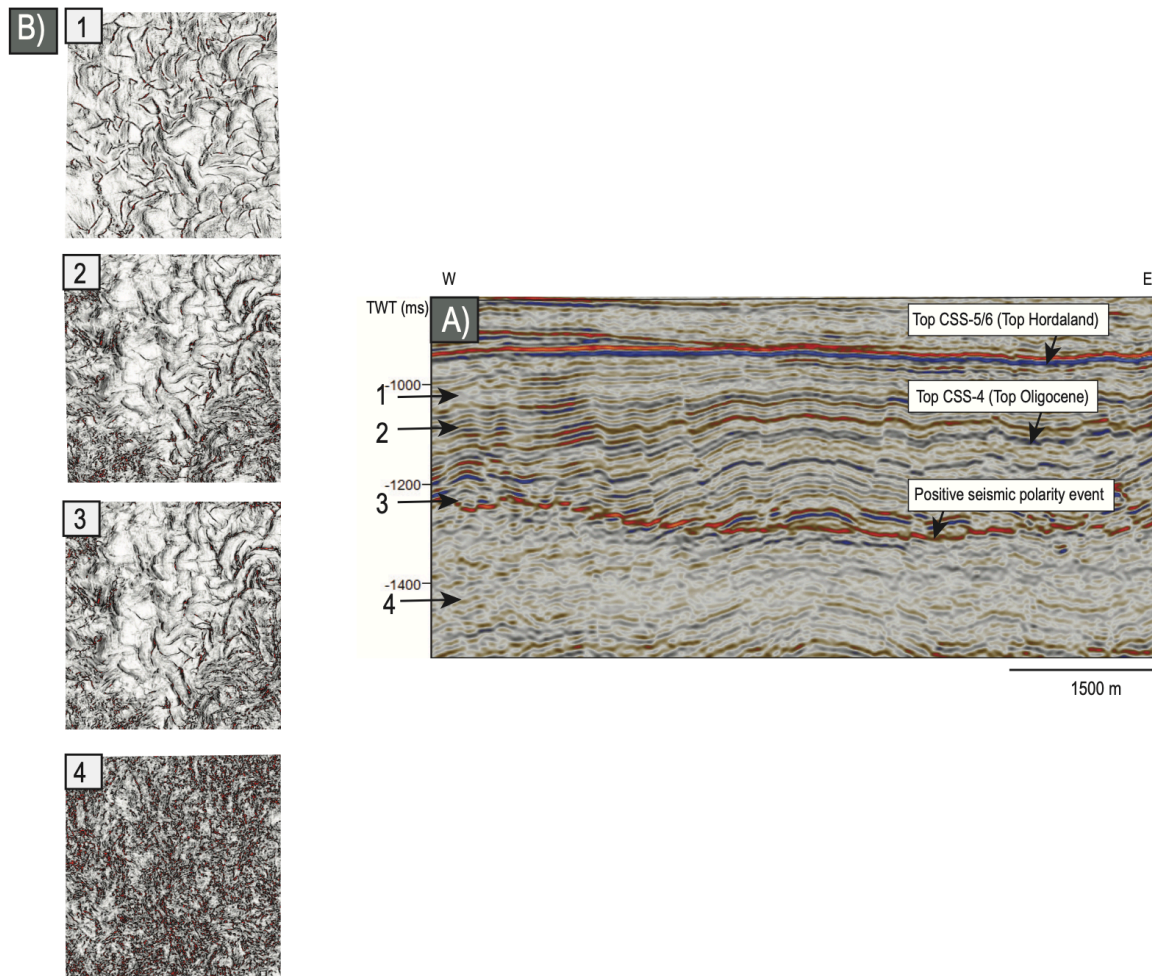


Figure 5-35: *A) Seismic cross-section displaying polygonal faulted CSS-4. CSS-4 holds a flat seismic reflection event dividing the sequence into two distinct units. B) Variance attribute maps displaying various plan form patterns of the polygonal faults from below the flat seismic reflection event (4) towards the top of the sequence (2) and into the overlying sequence (1).*

5.6 CSS-5/6 (Lower Miocene sequence)

The sequence corresponds to the Lower Miocene sequence and is bound by top CSS-4 and top CSS-5/6. The sequence appears with a varying thickness, filling in fluctuating topography from underlying CSS-4. The sequence reaches a maximum thickness of ~200 ms near the North Viking Graben in the basin center (section 4.2.2). The seismic characteristic of the sequence is relatively uniform with continuous seismic reflections. The sequence appears extensive further south but thins and transpires towards the north (figure 5-36). The sequence is mainly situated distally near the basin center and is not observed ascending at the basin flanks. The sequence

displays a seismic signature of onlapping onto underlying CSS-4, displayed on the western and eastern basin flank.

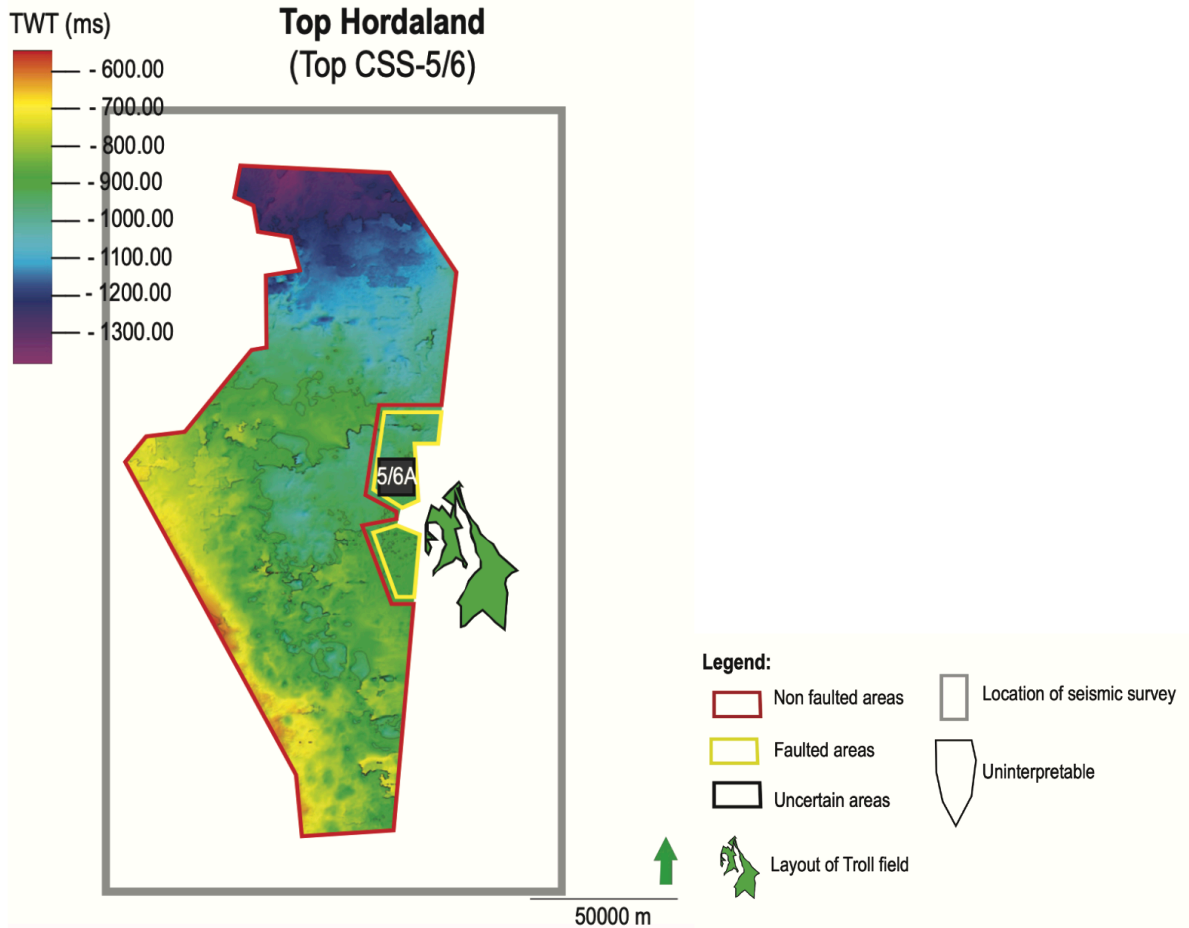


Figure 5-36: Top CSS-5/6 (Top Hordaland) surface map displaying one subarea within the faulted area of the horizon. Remaining areas of the surface map display non-faulted and uncertain areas. The layout of the Troll field is used as an indicator for approximate location.

Subarea 5/6A

The area is located on the eastern basin slope, where the sequence is characterized by low-medium amplitude reflections with minor normal faults (figure 5-37A). The variance map of top CSS-5/6 displays a polygonal geometry of isolated to curved plan form patterns of the polygonal faults that show moderate connectivity of $0.95 C_b$ (figure 5-37B).

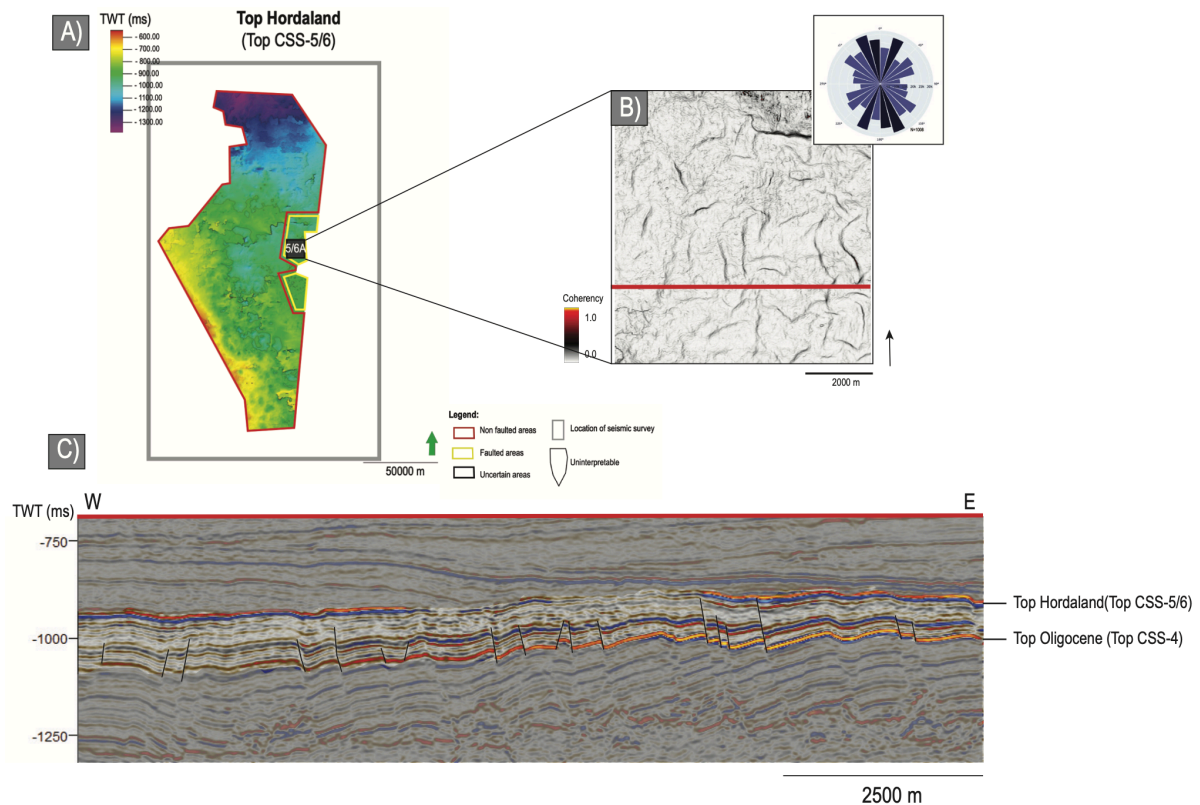


Figure 5-37: A) Top Hordaland surface map displaying three subareas within the faulted area of the horizon. B) Variance attribute map of subarea 5/6 displaying plan form pattern of the polygonal faults. The red line represents the seismic cross-section. The variance map is combined with a rose diagram displaying orientation trends of the subarea, where orientation trends are marked in dark blue. C) Seismic cross-section of polygonal faults situated in CSS-5/6 (Lower Miocene sequence).

The sequence shows two separate units, an upper unit that displays transparent, low amplitude reflections and a lower unit that displays medium amplitude faulted reflections (figure 5-37C). The polygonal faults in the lower unit exhibit planar to listric fault plane geometries, where the site of maximum fault displacement is located near top CSS-4 (figure 5-37C). Top CSS-4 displays a high amplitude, faulted reflection with fault traces intersecting into the underlying sequence (figure 5-37C). Seismic cross-sections display fault terminations in the transition between the two units, and top CSS-5/6 are generally not displaced by faulting. Observations from the rose diagram display a slightly favored orientation trend of the polygonal faults (NNW-SSE and NNE-SSW). The contour maps show the highest connectivity of faults in the sequence's western half (figures 5-37B and 5-38).

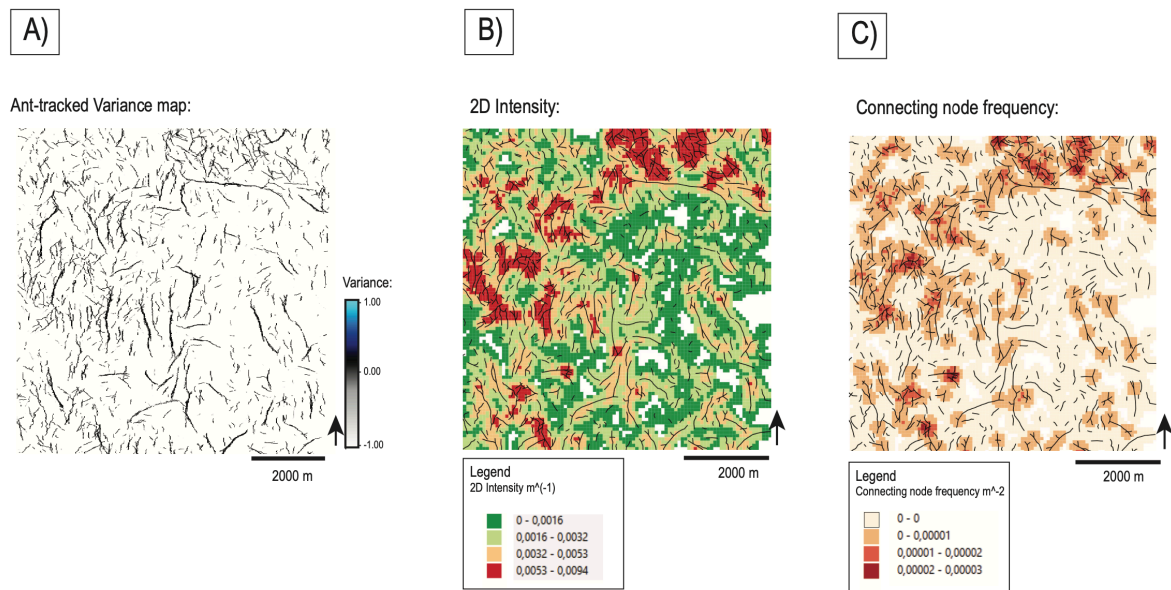


Figure 5-38: Map views of polygonal fault patterns of subarea 5/6A. **A)** Ant-tracked variance map used for manual fault interpretation and foundation for contour maps, **B)** 2D intensity map (m^{-1}) displaying intensity variations, and **C)** connecting node frequency map (m^{-2}). The combination of map views shows increased connectivity and intensity on the northwestern half of the area.

5.7 CSS-7 (Upper Miocene sequence)

The sequence corresponds to the Upper Miocene sequence and is bound by top CSS-5/6 and top CSS-7. The sequence displays various thicknesses through the study area reaching maximum thickness in the basin center of ~ 190 ms (section 4.2.2). The seismic signature is alternating between high and low seismic amplitude reflections. The sequence is present in a limited area but is present further north and south in the study area (figure 5-39). The sequence onlaps onto the underlying CSS-5/6 on the eastern basin flank and onto CSS-4 on the western basin flank.

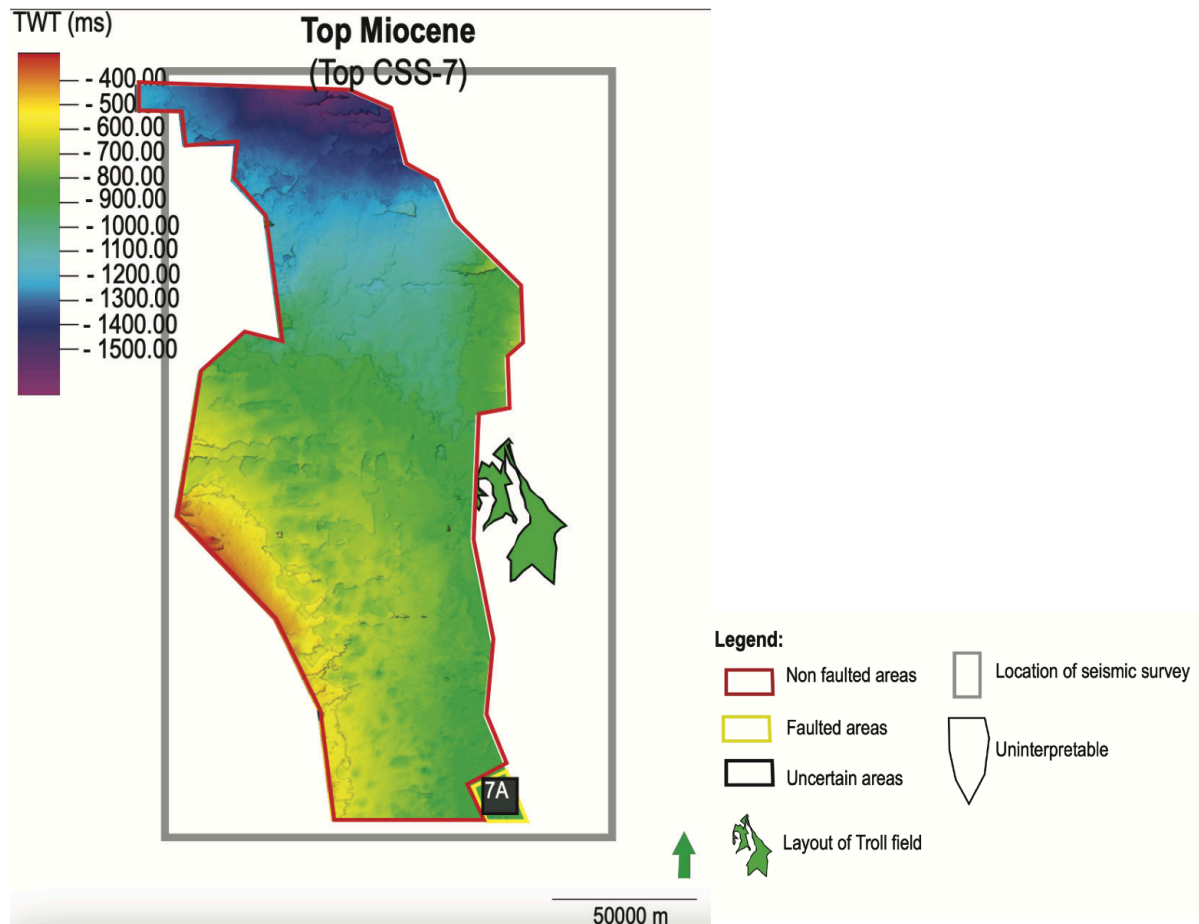


Figure 5-39: Top CSS-7 (Top Miocene) surface map displaying one subarea within the faulted area of the horizon. Remaining areas of the surface map display non-faulted and uncertain areas. The layout of the Troll field is used as an indicator for approximate location.

Subarea 7A

The area is located on the southeastern basin flank, where the sequence is characterized with medium amplitude, continuous reflections that display minor normal faults (figure 5-40A). The seismic reflections evolve to a more chaotic approach towards the west in the sequence with a loss of continuity (figure 5-40B). The variance map of top CSS-7 displays a polygonal geometry of rectangular to curved plan form patterns of faults, which exhibit moderate connectivity of $0.99 C_b$ (figure 5-40B).

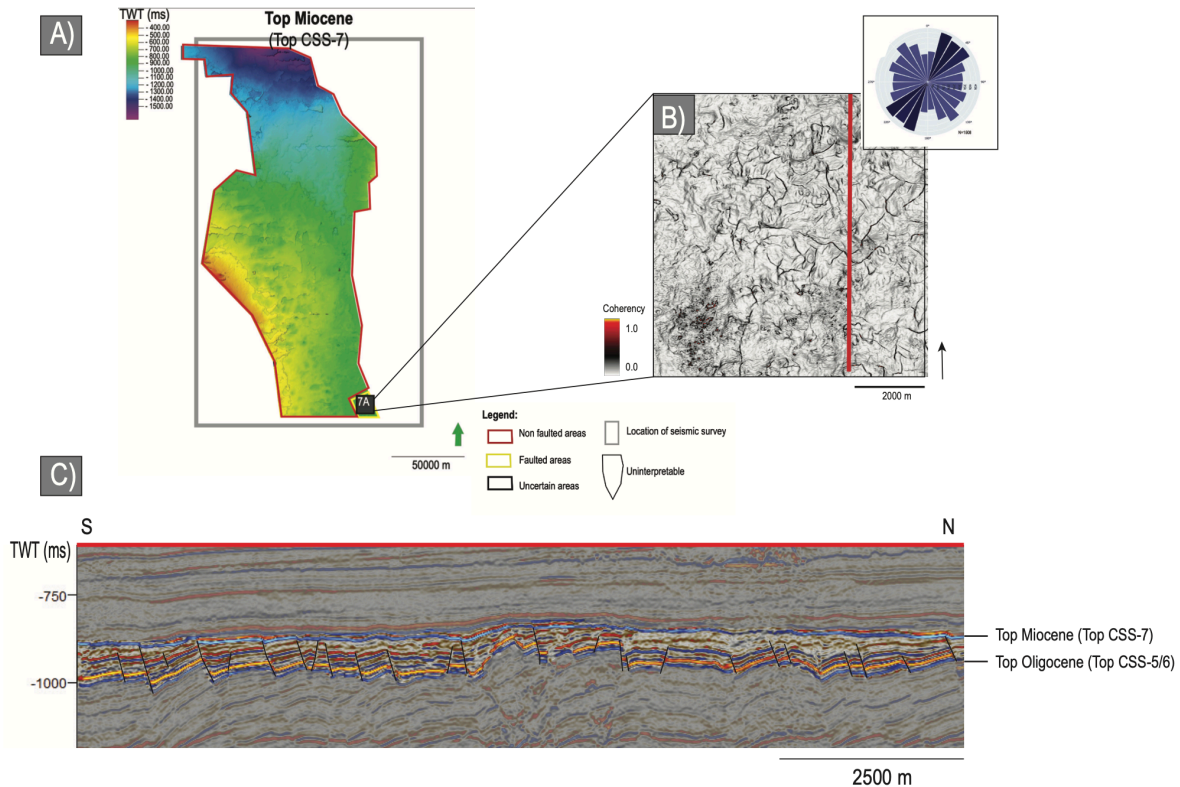


Figure 5-40: A) Top Miocene surface map displaying three subareas within the faulted area of the horizon. B) Variance attribute map of subarea 7A displaying plan form pattern of the polygonal faults. The red line represents the seismic cross-section. The variance map is combined with a rose diagram displaying orientation trends of the subarea, where orientation trends are marked in dark blue. C) Seismic cross-section of polygonal faults situated in CSS-7 (Upper Miocene sequence).

Top CSS-7 characterize the site of fault tips and termination of faults at this stratigraphic level (figure 5-40C). The fault plane displays a planar geometry and intersects through the sequence, with the site of maximum displacement is located near top CSS-5/6 (figure 5-40C). The polygonal faults show a gentler dip of the fault planes near the base and intersect into the underlying sequence. The faults show slightly preferred orientation trends (NNE-SSW) (figure 5-40B).

5.8 Summary of seismic and topological observations

A summary of the results is as follows: (1) Polygonal faults are situated in sedimentary successions ranging below Intra Paleocene to Top Miocene in the study area, (2) Polygonal faults is distributed on the eastern half of the study area from the basin flanks, basin slope reaching the basin floor, (3) The fault plane dip range from planar to gently listric, (4) The strike orientations of the polygonal faults display slightly preferable orientations of NNW-SSE, NNE-SSW, NW-SE, NE-SW, N-S and E-W, and (5) Connectivity's ranging between 0.65 – 1.30 C_B (figures 5-41 and 5-42).

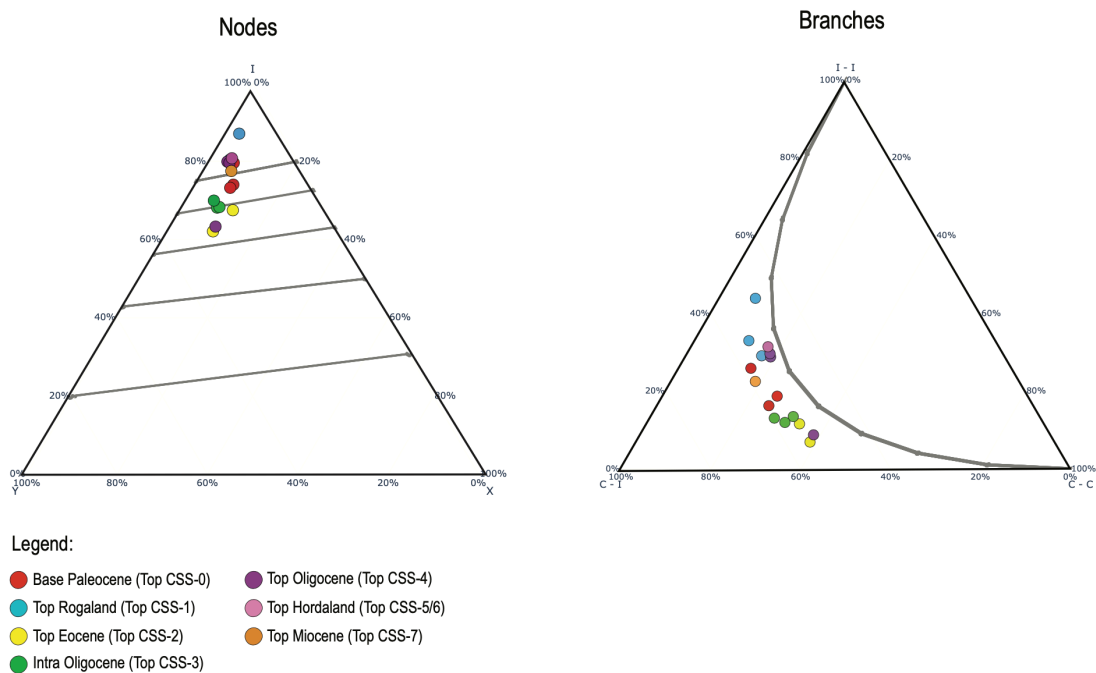


Figure 5-41: Ternary diagrams displaying the nodes and branches distribution based on stratigraphic levels.

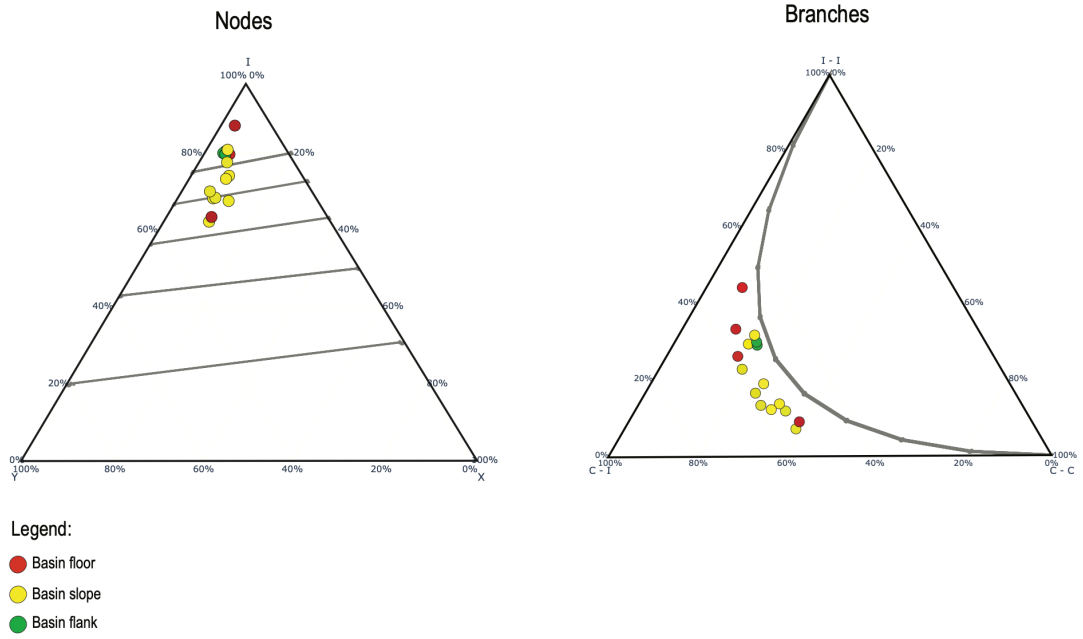


Figure 5-42: Ternary diagrams displaying the nodes and branches distribution based on basin location.

6. Summary and interpretation of observations

The summary and interpretation of observations contain a review of the seismic imaging of polygonal faults. After that, the kinematics for polygonal fault systems are discussed and interpreted. Based on the interpretation, a proposed classification system of the polygonal faults will follow. Lastly, suggested trigger mechanisms will be considered of the various polygonal fault systems in the study area.

6.1 Seismic expression of polygonal faults

Seismic observations of polygonal faults display a set of various fault patterns. Although minor subareas display minimalized parts of the abundant fault systems, the faults key pattern and seismic signatures were still identified. Below is a list of key seismic signature of the polygonal faults in the study area:

1. Polygonal faults are easily detected in plan view with complex geometries, where variance and ant-tracked attribute maps display the most easily recognizable fault traces of the faults. The fault traces form a distinct, polygonal structural pattern (figure 6-1).

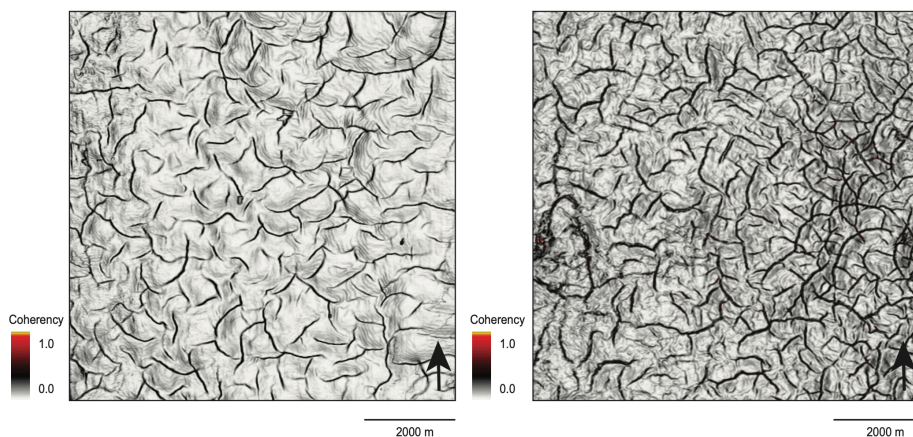


Figure 6-1: Seismic expression of polygonal fault pattern appreciated from variance attribute maps from plan view.

2. Polygonal fault systems are situated in units displaying low to high amplitude reflections that appear continuous, with clear off-sets of the polygonal fault displacement (figure 6-2).

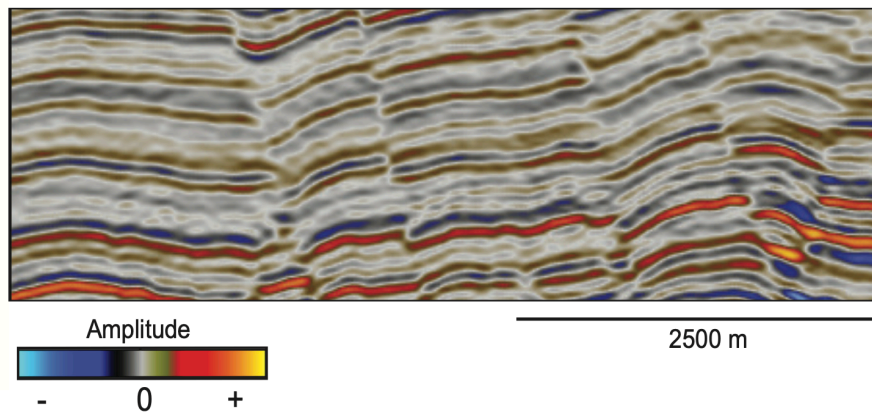


Figure 6-2: Seismic cross-section of the polygonal faults seismic expression display low to high amplitude reflections.

3. Polygonal faults develop in restricted sequences bound by sequence boundaries. A high amplitude reflection characterizes sequence boundaries of each sequence, where each sequence displays a specific seismic signature and physical properties (figure 6-3).

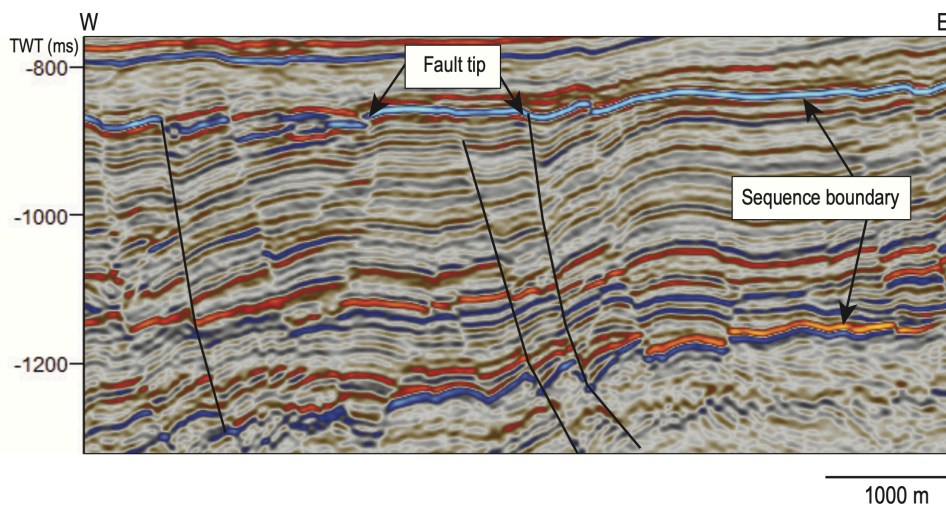


Figure 6-3: Seismic cross-section of polygonal faults restricted within a sequence. The sequence display two bright amplitude reflections as sequence boundaries. Polygonal faults are observed to develop isolated in restricted sequences and display distinct geometries.

4. Fault planes are alternating with a planar and gently listric geometry within sequences. Two outcomes are commonly observed. Firstly, fault planes generally are planar when bound to one sequence, and secondly, where fault planes appear planar to gently listric when bound to one sequence (figure 6-4).

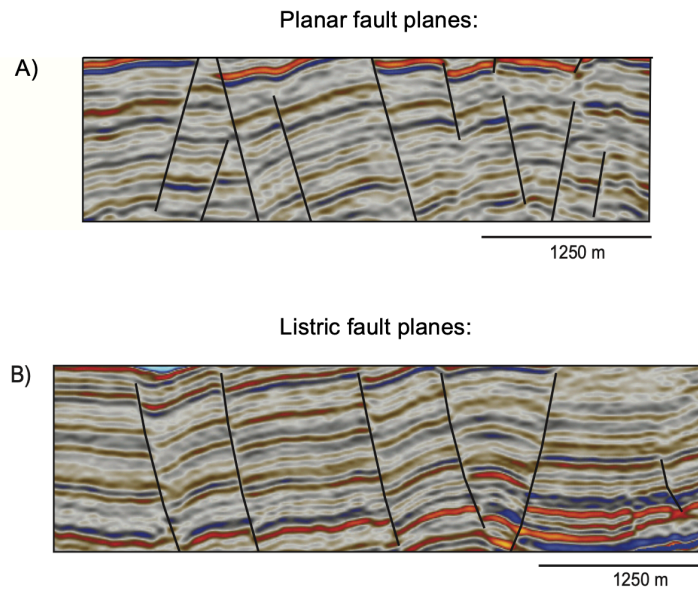


Figure 6-4: Polygonal faults display planar to gently listric fault planes when restricted to a sequence, **A)** Planar fault plane geometry restricted to a sequence, and **B)** planar to gently listric fault plane geometry restricted to a sequence.

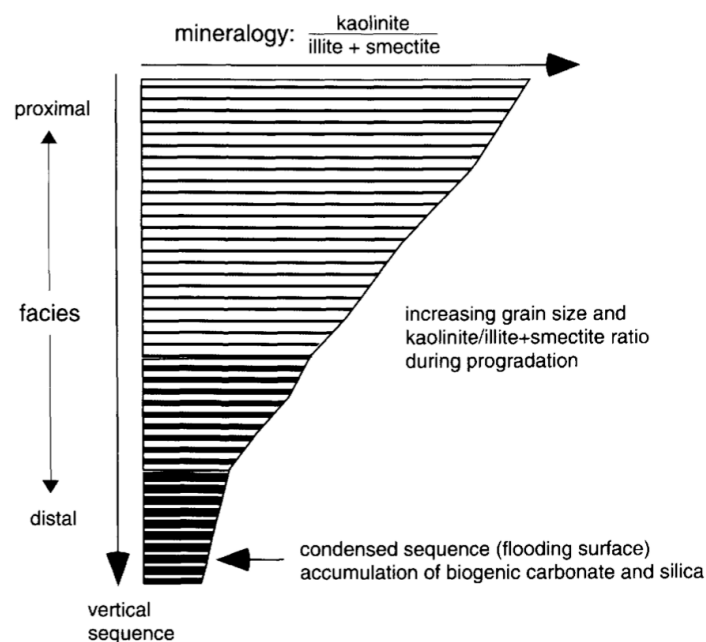
6.2 Kinematics for polygonal fault systems

6.2.1 Basin distribution

Polygonal faults appear in constrained areas in the northern North Sea, restricted to the northern basin center and eastern basin flank. The western basin flank and southern basin center exhibit an absence of polygonal fault systems (figure 4-12). The present polygonal faults display vertical variations observable within interpreted sequences. The distribution of polygonal faults in CSS-0 and CSS-1 is limited to the northern basin center and minor areas towards the eastern basin flank. Polygonal faults in CSS-2, CSS-3, and CSS-4 are mainly situated on the eastern half of the study area, covering a larger area than the underlying sequences, where the polygonal faults in CSS-5/6 and CSS-7 are restricted to minor areas on the eastern basin flank (figure 4-12).

The absence of polygonal faults can be related to either lithological variations or transparent to chaotic seismic imaging within sequences. Lithology variations are associated with the observation of vertical variations of polygonal fault systems, which are dependent on regional clay distribution within the basin at the time of deposition. The regional clay distribution is linked to the main provenance area and uplift events that affect the distribution of polygonal

faults based on an exclusive relationship related to mineralogy, grain size, and physical properties (Dewhurst et al., 1999; Thyberg et al., 2000). The main provenance area in the Cenozoic period is the East Shetland Platform located west of the study area (figure 2-1). The western location of the East Shetland Platform expresses that the eastern half of the study area is located distally from the main provenance area, possibly referred to as basin floor location under a time of deposition concerning various uplift events during the Cenozoic (Faleide et al., 2002). The mineral distribution of clays can illustrate an approximate distance of prograding clays. A high sea-level can ideally characterize a high concentration of illite and smectite distally linked to the polygonal faults at the eastern half, whereas kaolinite can be found more proximal towards the provenance area based on larger crystalline structures (figure 6-5) (Gibbs, 1977; Thyberg et al., 2000). Large crystalline structures and coarse-grained sediments may influence the formation of polygonal faults as they disappear upslope in basinal settings towards the sediment source towards the East Shetland Platform in the west (Dewhurst et al., 1999). As suggested by Cartwright et al. (2003) are polygonal faults are poorly described in coarse-grained sediments, and frequent sediment input from the western half may have led to coarse-grained lithologies and may reflect the lack of polygonal faults on the western half of the area.



Prograding mudstone sequences

Figure 6-5: The presence of restricted mineralogies is suggested to be dependent on the main provenance area. A proximal location to the source will exhibit a high kaolinite content regarding large crystalline structures, where a distal location to the source will exhibit a larger smectite and illite content regarding minor crystalline structures. The illustration and suggestion are retrieved from Thyberg et al. (1999).

6.2.2 Fault plane geometries

Polygonal faults exhibit planar to gently listric fault plane geometries, where a varying fault plane geometry between stratigraphic sequences is expected as polygonal faults develop in isolated, constrained sequences (figure 6-4). There is no visible correlation of fault plane geometries and basin locations, hence correlations between stratigraphic sequences.

Sequence CSS-2, CSS-5/6, and CSS-7 display polygonal faults with restricted planar fault plane geometries, with an average sequence thickness of ~125-435 ms (figure 6-6). Planar fault plane geometries can be associated with increased vertical stress, dependent on the amount of overburden load, lithologies not displaying volume reductions, and extension from sliding. The observations of planar fault planes in this study reject the theory of Stuevold et al. (2003) that suggested that planar fault plane geometries are related to sequences thickness with a moderate thickness (<200-300 m). The theory suggests lower vertical stress applied to sequences holding a moderate thickness rather than thick sequences. As suggested by Dewhurst et al. (1999) has a relationship linked to grain size has been favored for planar fault planes rather than burial depth and sequence thickness.

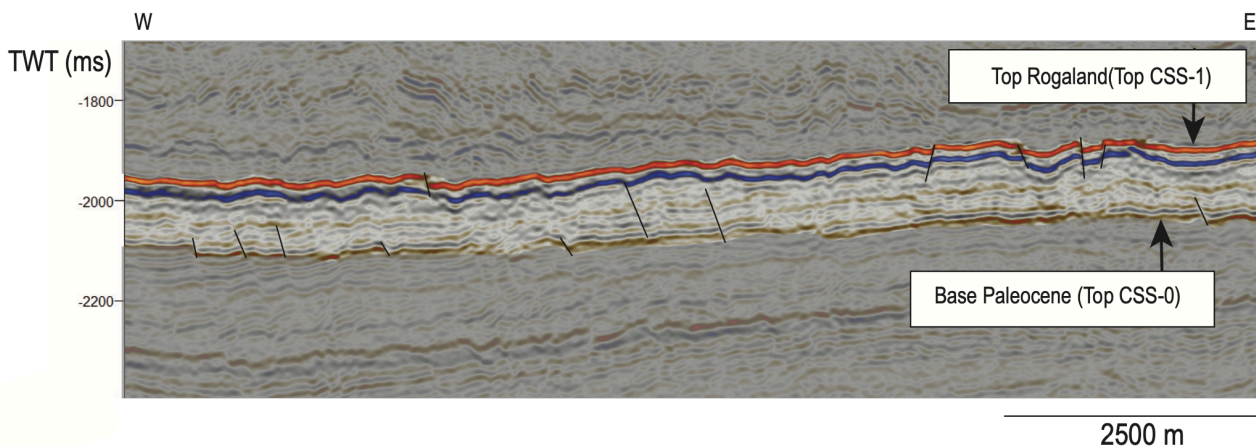


Figure 6-6: Seismic cross-section displaying restricted planar fault plane geometries of polygonal faults in CSS-2, CSS-5/6, and CSS-7.

Sequence CSS-1, CSS-3, and CSS-4 display polygonal faulted subareas with alternating planar to gently listric fault planes, with average sequence thicknesses of ~45-285 ms. Planar to gently listric fault plane geometries can be associated with compaction, volume reduction, or increased extension from sliding events. We can assume that volume reduction of sediments initiates the

formation of listric fault planes. A planar fault plane intersecting layers will eventually change geometry to a more listric approach under volume reduction. The layers that experience the most shrinkage display the most listric fault planes. Compaction or volume reduction of sequences leads to changes in temperature, pore pressure, and stress properties, triggering abrupt mineralogy alternations within a sequence. These changes can be linked to a pure compaction effect caused by porosity-depth trends, where compaction results from increasing pressure leading to physical processes and chemical cementation (Sclater & Christie, 1980).

CSS-4 displays a flat seismic reflection event interpreted as a diagenetic event of opal A to opal CT transformation zone, representing a volume reduction. Sediments below the transformation zone are less resistant to physical property changes in response to increased temperature and pressure gradients. The fault planes illustrate alternation to a gentler dip in interaction with volume reduction (figure 6-7). The relationship between fault dip plane alternation and transformation zone is observed in the entire sequence where the opal transformation is present. Gravitational sliding could generate listric-shaped fault planes through additional sliding or tilting but would expect uniform fault planes to dip towards the shelf and rotated beddings. However, do CSS-3 display listric fault planes and two orientation sets from faulting that could indicate bidirectional slab sliding initiated from sliding from the basin slope, resulting in two dominant fault orientation sets (figure 6-10).

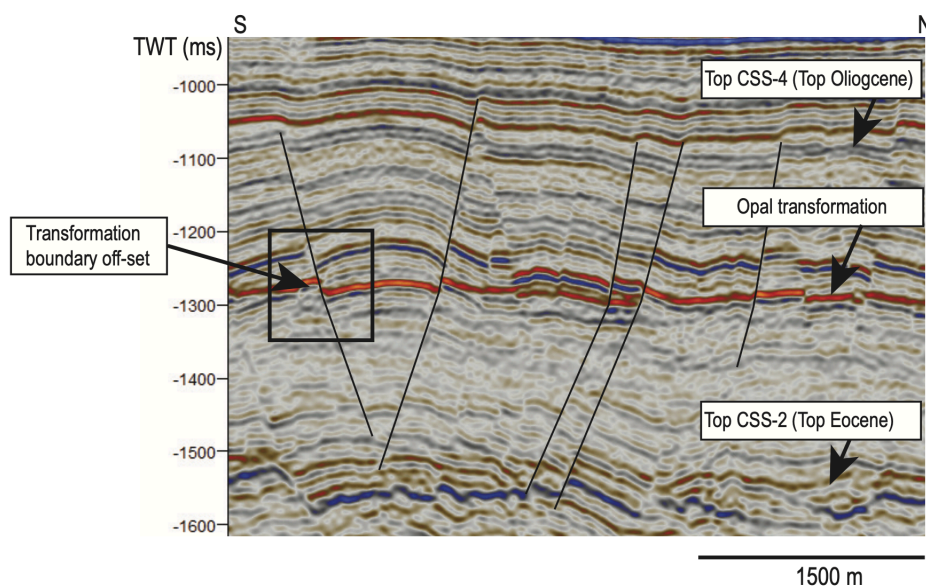


Figure 6-7: Seismic cross-section displaying alternation of fault plane dip in CSS-4. The fault plane alters to a gentler dip beneath the opal A to opal CT transformation zone. The black square on the left side of the cross-section displays the opal transformation as a flat seismic event displaced by the faulting.

6.2.3 Fault displacement

The site of maximum fault displacement specifies where the initial fault nucleation started, and multiple sites of maximum displacement are observed (figure 6-8). Multiple sites of maximum fault displacement observed from CSS-1, CSS-2, CSS-5/6, and CSS-7 indicate various facies related to lithology variations within sequences. Mixed lithologies can inhibit uniform nucleation of faults and develop various sites of maximum fault displacement. They can be associated with frequent uplift events in Late Paleocene-Early Eocene and Miocene, resulting in significant sandy inputs mixed into present clay lithologies. As suggested in studies done by Dewhurst et al. (1999), Thyberg et al. (1999), and Stuevold et al. (2003), explanations for the site of maximum fault displacement are linked to lithology variations, sediment supply, and tectonic movements.

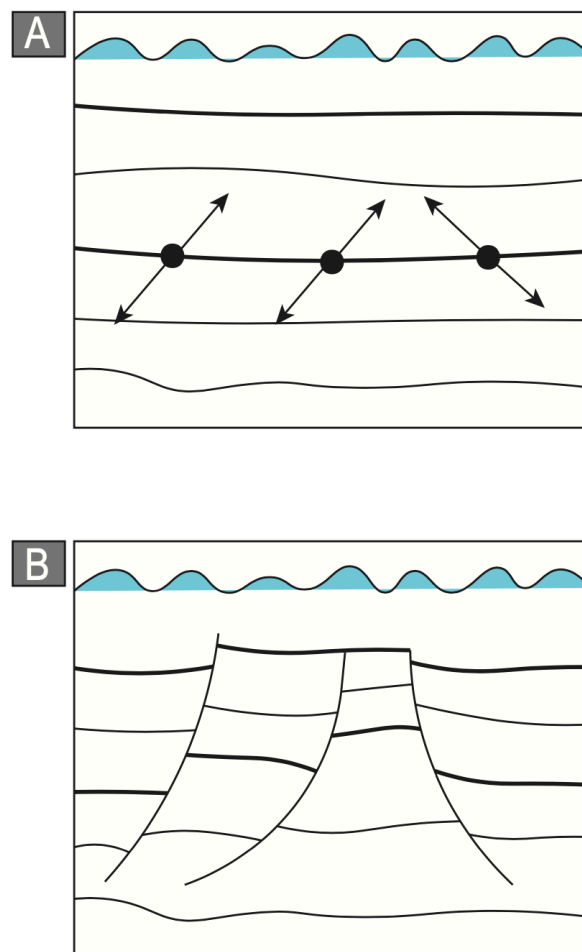


Figure 6-8: Modified figure of Cartwright (2003), displaying fault propagating of polygonal faults and maximum displacement at the site of initial nucleation point. **A)** Location of initial fault nucleation, **B)** Fault growth and propagation of adjacent sediments.

A relatively constant site of maximum fault displacement is observed in the Oligocene sequences, CSS-3 and CSS-4. The maximum fault displacement is displayed near the base of CSS-3 and in the upper unit of CSS-4, suggesting sites of initial nucleation which could be related to homogenous lithologies within the sequences.

The displacement trend in CSS-3 is associated with fault interaction from adjacent polygonal faulted sequences (figures 5-21 and 5-22). The polygonal faulted base of the CSS-3 displays alternated, rotated reflections that indicate a connection to compaction, volume reduction, or sliding within the sequence (figure 6-9). The maximum displacement trend observed in CSS-4 is situated above the opal A/CT transformation zone, displaying a porosity reduction and reduced sediment strengths linked to shrinkage. The Oligocene sequences are the only sequences displaying a constant fault displacement trend. They possibly could be linked to the high smectite-content of the period, which is vulnerable for changes in physical properties potentially leading to mechanical compaction and subsidence of sediments (Stuevold et al., 2003; Davies et al., 2009). The relationship of fault displacement and curvature of fault planes can be correlated. Hence no measurements have previously been conducted (Watterson et al., 2000; Cartwright et al., 2003).

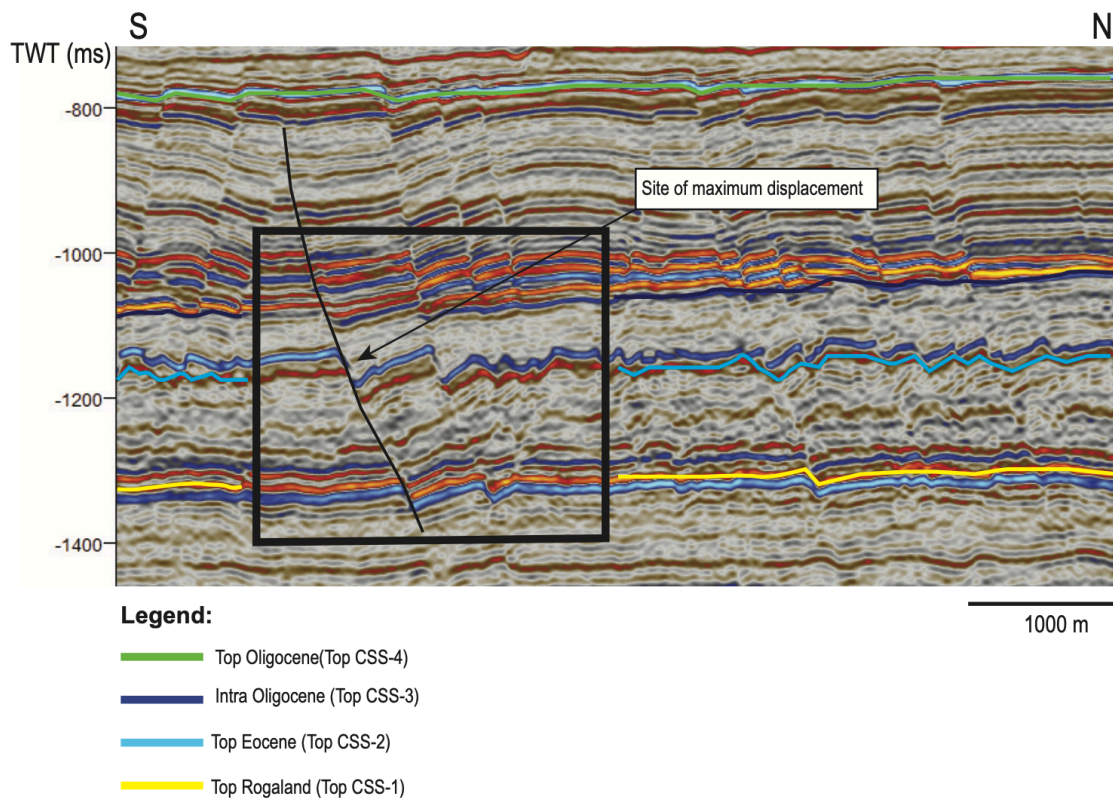


Figure 6-9: Seismic cross-section displaying the site of maximum displacement of polygonal faults at the base of CSS-3 at Top CSS-2. The site of maximum displacement can be associated with the site of initial fault nucleation.

6.2.4 Fault orientation

All polygonal faulted sequences display fault strikes in almost all orientations. CSS-1 displays a pronounced N-S trend compared to the remaining sequences, suggesting anisotropic stress and movement (figure 6-10). The remaining sequences reveal some preferred orientation trends, which may result from random distribution or geological processes. Polygonal faulted sequences that display subareas with the same preferred orientations are possibly indicating a trend.

The pronounced N-S orientation trend of the polygonal faults in CSS-1 may hold some tectonic imprints of the uplift event of the magmatic plume and East Shetland Platform in the period of Paleocene-Early Eocene in communication with sliding and toe thrusts as a likely result. The gravitational processes are anticipated to influence the orientation of the polygonal faults with an almost uniform dip in relation to the slope, close to orientations displayed from the faults in

CSS-1 (figure 6-10). Additional mechanisms as additional loading may have initiated the remaining, more random orientation trends in the sequence.

The remaining sequences display more inconsistent orientation trends from the rose diagrams (figure 6-10). Clear orientation sets are observed in CSS-2 and slightly in CSS-3 (figure 6-10). The preferred orientation trends from the two sequences tend to develop as sets linked to submarine slides influenced by bidirectional sliding. Bidirectional sliding results from tilting and rejuvenation, which could support of previously observed CSS-2 exhibiting prograding units that display alternating amplitudes (figure 5-16) (Cox et al., 2020). The clear onlap surface of top CSS-3 indicates flank uplift of the sequence before deposition of overlying sequence in Intra Oligocene (figure 5-20). CSS-4 displays a slightly preferred orientation towards NW-SE in some areas (figure 6-10). Clausen et al. (1999) suggested a preferred NW-SE orientation trend of the Upper Oligocene polygonal fault near the Horda Platform, related to tectonic uplift and interaction of additional trigger mechanism.

Subarea orientations:

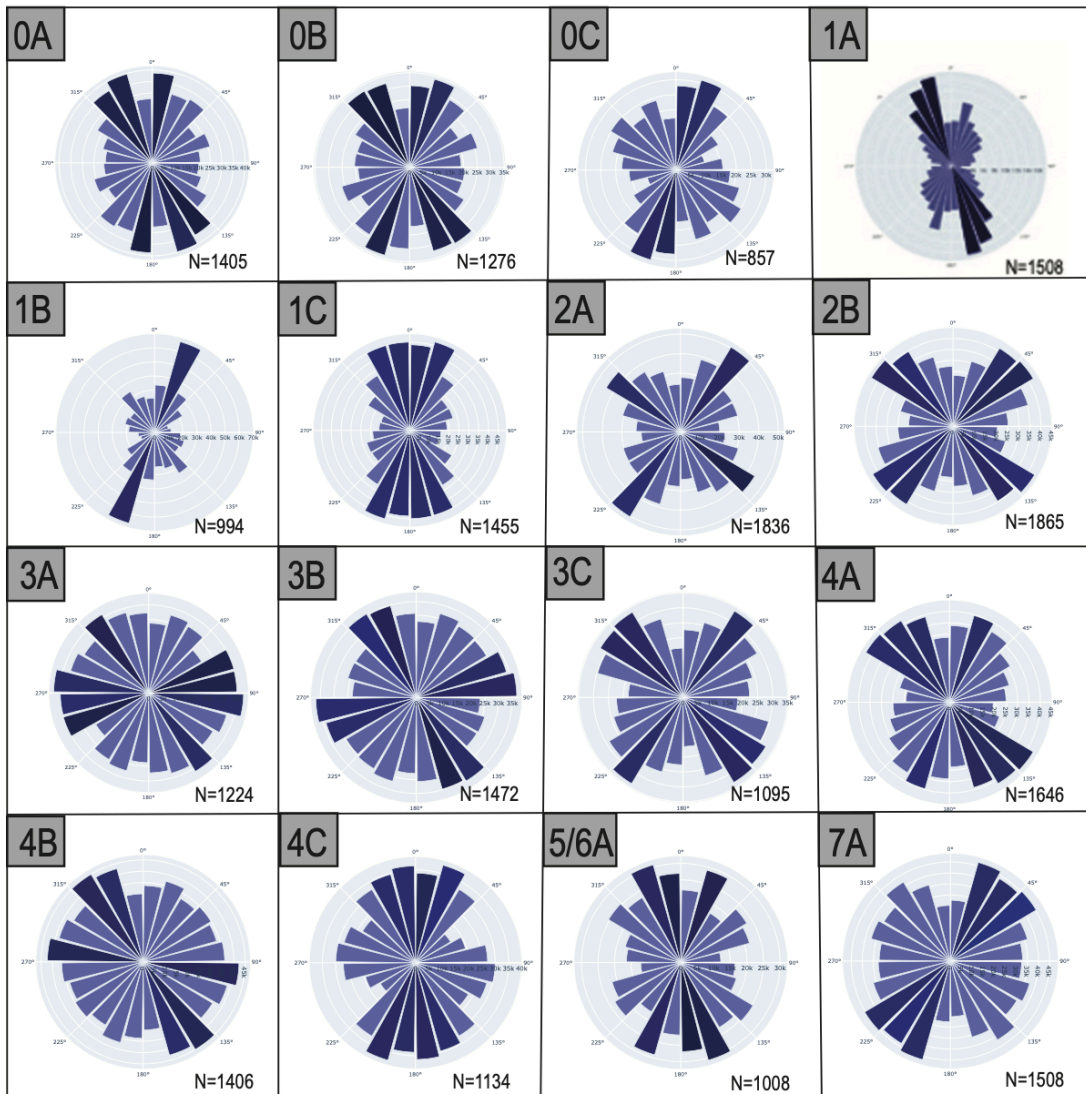


Figure 6-10: Rose diagrams of 16 subareas weighted by length retrieved from topological analysis in Network GT. The rose diagrams display the fault orientation of each subarea discussed in this thesis. Slightly preferred orientation trends are marked in a darker blue. Top CSS-0 is represented by 0A, 0B, and 0C, Top CSS-1 is represented by 1A, 1B, and 1C, Top CSS-2 is represented by 2A and 2B, Top CSS-3 is represented by 3A, 3B, and 3C, Top CSS-4 is represented by 4A, 4B, and 4C, Top CSS-5/6 is represented by 5/6A, and Top CSS-7 is represented by 7A.

To state slightly preferred orientation trends of a polygonal faults systems may be considered vague, regarding the fault systems anisotropic behavior. Preferred orientation trends may be an outcome of a random distribution of polygonal fault orientations. Figure 6-11 displays how synthetic data, computed in Python, distribute 1.000 fault orientations. The results can potentially clarify preferred orientation trends based on an inconstant distribution of fault orientations.

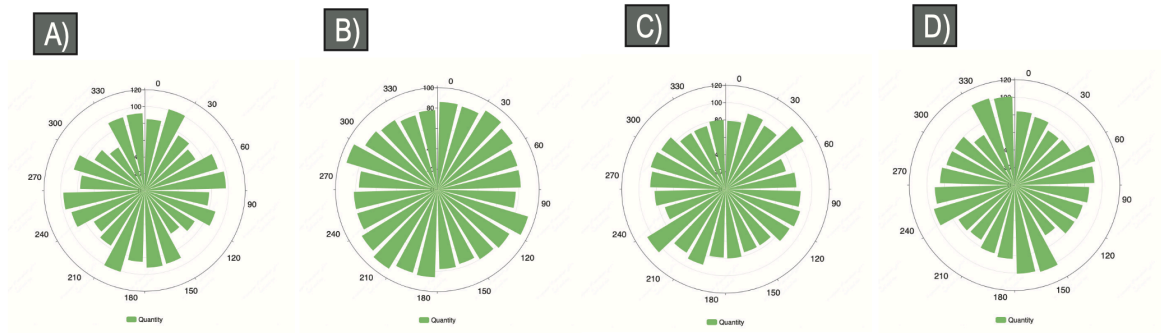


Figure 6-11: Rose diagrams displaying randomly generated fault orientations for four false polygonal fault networks. The rose diagram displays slightly preferred orientation trends based on a random selection of 1000 fault orientations. **A)** Display slightly preferred N-S and E-W trends, **B)** display randomly distributed orientation trends, **C)** display slightly preferred WSW-ENE trends, and **D)** display slightly preferred NNW-SSE trends.

6.3 Proposed classification of polygonal faults

After interpreting polygonal faulted areas concerning stratigraphy and basin location, the classification of polygonal faults was based on sequences at a stratigraphic level (table 6-1 and figure 6-12). The results exhibited several trends and similarities related to stratigraphy rather than basin location. The polygonal fault classification does not include the faults located below the Cenozoic sequences. A summarizing argumentation table of the potential trigger mechanism of the polygonal faulted subareas is displayed in table 6-2.

Table 6-1: Poly class characteristics of polygonal faults restricted to one class.

Classification	1. Poly class	2. Poly class	3. Poly class	4. Poly class
Subareas	0A, 0B, 0C, 1A, 1B, 1C	2A, 2B, 4A, 4B, 4C	3A, 3B, 3C	5/6A, 7A
Sequence	Paleocene-Early Eocene	Eocene and Upper Oligocene	Lower Oligocene	Lower and Upper Miocene
Characteristics	Isolated fault traces, N-S preferred strike (figure 6-13)	Horst/graben structures, remobilized sediments, high smectite content (figure 6-13)	Wedge sequence, connected faults from adjacent sequences (figure 6-13)	Hold fault tips, faults situated in lower unit of sequence (figure 6-13)
Preferred strike	N-S (<i>NNW-SEE, NNE-SSW</i>)	N-S, NW-SE, NE-SW	E-W, NW-SE, NE-SW	NNW-SEE, NNE-SSW, NE-SW
Site of maximum fault displacement	Inconsistent	Constant	Constant	Inconsistent
Plan form pattern	Isolated and rectangular	Rectangular and curved	Rectangular and curved	Isolated, rectangular, and curved
Average sequence thicknesses	~ 147-247 ms	~ 265-433 ms	~ 45-210 ms	~ 126-151 ms
Connectivity (C_b)	0.65 – 0.91 (figure 5-41)	0.90 – 1.30 (figure 5-41)	1.16 - 1.20 (figure 5-41)	0.86 - 0.98 (figure 5-41)
Additional structures	-	Horst/grabens Mounds Sand injectites	-	-

Poly class characteristics:

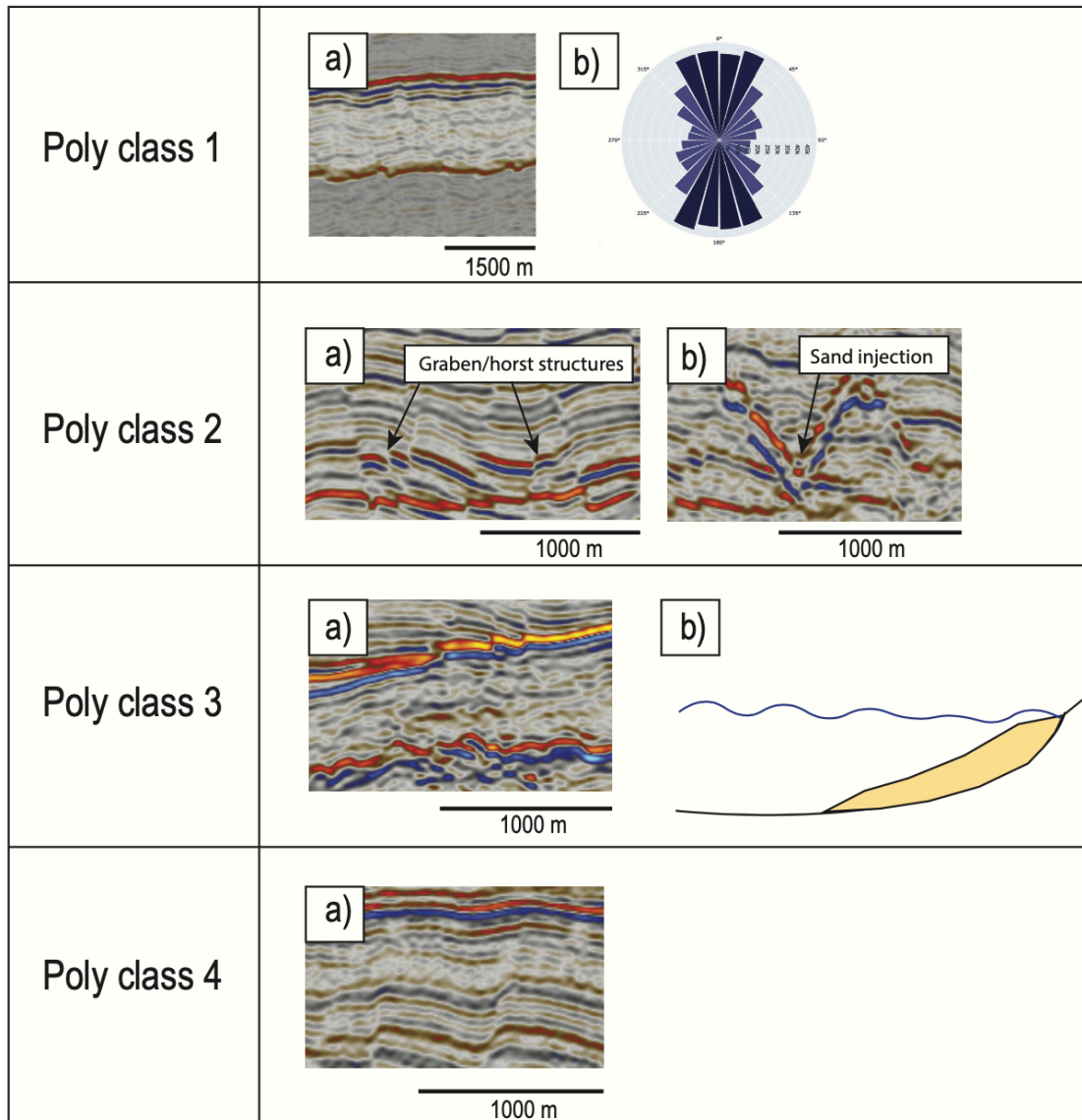


Figure 6-12: Illustration of the four polygonal fault classes' main characteristics. **Poly class 1:** **a)** Faulted base of the sequence translating into more isolated fault traces towards the top, and **b)** preferred N-S orientation of polygonal faults in restricted poly class. **Poly class 2:** **a)** Connected polygonal faults displaying horst/grabens, and **b)** structures as sand injections are commonly located within the poly class. **Poly class 3:** **a)** Polygonal faulted base and top intersecting with adjacent sequences, and **b)** prograding wedge sequence holding polygonal faults in this poly class. **Poly class 4:** **a)** Polygonal faults delimited within sequence due to coarsening upward trends.

6.4 Suggested trigger mechanisms

Suggested formation of 1. Poly class

The polygonal faults in the Paleocene-Early Eocene sequence (CSS-1) are systematically arranged into poly class 1 (figure 6-13). The poly class display: a) dominant N-S orientation, b) inconsistent site of maximum fault displacement, c) isolated and rectangular plan form pattern, d) average sequence thicknesses of ~147-247 ms, and e) connectivities of 0.65 – 0.91 (C_b).

The dominant orientation can be related to reduced horizontal stress in one direction and tensile fracturing. However, may the faults be influenced by uplift and gravitational processes of turbiditic sands influencing the fault orientations to the slope (figure 6-10). The dominant orientation of the polygonal faults may also be affected by the propagation of underlying faults op Upper Mesozoic age. Thus, the fault traces of the Upper Mesozoic age might hold tectonic imprints from previous tectonic events that can illuminate the dominant N-S trend observed. This theory is associated with minor and more extensive faults in the sequence observed from plan view (figure 5-12). The longer fault lengths could be linked to previously existing faults that have undergone numerous strain events than the minor fault lengths.

The characteristics of isolated, poorly connected (C_B) polygonal faults seem to be related to lithology variations within the sequence. Lithology variations may result from sandy inputs mixed into underlying clays in the Paleocene, and the increased sand ratio coincides with less dense polygonal faults towards the top of the sequence (figure 6-13). Poorly described occurrence of polygonal faults in sand-dominated units supports the inconsistent site of maximum fault displacement within the sequence. Poorly described occurrence of polygonal faults in sand-dominated units supports the loss in connectivity and isolated fault patterns. The observation of relatively isolated faults in CSS-1 coincides nicely with the phases of uplift and significant turbidite deposits from the East Shetland Platform in the Paleocene-Early Eocene. The contour maps of 2D intensity and connecting node frequency show increased connectivity of polygonal faults on the eastern half of the sequence located distally from the main provenance area (figures 5-9 and 5-11). The altering clay and sand lithology influenced by gravitational processes and gravitational loading are interpreted as potential trigger mechanisms of poorly connected, isolated, N-S trending polygonal faults.

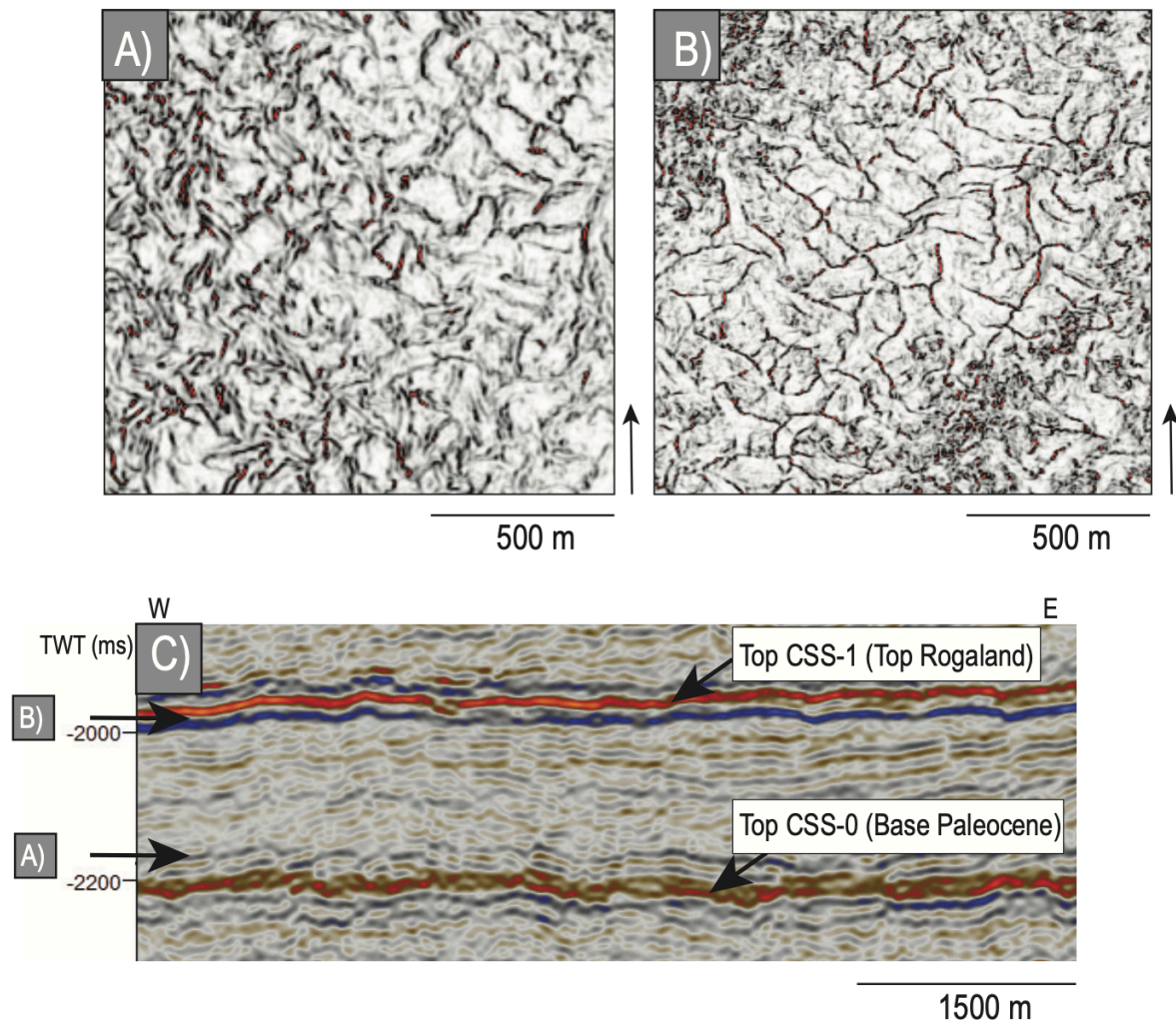


Figure 6-13: Plan form pattern from variance attribute maps of polygonal faults in CSS-1 (Paleocene-Early Eocene sequence). **A)** Variance attribute map close to Top CSS-0, acting as the base of CSS-1 displaying low-resolution fault patterns, **B)** variance attribute map close to Top CSS-1 displaying more isolated fault traces and better resolution of the plan form pattern, and **C)** seismic section displaying the position of where the attribute maps were extracted.

Turbiditic sands and sandy clinofolds fed into the basin in the Paleocene are acting as additional load to underlying smectite-rich clays. The additional load acts as gravitational load, increasing the vertical stress and potentially trigger sediment failure. Sediment failure occurs only in sediments with low friction values, dependent on an additional mechanism for initial nucleation generated by large shear stress and compaction. These mechanisms would result in the growth and development of fractures and faults. However, the additional sandy load of underlying clays is complementary for density inversion, as they have a higher density than clay, leading to differential compaction and fluid escape. The escaped fluids generated from

density inversion of clays are linked to fracturing and potential polygonal fault formation. This theory coincides with the regional uplifts by a magmatic plume and sands deposited from the East Shetland Platform in the Paleocene-Early Eocene period.

The previously discussed universal relationship of density inversion folds and graben/horsts related to polygonal faults is not observed in this poly class. However, is it possible that the mixture of sand and clays may form polygonal faults from density inversion regardless of inversion folds. Considering Henriot et al. (1988) statement, the universal relationship may show some weaknesses from clays holding mixed intervals of sand. Polygonal faults may form from this mixed lithology, but the coarse grain size of sands can potentially delimit the formation process of inversion folds.

The trigger mechanisms of syneresis and particle dissolution are unlikely to be the trigger mechanism of polygonal faults of this poly class based on the seismic data, with a lack of recognizable seismic patterns. Syneresis is a poorly understood mechanism, missing experimental work on smectite-rich sediments, and triggering of faults. With a lack of experimental work, the mechanism does not hold any recognizable seismic patterns. The presence of common structures of syneresis as cracks, craters, fissures, and mounds would support syneresis, but none of these structures are observed within the polygonal faulted sequence. Authors agree that fault traces triggered by syneresis should occur sporadically within a sequence regarding exclusive lithology of gels (Walstra, 1993; Cartwright et al., 2003). Sporadic fault traces are not reliable for this poly class, as the fault patterns appear close to uniform within the sequence. The mechanism of particle dissolution can display recognizable seismic patterns as seismic reflection events if a significant volume change (porosity reduction) occurs over a narrow temperature interval (Davies & Clark, 2006). Particle dissolution occurring over a broader depth and temperature interval does not hold any seismic traces and is hard to observe from seismic images. The mechanisms of particle dissolution are hard to state with a lack of mineralogy, geochemical data, and seismic traces.

Suggested formation of 2. Poly class

The polygonal faults in the Eocene and Upper Oligocene sequences (CSS-2 and CSS-4) are systematically arranged into poly class 2. The poly class display: a) slightly preferred N-S, NW-SE, NE-SW orientations (figure 6-10), b) constant site of maximum fault displacement, c)

rectangular and curved plan form pattern, d) average sequence thicknesses of ~265-433 ms, e) connectivities of 0.90 – 1.30 (C_b), and f) additional structures of horst/grabens, mounds, and sand injections. The sequences of this poly class contain the highest smectite content of all sequences in the Cenozoic.

The sequences holding this poly class are relatively thick (265-433 ms), which could be related to uplift events or sea-level fall during deposition influencing the rate of sediment deposition. An increased rate of sediment dispersal into the basin generates an additional load on underlying smectite-rich clays. Additional loading is linked to the trigger mechanism of gravitational load that is a reliable mechanism of polygonal faults. The mechanism is reliable as it coincides with soft sediment remobilization structures (sand injections and mounds) resulting from compaction and fluidization. The process of fluidization can be linked to the fracturing of overlying sediments, such as fluids escape. Gravitational loading is a potential trigger mechanism of this poly class based on the findings of soft sediment remobilization structures in the polygonal faulted sequences. As previously discussed, the mechanism of gravitational loading is dependent on an additional mechanism causing large shear stress for nucleation (Goult, 2008).

Density inversion is a potential trigger mechanism concerning the occurrence of density inversion folds displaying graben/horst structures (figures 5-17, 5-31, and 5-34). The density inversion folds are results of fluid escape during differential compaction. A universal relationship of density inversion structures and polygonal faults is present within CSS-2 and CSS-4 holding this fault class. On the other hand, is the relationship not observed on the southeastern slope of the Eocene sequence, implicating either another trigger mechanism or physical property variations blocking the development of density inversion folds. Density inversion is interpreted as a potential trigger mechanism of this polygonal fault class interacting with gravitational instabilities (Henriet et al., 1988; Clausen et al., 1999).

Particle dissolution is, similarly to density inversion, suggested as a potential trigger mechanism linked to gravitational loading. Particle dissolution is only identified in the polygonal faults in CSS-4 and will not take CSS-2 into account. The opal transformation boundary represents an evident particle dissolution but appears somewhat questionable for the formation of polygonal faults, as it is displaced by faults (figure 6-7). The maximum fault displacement is found in the

upper unit above the transformation event, indicating the site of nucleation. As previous studies have highlighted, the relationship between polygonal faults and the opal transformation related to compaction and lithification processes is still unclear (Skempton, 1969; Cartwright, 2011). Particle dissolution is a suggested trigger mechanism of polygonal faults in CSS-4 showing physical property changes that induce contraction-driven shear failure (figures 5-26, 5-28, and 5-31). Polygonal faults seem to develop regardless of particle dissolution (CSS-2) based on seismic observations.

The mechanism of gravitational sliding is interpreted to be a potential trigger mechanism, based on the appearance of N-S trending mounds oriented perpendicular to the slope gradient in CSS-4, as well as orientation sets linked to slab slides in CSS-2. The N-S trending mounds in CSS-4 are possibly related to gravitational sliding. Large piles of chaotic reflections within the sequence indicate a sliding event causing the accumulation of sediment piles holding reverse faults near the basin slope transition (figure 6-14). The N-S-oriented mounds are situated close to the base of the opal transformation zone, acting as a detachment surface. The detachment surface can develop within stratigraphic sequences, where underlying rocks are unaffected by sliding events (Hesthammer & Fossen, 1999). These observations coincide well with sliding on the eastern flank that resulted from the uplift in the Early Miocene. The orientation sets (NW-SE, NE-SW) of CSS-2 could express bidirectional sliding from slab slides. Most of the faults in this sequence are located at the eastern basin flank exposed for uplift events. The observations of CSS-2 correspond with uplift events in the Early Oligocene and the rejuvenation of sediment deposits. The gravitational sliding mechanism is also supported by the increase in sediment thickness in the basin center with a decrease in thickness towards the flanks (figure 5-13).

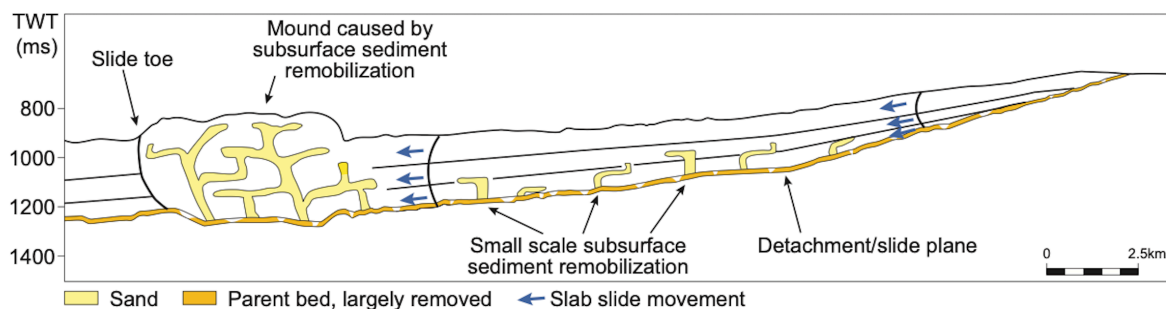


Figure 6-14: Illustration retrieved from Hermanrud et al. (2019). The illustration displays slab sliding along a detachment surface initiated during periods of flank uplift. Slab sliding results in the formation of mounds and sand injections situated close to a detachment boundary. Illustration reflects observations done from the base of the eastern basin flank in CSS-4.

The mechanism of syneresis is interpreted to be unlikely to trigger the polygonal faults of this poly class based on seismic observations. As previously discussed, syneresis is poorly described in smectite-rich lithologies. Syneresis is associated with various fracture nucleation sites and can result in fractures propagate up and down in a unit (Dewhurst et al., 1999). The initial nucleation of faulting in the sequences is restricted to the upper unit, not displaying various nucleation sites. In addition, are the polygonal faults within this fault class broadly developed within the restricted sequences, not coinciding with minor, restricted sites of syneresis (Cartwright et al., 2003). The fault class holds varying lithologies of clays and sand from remobilization, weakening the mechanism of syneresis, as the faults tend to die out with coarse-grained sediments (Dewhurst et al., 1999).

Suggested formation of 3. Poly class

The polygonal faults in the Lower Oligocene sequence (CSS-3) are systematically arranged into poly class 3. The poly class display: a) slightly preferred E-W, NW-SE, NE-SW orientations (figure 6-10), b) constant site of maximum fault displacement, c) rectangular and curved plan form pattern, d) average sequence thicknesses of ~45-210 ms, and e) connectivities of 1.16 – 1.20 (C_b).

The fault systems display preferred orientations of E-W, NW-SE, and NE-SW with no biased orientations regarding the position of the eastern basin slope. However, the faults display two orientation sets (NW-SE, NE-SW) (figure 6-10), which are suggested to form from bidirectional slab slides from mass transport deposits along the basin flank. The mass transport deposits can express orientation sets when formed under uplift and rejuvenation (Cox et al., 2020). The uplift event in the Early Oligocene coincides with the traces of a prograding wedge as deposited from the period and potential mass transport deposits (figure 5-19). In addition to sliding, can underlying, previous faults influence the orientation of faults as imprints. The connection of fault planes into adjacent sequences coincides with fault propagation and potentially influence by older fault traces (figures 5-21 and 5-22).

The depositional history and extent of CSS-3 in the basin may lack some seismic interpretation, but this is not further considered as polygonal faults are the main topic. The prograding trend of CSS-3 from the eastern basin flank and Norwegian margin display well-developed polygonal faults distally in the sequence. Denser polygonal fault systems developed in the western part of

the sequence are characterized with clays based on the distance from the provenance area and increased smectite content (figure 6-5). The onlapping of CSS-4 at the proximal part of the wedge, generates smaller vertical stress than the vertical stress acting more distal of the wedge, based on the thickness of overlying CSS-4. The amount of vertical stress and gravitational load is linked to the significant difference in polygonal fault development from the east to the west on the wedge sequence (figure 6-15). However, indicate the onlap surface flank uplift of the eastern flank before deposition of CSS-4. The altering fault plane from connected overlying faults is linked to physical property changes between sequences (figures 5-21, 5-22, and 5-23). The additional loading of CSS-3 may lead to compactional loading, resulting in shear fractures and polygonal fault development. The most pronounced displacement from faulting is located near the base of the sequence and is related to the initial site of fault nucleation (figure 5-22).

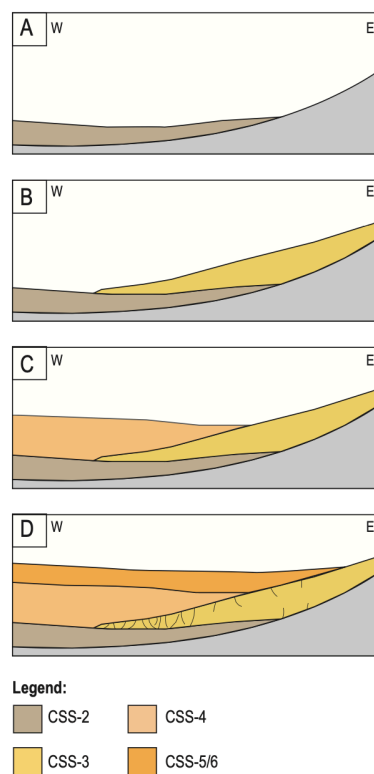


Figure 6-15: Illustration of a suggested formation of polygonal faults in CSS-3. **A)** Time before deposition of wedge sequence, **B)** deposition of Wedge sequence from the eastern margin (Norwegian margin), the distal areas of the wedge sequence hold a minor thickness and the possibility of higher smectite content due to the distal location concerning provenance area, **C)** deposition of additional sequence creating an additional load and vertical stress, and **D)** deposition of a new sequence and additional load leading to fracture of underlying weak, smectite-rich areas of wedge sequence.

Syneresis and particle dissolution are unlikely to trigger this poly class, as the shallow depth conditions (< 100m) desired were most likely not fulfilled. The polygonal faults of CSS-3 are

linked to the adjacent, thick CSS-4 and were most likely located at deeper depths when the faulting occurred (figure 20A). The particle dissolution mechanism described in poly class 1 is hard to state with a lack of mineralogy data and no observable seismic patterns.

Suggested formation of 4. Poly class

The polygonal faults in the Miocene sequences (CSS-5/6, CSS-7) are systematically arranged into poly class 4. The poly class display, a) slightly preferred NNW-SSE, NNE-SSW, NE-SW orientations (figure 6-10), b) inconsistent site of maximum fault displacement, c) isolated, rectangular, and curved plan form pattern, d) average sequence thicknesses of ~126-151 ms, and e) connectivities of 0.86 – 0.98 (C_b).

The polygonal faults are characterized by planar fault planes situated in the lower areas of the sequences (figures 5-37A and 5-40A). Thick, sandy lithologies of the Skade and Utsira Fm. are situated in the upper unit of the sequences, acting as an additional load of underlying clays. The faults do not propagate above the sequences, which coincide with coarsening upward trends and glacial influenced sediments, hindering polygonal fault formation and delimitation by grain size in the Pliocene and Pleistocene periods.

The dense, thick sand deposits overlaying clays support gravitational loading as a potential mechanism. Gravitational loading generates sediment failure based on additional vertical loading and is initiated by a compactional event associated with density inversion, syneresis, or particle dissolution. The sequences do not exhibit density inversion folds or graben/horst and do not perceive the universal relationship between density inversion folds and polygonal faults (Henriet et al., 1988). Similarly, as with previous poly classes, this relationship may not always be observable based on physical property variations or other disturbances of clay distribution. The occurrence of this poly class is restricted in minor areas (~56 – 150 km²) and may be associated with restricted lithologies of gels, described from the mechanism of syneresis. The restricted occurrence of the poly class from the Miocene period has previously been interpreted to display isolated fault traces. The signature of polygonal fault tips near the top of the sequences could be related to the observed coarsening upward trend in Miocene. This trend is related to rapid deposition and decrease in sea-level, demonstrating nucleation near the surface, where faults are potentially triggered by syneresis.

Gravitational sliding may act as a contributing factor in the formation of this fault class, as glacio-eustatic changes in Mid-Miocene leading to the uplift of the western flank could be related to the sliding of clays in the period. The poly class is restricted to minor areas on the western slope holding diverse distribution orientations of the polygonal faults. This leads to an interpretation that gravitational sliding does not act as the only contributor to the formation of polygonal faults. The mechanism of particle dissolution is interpreted to be unlikely to trigger the polygonal faults of poly class 4. Particle dissolution is rejected based on the lack of seismic transformation events and mineralogy data in the seismic work.

Table 6-2: Argumentation table for potential trigger mechanisms of polygonal faults in the Cenozoic successions of the northern North Sea.

Trigger mechanisms					
Poly class	Sequence	Density inversion	Gravitational sliding	Gravitational loading	Syneresis and particle dissolution
1	CSS-1A	Potential: sediments can potentially facilitate differential compaction, but lack density inversion folds	Potential: preferred N-S orientation coincides with perpendicular orientation of slope	Potential: vertical loading of sequence, need combination with additional mechanism	Unlikely to: no observable physical property changes (lack of mineralogy data)
1	CSS-1B	Potential: sediments can potentially facilitate differential compaction, but lack density inversion folds	Potential: preferred N-S orientation coincides with perpendicular orientation of slope	Potential: vertical loading of sequence, need combination with additional mechanism	Unlikely to: no observable physical property changes (lack of mineralogy data)
1	CSS-1C	Potential: sediments can potentially facilitate differential compaction, but lack density inversion folds	Potential: preferred N-S orientation coincides with perpendicular orientation of slope	Potential: vertical loading of sequence, need combination with additional mechanism	Unlikely to: no observable physical property changes (lack of mineralogy data)
2	CSS-2A	Potential: sediments can potentially facilitate differential compaction, but lack density inversion folds	Potential: two preferred orientation trends may indicate slab sliding	Potential: soft sediment remobilization structures fluidized	Unlikely to: no observable physical property changes (lack of mineralogy data)
2	CSS-2B	Potential: presence of density inversion folds, graben, and horst	Potential: two preferred orientation trends may indicate slab sliding	Potential: soft sediment	Unlikely to: no observable physical

				remobilization structures fluidized	property changes (lack of mineralogy data)
3	CSS-3A	Potential: sediments can potentially facilitate differential compaction, but lack density inversion folds	Unlikely to: no visible seismic trends indicate relation to slope and sliding	Potential: vertical loading of sequence, need combination with additional mechanism	Unlikely to: no observable physical property changes (lack of mineralogy data)
3	CSS-3B	Potential: sediments can potentially facilitate differential compaction, but lack density inversion folds	Potential: two preferred orientation trends may indicate slab sliding	Potential: vertical loading of sequence, need combination with additional mechanism	Unlikely to: no observable physical property changes (lack of mineralogy data)
3	CSS-3C	Potential: sediments can potentially facilitate differential compaction, but lack density inversion folds	Potential: two preferred orientation trends may indicate slab sliding	Potential: vertical loading of sequence, need combination with additional mechanism	Unlikely to: no observable physical property changes (lack of mineralogy data)
2	CSS-4A	Potential: presence of density inversion folds and graben/horst in sequence	Potential: mounded N-S orientated features coincides with perpendicular orientation of slope	Potential: soft sediment remobilization structures fluidized	Potential: polygonal faults in units above and below diagenetic boundary
2	CSS-4B	Potential: presence of density inversion folds and graben/horst in sequence	Potential: mounded N-S orientated features coincides with perpendicular orientation of slope	Potential: soft sediment remobilization structures fluidized	Potential: polygonal faults in units above and below diagenetic boundary
2	CSS-4C	Potential: presence of density inversion folds and graben/horst in sequence	Potential: mounded N-S orientated features coincides with perpendicular orientation of slope	Potential: soft sediment remobilization structures fluidized	Potential: polygonal faults in units above and below diagenetic boundary

4	CSS-5/6A	Potential: sediments can potentially facilitate differential compaction, but lack density inversion folds	Unlikely to: no visible seismic trends indicate relation to slope and sliding	Potential: vertical loading of sequence, need combination with additional mechanism	Unlikely to: no observable physical property changes (lack of mineralogy data)
4	CSS-7A	Potential: sediments can potentially facilitate differential compaction, but lack density inversion folds	Unlikely to: no visible seismic trends indicate relation to slope and sliding	Potential: vertical loading of sequence, need combination with additional mechanism	Unlikely to: no observable physical property changes (lack of mineralogy data)

7. Future work

This study has presented new, additional information on polygonal fault systems situated within the northern North Sea Paleocene-Miocene interval. Distribution maps of polygonal faults within the stratigraphic intervals may be sufficient for further work. As this study investigated subareas of the large-scale fault systems, it remains more detailed work. Suggestions for future work are listed below.

- Perform a similar, detailed study on a restricted area to fully understand the detailed pattern and behavior of the polygonal faults at stratigraphic levels. A large study area as in this study may not be beneficial and can possibly avoid the fault system essential fault patterns and geometries.
- Access to mineralogy data from the Cenozoic successions would be beneficial to further investigate the mineralogy of the various sequences. Geochemical data would be helpful when discussing potential trigger mechanisms and reject some mechanisms related to restricted mineralogies.
- Extend the topological analysis of the polygonal faults with automatic interpretation on an entire stratigraphic horizon. This would display more large-scale data on the fault systems and display prominent trends and patterns of entire polygonal fault systems.
- Detailed interpretation at stratigraphic levels to see how polygonal faults connect and give a more precise vision of how the polygonal faults interact with adjacent sequences in the stratigraphy.
- Experiments on uncertain trigger mechanisms to approve or reject the processes as potential mechanisms of polygonal fault formations. Uncertain trigger mechanisms are difficult to relate to as little knowledge of the processes.
- Compare similar studies in other sedimentary basins and observe a connection between polygonal faults at stratigraphic levels rather than basin locations.
- Further investigate polygonal fault systems in the Upper Mesozoic sequences to study similarities or differences of the Lower Cenozoic fault systems.

8. Conclusion

Seismic interpretation of polygonal faults in the Paleocene to Miocene sequences of the northern North Sea have been conducted. The polygonal distribution and patterns have been the main aim of this study, and the key findings of this thesis are as follows:

- The polygonal faults are developed in six stratigraphic sequences from Paleocene to Miocene, displaying a wide range of seismic signatures, geometries, and topologies. In addition, the Upper Mesozoic sediments display fault patterns related to Lower Cenozoic faulting.
- Polygonal faults are restricted to the eastern half of the study area. The finding shows that with increased distance from the provenance area in the west, at the East Shetland Platform, there is decreasing grain size and potentially increasing smectite production, which controls the distribution of polygonal faults.
- Four polygonal fault classes are recognized from the seismic interpretation and are restricted to stratigraphic sequences, strongly associated with uplift and lithologies.
 - The Paleocene-Early Eocene sequence (CSS-1) exhibits poorly connected, N-S trending polygonal faults parallel to the slope. The faults are influenced by uplift and sandy deposits influencing the clay lithology assemblages of the sediments in the Late Paleocene-Early Eocene.
 - Lower Oligocene sequence (CSS-3) wedges out from the eastern margin, where faults intersect adjacent sequences and display a prograding fault pattern most likely concerning provenance area, grain size, and smectite distribution.
 - Eocene and Oligocene sequences (CSS-2 and CSS-4) display the highest densities and frequencies of polygonal fault in this study, related to the highest smectite content of clays, indicating an essential relationship between polygonal faults and clay lithologies. The sequences exhibit remobilization structures, N-S trending mounds, and fault orientation sets, demonstrating compactional loading, fluidization, and gravitational sliding initiated by western flank uplifts in the Oligocene-Miocene transition.
 - Miocene sequences (CSS-5/6 and CSS-7) are associated with lithology changes linked to coarsening upward trends. The fault tips at the Miocene-Pliocene transition terminate as the clay lithologies phase out into coarser lithologies.

-
- The most probable formation of polygonal faults is an interaction between internal (volume reduction) and external (sliding, loading) processes. The most reliable mechanism discussed in this study, based on seismic data, is gravitational loading, gravitational sliding, and density inversion. The mechanisms correlate with seismic observations of density folds, remobilization structures, and orientation trends. The two remaining syneresis and particle dissolution mechanisms are less probable trigger mechanisms due to uncertain seismic characteristics in this study.
 - The large-scale seismic interpretation job of the northern North Sea can provide a basis for a potential update of the Cenozoic stratigraphic framework, and a basis for a PhD as lots of observations have not been covered and discussed in this thesis regarding the scope of the study area.

References

- Andresen, K. J., & Clausen, O. (2014). An integrated subsurface analysis of clastic remobilization and injection; a case study from the Oligocene succession of the eastern North Sea. *Basin Research*, 26(5), 641-674.
- Bjørlykke, K. (1998). Clay mineral diagenesis in sedimentary basins—a key to the prediction of rock properties. Examples from the North Sea Basin. *Clay Minerals*, 33(1), 15-34.
- Blatt, H. (1979). Diagenetic processes in sandstones.
- Bramlette, M. N. (1946). *The Monterey Formation of California and the origin of its siliceous rocks* (Vol. 212): US Government Printing Office.
- Briedis, N. A., Bergslien, D., Hjellbakk, A., Hill, R. E., & Moir, G. J. (2007). Recognition criteria, significance to field performance, and reservoir modeling of sand injections in the Balder field, North Sea.
- Burst, J. F. (1969). Diagenesis of Gulf Coast clayey sediments and its possible relation to petroleum migration. *AAPG bulletin*, 53(1), 73-93.
- Cartwright, J. (2011). Diagenetically induced shear failure of fine-grained sediments and the development of polygonal fault systems. *Marine and Petroleum Geology*, 28(9), 1593-1610.
- Cartwright, J., James, D., & Bolton, A. (2003). The genesis of polygonal fault systems: a review. *Geological Society, London, Special Publications*, 216(1), 223-243.
- Cartwright, J. A. (1994). Episodic basin-wide fluid expulsion from geopressed shale sequences in the North Sea basin. *Geology*, 22(5), 447-450.
- Cartwright, J. t., & Dewhurst, D. (1998). Layer-bound compaction faults in fine-grained sediments. *Geological Society of America Bulletin*, 110(10), 1242-1257.
- Chopra, S., & Marfurt, K. J. (2005). Seismic attributes—A historical perspective. *Geophysics*, 70(5), 3SO-28SO.
- Clausen, J., Gabrielsen, R., Reksnes, P., & Nysaether, E. (1999). Development of intraformational (Oligocene–Miocene) faults in the northern North Sea: influence of remote stresses and doming of Fennoscandia. *Journal of Structural Geology*, 21(10), 1457-1475.
- Copestake, P., Sims, A. P., Crittenden, S., Hamar, G. P., Ineson, J. R., Rose, P. T., & Tringham, M. E. (2003). *Lower Cretaceous: The Millennium Atlas: petroleum geology of the central and northern North Sea*. London.
- Cox, D. R., Huuse, M., Newton, A. M., Gannon, P., & Clayburn, J. (2020). Slip sliding away: Enigma of large sandy blocks within a gas-bearing mass transport deposit, offshore northwestern Greenland. *AAPG bulletin*, 104(5), 1011-1043.
- Davies, R., Ireland, M., & Cartwright, J. (2009). Differential compaction due to the irregular topology of a diagenetic reaction boundary: a new mechanism for the formation of polygonal faults. *Basin Research*, 21(3), 354-359.
- Davies, R. J., & Clark, I. R. (2006). Submarine slope failure primed and triggered by silica and its diagenesis. *Basin Research*, 18(3), 339-350.
- Davies, R. J., & Ireland, M. T. (2011). Initiation and propagation of polygonal fault arrays by thermally triggered volume reduction reactions in siliceous sediment. *Marine Geology*, 289(1-4), 150-158.
- Dewhurst, D. N., Cartwright, J. A., & Lonergan, L. (1999). The development of polygonal fault systems by syneresis of colloidal sediments. *Marine and Petroleum Geology*, 16(8), 793-810.
- Diskos. (2021). Well data. Retrieved from <http://www.diskos.cgg.com>

- Duffy, O. B., Nixon, C. W., Bell, R. E., Jackson, C. A.-L., Gawthorpe, R. L., Sanderson, D. J., & Whipp, P. S. (2017). The topology of evolving rift fault networks: Single-phase vs multi-phase rifts. *Journal of Structural Geology*, *96*, 192-202.
- Dypvik, H. (1983). Clay mineral transformations in Tertiary and Mesozoic sediments from North Sea. *AAPG bulletin*, *67*(1), 160-165.
- Eidvin, T., Jansen, E., Rundberg, Y., Brekke, H., & Grogan, P. (2000). The upper Cainozoic of the Norwegian continental shelf correlated with the deep sea record of the Norwegian Sea and the North Atlantic. *Marine and Petroleum Geology*, *17*(5), 579-600.
- Ellis, A., & Dryden, W. (1987). *The practice of rational-emotive therapy (RET)*: Springer Publishing Co.
- Faleide, J. I., Kyrkjebø, R., Kjennerud, T., Gabrielsen, R. H., Jordt, H., Fanavoll, S., & Bjerke, M. D. (2002). Tectonic impact on sedimentary processes during Cenozoic evolution of the northern North Sea and surrounding areas. *Geological Society, London, Special Publications*, *196*(1), 235-269.
- Fazlikhani, H., Fossen, H., Gawthorpe, R. L., Faleide, J. I., & Bell, R. E. (2017). Basement structure and its influence on the structural configuration of the northern North Sea rift. *Tectonics*, *36*(6), 1151-1177.
- Fossen, H. (2016). *Structural geology*: Cambridge University Press.
- Fossen, H., Khani, H. F., Faleide, J. I., Ksienzyk, A. K., & Dunlap, W. J. (2017). Post-Caledonian extension in the West Norway–northern North Sea region: the role of structural inheritance. *Geological Society, London, Special Publications*, *439*(1), 465-486.
- Fraser, S., Robinson, A., Johnson, H., Underhill, J., Kadolsky, D., Connell, R., . . . Ravnås, R. (2003). *Upper Jurassic: The Millennium Atlas: Petroleum Geology of the Central and Northern North Sea*. London.
- Færseth, R. (1996). Interaction of Permo-Triassic and Jurassic extensional fault-blocks during the development of the northern North Sea. *Journal of the Geological Society*, *153*(6), 931-944.
- Gibbs, R. J. (1977). Clay mineral segregation in the marine environment. *Journal of Sedimentary Research*, *47*(1), 237-243.
- Glennie, K. W. (2009). *Petroleum Geology of the North Sea: Basic concepts and recent advances*: John Wiley & Sons.
- Goldsmith, P. J., Hudson, G., & Van Veen, P. (2003). *Triassic: The Millennium Atlas: Petroleum Geology of the Central and Northern North Sea*. London.
- Goult, N. (2001). Polygonal fault networks in fine-grained sediments—an alternative to the syneresis mechanism. *First break.*, *19*(2), 69-73.
- Goult, N. (2002). Mechanics of layer-bound polygonal faulting in fine-grained sediments. *Journal of the Geological Society*, *159*(3), 239-246.
- Goult, N. (2008). Geomechanics of polygonal fault systems: a review. *Petroleum Geoscience*, *14*(4), 389-397.
- Helland-Hansen, W., Ashton, M., Lømo, L., & Steel, R. (1992). Advance and retreat of the Brent delta: recent contributions to the depositional model. *Geological Society, London, Special Publications*, *61*(1), 109-127.
- Henriet, J., De Batist, M., Van Vaerenbergh, W., & Verschuren, M. (1988). Seismic facies and clay tectonic features of the Ypresian clay in the southern North Sea. *Bulletin van de Belgische Vereniging voor Geologie*, *97*, 457-472.
- Hermanrud, C., Christensen, E., Haugvaldstad, M., Røynestad, L., Tjensvold, I., & Watsend, L. (2019). Triggers of sand remobilization in deep marine deposits. *Geological Society, London, Special Publications*, *493*.

- Hermanrud, C., & Undertun, O. (2019). Resolution limits of fluid overpressures from mineralogy, porosity, and sonic velocity variations in North Sea mudrocks. *AAPG bulletin*, 103(11), 2665-2695.
- Hesthammer, J., & Fossen, H. (1999). Evolution and geometries of gravitational collapse structures with examples from the Statfjord Field, northern North Sea. *Marine and Petroleum Geology*, 16(3), 259-281.
- Higgins, J. A., Blättler, C., Lundstrom, E., Santiago-Ramos, D., Akhtar, A., Ahm, A. C., . . . Murray, S. (2018). Mineralogy, early marine diagenesis, and the chemistry of shallow-water carbonate sediments. *Geochimica et Cosmochimica Acta*, 220, 512-534.
- Higgs, W., & McClay, K. (1993). Analogue sandbox modelling of Miocene extensional faulting in the Outer Moray Firth. *Geological Society, London, Special Publications*, 71(1), 141-162.
- Hurst, A., Scott, A., & Vigorito, M. (2011). Physical characteristics of sand injectites. *Earth-Science Reviews*, 106(3-4), 215-246.
- Husmo, T., Hamar, G., Høiland, O., Johannessen, E., Rømuld, A., Spencer, A., & Titterton, R. (2003). *Lower and Middle Jurassic: The Millennium Atlas: Petroleum Geology of the Central and Northern North Sea*. London.
- Huuse, M., Jackson, C. A. L., Van Rensbergen, P., Davies, R. J., Flemings, P. B., & Dixon, R. J. (2010). Subsurface sediment remobilization and fluid flow in sedimentary basins: an overview. *Basin Research*, 22(4), 342-360.
- Ireland, M. T., Davies, R. J., Goult, N. R., & Carruthers, D. (2011). Structure of a silica diagenetic transformation zone: the Gjallar Ridge, offshore Norway. *Sedimentology*, 58(2), 424-441.
- Isaksen, D., & Tonstad, K. (1989). *A revised Cretaceous and Tertiary lithostratigraphic nomenclature for the Norwegian North Sea*: Norwegian Petroleum Directorate.
- Isaksen, G. H. (2004). Central North Sea hydrocarbon systems: Generation, migration, entrapment, and thermal degradation of oil and gas. *AAPG bulletin*, 88(11), 1545-1572.
- Jackson, C. A.-L. (2007). The Geometry, distribution, and development of clastic injections in slope systems: Seismic examples from the Upper Cretaceous Kyrre Formation, Mly Slope, Norwegian Margin.
- Jolly, R. J., & Lonergan, L. (2002). Mechanisms and controls on the formation of sand intrusions. *Journal of the Geological Society*, 159(5), 605-617.
- Jordt, H., Faleide, J. I., Bjørlykke, K., & Ibrahim, M. T. (1995). Cenozoic sequence stratigraphy of the central and northern North Sea Basin: tectonic development, sediment distribution and provenance areas. *Marine and Petroleum Geology*, 12(8), 845-879.
- Jordt, H., Thyberg, B. I., & Nøttvedt, A. (2000). Cenozoic evolution of the central and northern North Sea with focus on differential vertical movements of the basin floor and surrounding clastic source areas. *Geological Society, London, Special Publications*, 167(1), 219-243.
- Kastner, M., Keene, J., & Gieskes, J. (1977). Diagenesis of siliceous oozes—I. Chemical controls on the rate of opal-A to opal-CT transformation—an experimental study. *Geochimica et Cosmochimica Acta*, 41(8), 1041-1059.
- Klopprogge, J. T., Komarneni, S., & Amonette, J. E. (1999). Synthesis of smectite clay minerals: a critical review. *Clays and Clay Minerals*, 47(5), 529-554.
- Laurent, D., Gay, A., Baudon, C., Berndt, C., Soliva, R., Planke, S., . . . Mangue, M. (2012). High-resolution architecture of a polygonal fault interval inferred from geomodel applied to 3D seismic data from the Gjallar Ridge, Vøring Basin, Offshore Norway. *Marine Geology*, 332, 134-151.

References

- Lonergan, L., Cartwright, J., & Jolly, R. (1998). The geometry of polygonal fault systems in Tertiary mudrocks of the North Sea. *Journal of Structural Geology*, 20(5), 529-548.
- Lonergan, L., & Cartwright, J. A. (1999). Polygonal faults and their influence on deep-water sandstone reservoir geometries, Alba Field, United Kingdom central North Sea. *AAPG bulletin*, 83(3), 410-432.
- Lonergan, L., Lee, N., Johnson, H. D., Cartwright, J. A., & Jolly, R. J. (2000). Remobilisation and injection in deepwater depositional systems: Implications for reservoir architecture and prediction.
- Lynne, B. Y., Campbell, K. A., Moore, J., & Browne, P. (2005). Diagenesis of 1900-year-old siliceous sinter (opal-A to quartz) at Opal Mound, Roosevelt Hot Springs, Utah, USA. *Sedimentary Geology*, 179(3-4), 249-278.
- Løseth, H., & Henriksen, S. (2005). *A Middle to Late Miocene compression phase along the Norwegian passive margin*. Paper presented at the Geological Society, London, Petroleum Geology Conference series.
- Løseth, H., Wensaas, L., Arntsen, B., & Hovland, M. (2003). Gas and fluid injection triggering shallow mud mobilization in the Hordaland Group, North Sea. *Geological Society, London, Special Publications*, 216(1), 139-157.
- Mai, H. T., Marfurt, K. J., & Chávez-Pérez, S. (2009). Coherence and volumetric curvatures and their spatial relationship to faults and folds, an example from Chicotepec basin, Mexico. In *SEG Technical Program Expanded Abstracts 2009* (pp. 1063-1067): Society of Exploration Geophysicists.
- Manzocchi, T. (2002). The connectivity of two-dimensional networks of spatially correlated fractures. *Water Resources Research*, 38(9), 1-1-1-20.
- Marcussen, Ø., Thyberg, B. I., Peltonen, C., Jahren, J., Bjørlykke, K., & Faleide, J. I. (2009). Physical properties of Cenozoic mudstones from the northern North Sea: Impact of clay mineralogy on compaction trends. *AAPG bulletin*, 93(1), 127-150.
- Martinsen, O., Bøen, F., Charnock, M., Mangerud, G., & Nøttvedt, A. (1999). *Cenozoic development of the Norwegian margin 60–64° N: sequences and sedimentary response to variable basin physiography and tectonic setting*. Paper presented at the Geological Society, London, Petroleum Geology Conference series.
- Mauldon, M., Dunne, W., & Rohrbach Jr, M. (2001). Circular scanlines and circular windows: new tools for characterizing the geometry of fracture traces. *Journal of Structural Geology*, 23(2-3), 247-258.
- Morley, C., & Nixon, C. (2016). Topological characteristics of simple and complex normal fault networks. *Journal of Structural Geology*, 84, 68-84.
- NASA. (2021). What is Permafrost. Retrieved from <https://climatekids.nasa.gov/permafrost/>
- Nixon, C. W., Nærland, K., Rotevatn, A., Dimmen, V., Sanderson, D. J., & Kristensen, T. B. (2020). Connectivity and network development of carbonate-hosted fault damage zones from western Malta. *Journal of Structural Geology*, 141, 104212.
- Nixon, C. W., Sanderson, D. J., & Bull, J. M. (2012). Analysis of a strike-slip fault network using high resolution multibeam bathymetry, offshore NW Devon UK. *Tectonophysics*, 541, 69-80.
- Nøttvedt, A., Gabrielsen, R., & Steel, R. (1995). Tectonostratigraphy and sedimentary architecture of rift basins, with reference to the northern North Sea. *Marine and Petroleum Geology*, 12(8), 881-901.
- NPD FactPages. (2021). Retrieved from <https://www.npd.no/fakta/nyheter/Faktasider-og-faktakart-teknisk-informasjon/>
- Nyberg, B., Nixon, C. W., & Sanderson, D. J. (2018). NetworkGT: A GIS tool for geometric and topological analysis of two-dimensional fracture networks. *Geosphere*, 14(4), 1618-1634.

- Nøttvedt, A. (2000). Integrated Basin Studies—Dynamics of the Norwegian Margin: an introduction. *Geological Society, London, Special Publications*, 167(1), 1-14.
- Olobayo, O. (2015). *Deposition, remobilization and fluid flow in sedimentary basins-case studies in the northern north sea and nigerian transform margin*: The University of Manchester (United Kingdom).
- Ortega, O., & Marrett, R. (2000). Prediction of macrofracture properties using microfracture information, Mesaverde Group sandstones, San Juan basin, New Mexico. *Journal of Structural Geology*, 22(5), 571-588.
- Pigott, J. D., Kang, M.-H., & Han, H.-C. (2013). First order seismic attributes for clastic seismic facies interpretation: Examples from the East China Sea. *Journal of Asian Earth Sciences*, 66, 34-54.
- Ravnås, R., Nøttvedt, A., Steel, R., & Windelstad, J. (2000). Syn-rift sedimentary architectures in the Northern North Sea. *Geological Society, London, Special Publications*, 167(1), 133-177.
- Rundberg, Y., & Eidvin, T. (2005). Controls on depositional history and architecture of the Oligocene-Miocene succession, northern North Sea Basin. In *Norwegian Petroleum Society Special Publications* (Vol. 12, pp. 207-239): Elsevier.
- Sanderson, D. J., & Nixon, C. W. (2015). The use of topology in fracture network characterization. *Journal of Structural Geology*, 72, 55-66.
- Sclater, J. G., & Christie, P. A. (1980). Continental stretching: An explanation of the post-Mid-Cretaceous subsidence of the central North Sea Basin. *Journal of Geophysical Research: Solid Earth*, 85(B7), 3711-3739.
- Shin, H., Santamarina, J. C., & Cartwright, J. A. (2008). Contraction-driven shear failure in compacting uncemented sediments. *Geology*, 36(12), 931-934.
- Simm, R., & White, R. (2002). Tutorial: Phase, polarity and the interpreter's wavelet. *first break*, 20(5).
- Simpson, R. W. (1997). Quantifying Anderson's fault types. *Journal of Geophysical Research: Solid Earth*, 102(B8), 17909-17919.
- Skempton, A. W. (1969). The consolidation of clays by gravitational compaction. *Quarterly Journal of the Geological Society*, 125(1-4), 373-411.
- Środoń, J. (1999). Nature of mixed-layer clays and mechanisms of their formation and alteration. *Annual Review of Earth and Planetary Sciences*, 27(1), 19-53.
- Stuevold, L. M., Faereth, R. B., Arnesen, L., Cartwright, J., & Möller, N. (2003). Polygonal faults in the Ormen Lange field, Møre basin, offshore mid Norway. *Geological Society, London, Special Publications*, 216(1), 263-281.
- Sun, Q., Wu, S., Yao, G., & Lü, F. (2009). Characteristics and formation mechanism of polygonal faults in Qiongdongnan Basin, northern South China Sea. *Journal of Earth Science*, 20(1), 180-192.
- Surlyk, F., Dons, T., Clausen, C. K., & Higham, J. (2003). *Upper Cretaceous: The Millennium Atlas: petroleum geology of the central and northern North Sea*.
- Thyberg, B., Jordt, H., Bjørlykke, K., & Faleide, J. (2000). Relationships between sequence stratigraphy, mineralogy and geochemistry in Cenozoic sediments of the northern North Sea. *Geological Society, London, Special Publications*, 167(1), 245-272.
- Thyberg, B. I., Stabell, B., Faleide, J. I., & Bjørlykke, K. (1999). Upper Oligocene diatomaceous deposits in the northern North Sea-silica diagenesis and paleogeographic implications. *Norsk Geologisk Tidsskrift*, 79(1), 3-18.
- Tjensvold, I. T. (2018). *Trigger mechanisms for sand intrusions* (MSc). University of Bergen, Vendeville, B., Cobbold, P., Davy, P., Choukroune, P., & Brun, J. (1987). Physical models of extensional tectonics at various scales. *Geological Society, London, Special Publications*, 28(1), 95-107.

References

- Vrolijk, P. (1990). On the mechanical role of smectite in subduction zones. *Geology*, 18(8), 703-707.
- Walstra, P. (1993). The syneresis of curd. In *Cheese: Chemistry, physics and microbiology* (pp. 141-191): Springer.
- Wang, J. R., & Schmugge, T. J. (1980). An empirical model for the complex dielectric permittivity of soils as a function of water content. *IEEE Transactions on Geoscience and Remote Sensing*(4), 288-295.
- Watterson, J., Walsh, J., Nicol, A., Nell, P., & Bretan, P. (2000). Geometry and origin of a polygonal fault system. *Journal of the Geological Society*, 157(1), 151-162.
- Weaver, C. E. (1989). Clays, Muds, and Shales: Development in Sedimentology, 44. In: Elsevier, Scientific Publication.
- White, W. A. (1961). Colloid phenomena in sedimentation of argillaceous rocks. *Journal of Sedimentary Research*, 31(4), 560-570.
- Wrona, T., Magee, C., Jackson, C. A., Huuse, M., & Taylor, K. G. (2017). Kinematics of polygonal fault systems: observations from the northern North Sea. *Frontiers in Earth Science*, 5, 101.
- Ziegler, P. (1975). Geologic evolution of North Sea and its tectonic framework. *AAPG bulletin*, 59(7), 1073-1097.
- Zweigel, P., Arts, R., Lothe, A. E., & Lindeberg, E. B. (2004). Reservoir geology of the Utsira Formation at the first industrial-scale underground CO₂ storage site (Sleipner area, North Sea). *Geological Society, London, Special Publications*, 233(1), 165-180.